PolyPublie
Polytechnique Montréal

POLYTECHNIQUE MONTRÉAL
UNIVERSITÉ D'INGÉNIERIE

Titre: Title:	A New Definition of the Representative Volument Element in Numerical Homogenization Problems and its Application to the Performance Evaluation of Analytical Homogenization Models.
Auteur: Author:	Hadi Moussaddy
Date:	2013
Type:	Mémoire ou thèse / Dissertation or Thesis
Référence: Citation:	Moussaddy, H. (2013). A New Definition of the Representative Volument Element in Numerical Homogenization Problems and its Application to the Performance Evaluation of Analytical Homogenization Models. [Thèse de doctorat, École Polytechnique de Montréal]. PolyPublie. https://publications.polymtl.ca/1091/

Document en libre accès dans PolyPublie
Open Access document in PolyPublie

URL de PolyPublie: PolyPublie URL:	https://publications.polymtl.ca/1091/
Directeurs de recherche: Advisors:	Daniel Therriault, & Martin Lévesque
Programme: Program:	Génie mécanique

Ce fichier a été téléchargé à partir de PolyPublie, le dépôt institutionnel de Polytechnique Montréal
This file has been downloaded from PolyPublie, the institutional repository of Polytechnique Montréal

https://publications.polymtl.ca

UNIVERSITÉ DE MONTRÉAL

A NEW DEFINITION OF THE REPRESENTATIVE VOLUMENT ELEMENT IN NUMERICAL HOMOGENIZATION PROBLEMS AND ITS APPLICATION TO THE PERFORMANCE EVALUATION OF ANALYTICAL HOMOGENIZATION MODELS

HADI MOUSSADDY
DÉPARTEMENT DE GÉNIE MÉCANIQUE
ÉCOLE POLYTECHNIQUE DE MONTRÉAL

THÈSE PRÉSENTÉE EN VUE DE L'OBTENTION
DU DIPLÔME DE PHILOSOPHIÆ DOCTOR
(GÉNIE MÉCANIQUE)
AVRIL 2013

© Hadi Moussaddy, 2013.

UNIVERSITÉ DE MONTRÉAL

ÉCOLE POLYTECHNIQUE DE MONTRÉAL

Cette thèse intitulée :

A NEW DEFINITION OF THE REPRESENTATIVE VOLUMENT ELEMENT IN NUMERICAL HOMOGENIZATION PROBLEMS AND ITS APPLICATION TO THE PERFORMANCE EVALUATION OF ANALYTICAL HOMOGENIZATION MODELS

présentée par : MOUSSADDY Hadi
en vue de l'obtention du diplôme de : Philosophiæ Doctor
a été dûment acceptée par le jury d'examen constitué de :

M. GOSSELIN Frédéric, Ph.D., président
M. THERRIAULT Daniel, Ph.D., membre et directeur de recherche
M. LÉVESQUE Martin, Ph.D., membre et codirecteur de recherche
M. LESSARD Larry, Ph.D., membre
M. BÖHM Helmut J., Techn. Doct., membre

To my parents
Safwan and Aisha

To my wife
Nour

To my whole family...

ACKNOWLEDGEMENTS

I would like to thank Pr. Daniel Therriault and Pr. Martin Lévesque for their guidance throughout this project. Your insightful criticism guided me to complete a rigorous work, while gaining scientific maturity. Also, I want to thank Pr. Böhm, Pr. Lessard and Pr. Henry for being my committee members and Pr. Gosselin for being the Jury president.

I owe special gratitude to the members of Laboratory for Multiscale Mechanics (LM2) research group. I would like to paricularly acknowledge the contributions of Maryam PahlavanPour by conducting parts of the analytical modeling included in this thesis, and for numerous fruitful dicussions all along this project. The discussions and support of Rouhollah Farahani, Amine El-Mourid, and Elias Ghossein are also gratefully acknowledged.

I would also like to thank the Fluids Dynamics Laboratory at École Polytechnique de Montréal for providing the computers that made this research possible.

I would like to thank the Natural Sciences and Engineering Research Council of Canada (NSERC) for their financial support through scholarships.

I would like to take this opportunity to thank my parents for providing unconditional support throughout the good and the bad times of a long journey. You were my source of motivation all along the project. Finally, I would like to thank my dear wife who provided me with her love and was admirably patient and understanding untill the end of my research.

RÉSUMÉ

Le Volume Élémentaire Représentatif (VÉR) joue un rôle important dans la mécanique des matériaux composites dans le but de déterminer leurs propriétés effectives. L'homogénéisation numérique permet de calculer avec précision les propriétés effectives des composites étant donné que le VÉR soit utilisé. Dans le cadre d'homogénéisation numérique, le VÉR réfère à un ensemble de volumes élémentaires du matériau qui produisent, en moyenne, les propriétés effective du composite. Plusieurs définitions quantitatives du VÉR, détaillant les méthodes de sa détermination, sont trouvées dans la littérature. Dans cette étude, les différentes définitions du VÉR sont évaluées vis à vis leurs estimations des propriétés effectives du composite. L'étude est réalisée sur une microstructure élastique bi-phasée, les composites renforcés par des fibres aléatoirement dispersées.

Des simulations par la méthode des éléments finis à grand nombre de degrés de liberté sur des volume de taille différentes sont parallélisées sur des serveurs de calculs. Les volumes élémentaires du matériau sont générées virtuellement et assujetties à des conditions aux rives périodiques. Il est démontré que les définitions populaires du VÉR, basées sur la convergence des propriétés moyennes, produisent des propriétés erronées. Une nouvelle définition du VÉR est introduite basée sur les variations statistiques des propriétés issues des volumes élémentaires. Cette définition est démontrée apte à estimer avec grande précision les propriétés effectives des composites à fibres aléatoires. De plus, la nouvelle définition permet de calculer les propriétés effectives à un VÉR plus petit que celui nécessaire selon les autres définitions, mais aussi de réduire considérablement le nombre de simulations nécessaires pour déterminer le VÉR.

Les propriétés effectives calculés par homogénéisation numériques sont comparées à celles des modèles d'homogénéisation analytiques. Les comparaisons sont réalisées sur une large gamme de rapports de forme des fibres (allant jusqu'à 120), de contraste des propriétés (allant jusqu'à 300) pour des fractions volumiques à moins de 20%. Le modèle de Mori-Tanaka, ainsi que les méthodes d'homogénéisation par deux étapes de Mori-Tanaka/Voigt et Lielens/Voigt produisent des estimations précises des propriétés effectives des composites à fibres aléatoirement dispersées et ce jusqu'au rapport de forme de 100. Ceci permet d'utiliser ces modèles analytiques dans un calcul rapide et de grande précision des propriétés effectives de ce type de composites. Pour des fibres de rapports de forme dépassant 100, une saturation de la rigidité effective est observée dans les résultats numériques et aucun des modèles analytiques ne produit des estimations précises des propriétés effectives pour cette gamme de microstructures.

Ce travail peut être vu comme une alerte concernant la validité des définitions du VÉR couramment utilisées dans la littérature. Ceci est une première étape envers l'optimisation des méthodes de détermination du VÉR visant à déterminer avec précision les propriétés effectives des composites. L'objectif est d'explorer de nouvelles définitions susceptibles à obtenir des volumes de plus petites tailles et dont le coût de détermination est moindre tout en préservant la précision des propriétés effectives calculées.

ABSTRACT

The Representative Volume Element (RVE) plays a central role in the mechanics of composite materials with respect to predicting their effective properties. Numerical homogenization delivers accurate estimations of composite effective properties when associated with a RVE. In computational homogenization, the RVE refers to an ensemble of random material volumes that yield, by an averaging procedure, the effective properties of the bulk material, within a tolerance. A large diversity of RVE quantitative definitions, providing computational methods to estimate the RVE size, are found in literature. In this study, the ability of the different RVE definitions to yield accurate effective properties is investigated. The assessment is conducted on a specific random microstructure, namely an elastic two-phase three dimensional composite reinforced by randomly oriented fibers.

Large scale finite element simulations of material volumes of different sizes are performed on high performance computational servers using parallel computing. The materials volumes are virtually generated and subjected to periodic boundary conditions. It is shown that most popular RVE definitions, based on convergence of the properties when increasing the material volume, yields inaccurate effective properties. A new RVE definition is introduced based on the statistical variations of the properties computed from material volumes. It is shown to produce more accurate estimations of the effective properties. In addition, the new definition produced RVE that are smaller in size than that of other RVE definitions ; also the number of necessary finite element simulations to determine the RVE is substantially reduced.

The computed effective properties are compared to that of analytical models. The comparisons are performed for a wide range of fibers aspect ratios (up to 120), properties contrast (up to 300) and volume fractions only up to 20% due to computational limits. The Mori-Tanaka model and the two-step analytical methods of Mori-Tanaka/Voigt and Lielens/Voigt are best suited for estimating the effective elastic properties of composites reinforced by randomly oriented fibers of aspect ratio up to 100. This finding allows the future utilization of those analytical models for very quick and accurate effective properties calculations for this class of composites. For aspect ratios larger than 100, a stiffening saturation occurs and no analytical model delivers accurate estimations of the effective properties.

The present work can be regarded as an awareness flag regarding the validity of currently utilized RVE determination techniques. Moreover, this study provides a first step towards optimization of the RVE determination methods for computing accurate effective properties. The aim is to explore new RVE definitions that yield smaller volumes and have lower determination costs, while yielding accurate effective properties.

TABLE OF CONTENTS

LIST OF TABLES

LIST OF FIGURES

LIST OF SYMBOLS AND ABBREVIATIONS

$\mathbf{x}$	Point coordinates vector
l_f	Fiber length
d_f	Fiber diameter
c_f	Fiber volume fraction
c_m	Matrix volume fraction
c^*	Lielens volume fraction
k	Bulk modulus
G	Shear modulus
Z	Either bulk or shear modulus
n	Number of fibers
r	Numer of realizations
s	Standard deviation
$\mathbf{u}_x$	Displacement at point $\mathbf{x}$
$\mathbf{C}$	Stiffness tensor
$\mathbf{C}^*$	Effective stiffness tensor
$\tilde{\mathbf{C}}$	Apparent stiffness tensor
$\overline{\mathbf{C}}$	Arithmetic mean stiffness tensor
$\underline{\mathbf{C}}$	Harmonic mean stiffness tensor
$\hat{\mathbf{C}}$	Average of arithmetic and harmonic means of stiffness tensors
$\mathbf{I}$	Identity tensor
$\mathbf{S}$	Eshelby tensor
$\mathbf{A}$	Strain localization tensor
$\mathbf{B}$	Stress concentration tensor
V	Volume
V^S	Boundaries of volume
$\mathbf{d}$	Fiber translation vector
e	Minimum distance between two fibers
$\mathbf{v}_{12}$	Minimum distance vector between two fibers

Greek symbols

α	Subregion of an aggregated composite
ρ	Fiber aspect ratio

(θ, ϕ, ψ)	Euler angles
$\boldsymbol{\omega}$	Rotation tensor
ε	Strain component
$\boldsymbol{\varepsilon}$	Strain tensor
E	Macroscopic strain component
$\mathbf{E}$	Macroscopic strain tensor
$\boldsymbol{\sigma}$	Stress tensor
σ	Stress component
$\boldsymbol{\Sigma}$	Macroscopic stress tensor
Σ	Macroscopic stress component
$\epsilon_n = \delta$	Volume size error
$\epsilon_r = \zeta$	Number of realizations error
$\epsilon_{tol} = tol$	Tolerance

Abbreviations

RVE	Representative volume element
FE	Finite element
ROFRC	Randomly oriented fiber reinforced composites
3D	Three-dimensional
AR	Aspect ratio
M	Method
M-T	Mori-Tanaka
Dil	Dilute solution
SC	Self-consistent
Li	Lielens
PCW	Ponte Castañeda and Willis
HS	Hashin and Shtrikman
er.	error

INTRODUCTION

Heterogeneous materials are used in engineering applications at a macroscopic scale that is orders of magnitude larger than that of their constituents. Micromechanical homogenization methods aim at predicting the macroscopic properties of heterogeneous materials based on the knowledge of the constitutive laws (e.g., elasticity) and of the microstructure (e.g., constituents properties and spatial arrangement), as schematized in Figure 0.1. Several seminal works exist on the topic, like those of Willis (1981), Mura (1982), Nemat-Nasser and Hori (1993), Suquet (1997), Ponte Castañeda and Suquet (1997), Bornert *et al.* (2001), Torquato (2002) and Milton (2002).

Analytical, as well as numerical, homogenization methods have been developed and applied for numerous types of composites. Analytical homogenization models, generally based on ideal representations, produce quick estimations or rigorous bounds for the effective properties of composites. Unless for very specific microstructures (see Ghossein and Lévesque (2012)), their accuracy has not been thoroughly evaluated and this has hindered their application into an industrial context.

Numerical homogenization is accomplished by simulating artificial loadings on three-dimensional (3D) representations of the material. The response of the volume is computed using numerical techniques such as the Finite Element (FE) and Fast Fourier Transform (FFT). The accuracy of the numerical homogenization relies on the elementary notion of the Representative Volume Element (RVE). In the framework of homogenization, a RVE basically refers to a material volume that is large enough to yield accurate effective properties of the bulk material. Simulating volumes that are smaller than the RVE produces properties that are different from those of the bulk composite. On the other hand, very large volumes

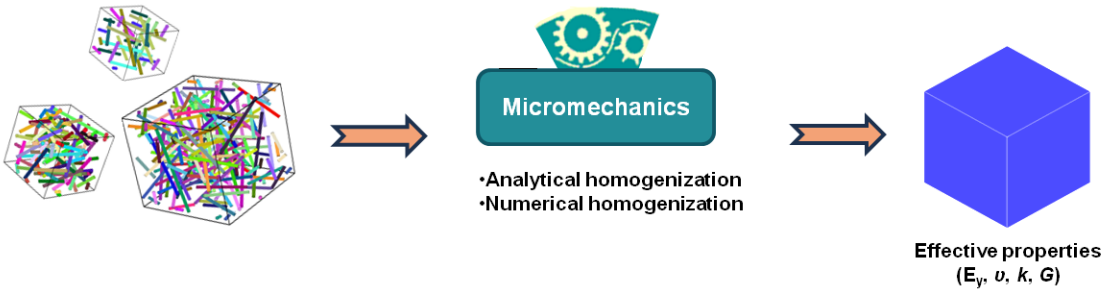

Figure 0.1 Bridging from the microscale to the macroscale through micromechanics.

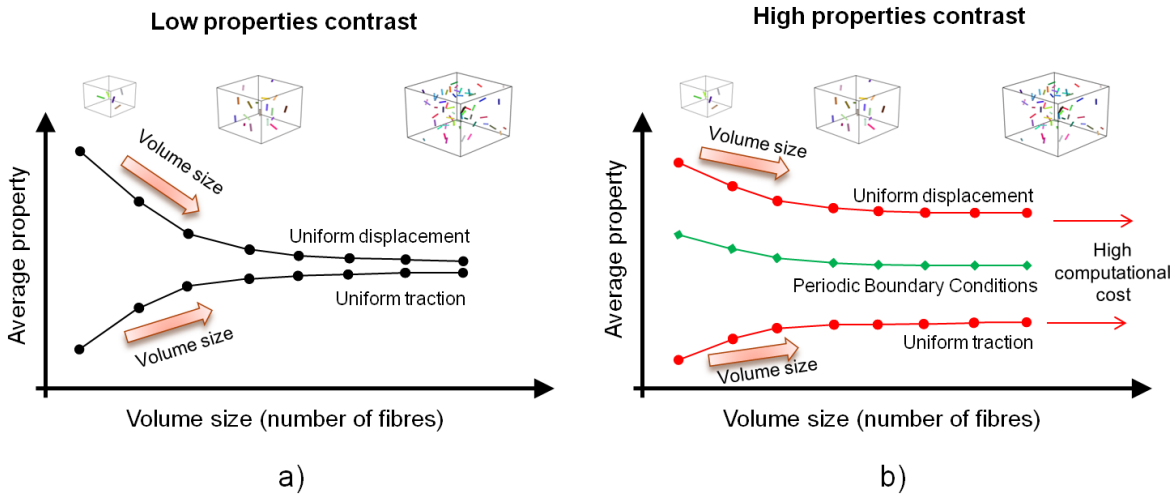

Figure 0.2 Representation of the convergence of the average properties with respect to the volume size under different boundary conditions for a) low properties contrast and b) high properties contrast.

are impossible to solve due to their computational burden, thus there is an interest to determine the minimal size RVE that delivers accurate predictions of the effective properties. Since the effective properties are initially unknown, it is not trivial to verify the validity of a RVE. The RVE is usually validated through the satisfaction of different physical and/or geometrical criteria proposed in literature (Kanit *et al.*, 2003; Stroeven *et al.*, 2004; Trias *et al.*, 2006; Gitman *et al.*, 2007; Pelissou *et al.*, 2009). However, only one criterion has been proven to rigorously determine effective properties with a given accuracy, by computing bounds on the effective properties of the bulk material. The bounds are obtained by applying uniform displacement and traction boundary conditions on a material volume of any size, as proven by Huet (1990). The larger the volume element, the tighter the bounds are, as shown in Figure 0.2a). The material volume size is usually increased until the bounds are close enough to guarantee a user-prescribed accuracy. Difficulties arise when dealing with high property contrasts between constituents, resulting in a large gap between both bounds and a very low convergence rates when increasing the volume size. Thus, very large material volumes are necessary to compute accurate properties, resulting in most cases in very high computational costs, as shown in Figure 0.2b). It has been shown (Kanit *et al.*, 2003) that by applying Periodic Boundary Conditions (PBC), one can compute accurate estimations at smaller material volumes than when using their uniform counterparts. Other sets of RVE criteria have been used in literature (compare Trias *et al.* (2006), Gitman *et al.* (2007)) using PBCs, but only to provide estimations of the effective properties of unknown accuracy. The ability of those

RVE quantitative definitions to deliver accurate effective proeprties has not been validated yet. Moreover, the RVE determination cost has led to its ignorance in many homogenization studies published in literature.

The principal objective of this thesis is to evaluate the performance, in terms of accuracy and computational cost, of various RVE quantitative definitions. As a second objective, and also as a rigourous case study, the thesis aims at evaluating the accuracy of analytical homogenization models for Randomly Oriented Fiber Reinforced Composites (ROFRC). Such materials have been studied by few authors (Böhm *et al.*, 2002; Kari *et al.*, 2007; Mortazavi *et al.*, 2013; Hua and Gu, 2013) but in all these studies, the RVE has never been clearly established, which questions the validity of the conclusions drawn.

The validation of the RVE determination methods would allow to valid modeling methods from the microscale to the macroscale. Results of validated RVEs can be used as benchmarks for ideal representations of the composite microstructure. ROFRCs can describe the microstructure of injection molded fiber reinforced composites, or even of nanocomposites reinforced by nanofibers. The latter is due to the complexity of nanoscale control and alignment of fibers.

The outcome of the thesis is a valid and efficient RVE definition for an accurate numerical modeling of composite materials. Effective properties issued from that RVE definition can be used as benchmarks for ideal representations of composite materials. ROFRCs studied in this thesis can be found in injection molded fiber composites and in nanocomposites reinforced by nanofibers. The latter is due to the complexity of orientation control at the nanoscale. By using accurate effective properties issued from numerical modeling of validated RVEs as benchmarks, the analytical models can be assessed. The outcome is the range of accuracy of the different analytical models, hence allowing an accurate and efficient homogenization of ROFRCs. Such validated analytical models are very useful for the industries (e.g., automotive) and can be further developed to implement imperfections in the composite microstructure.

This thesis is organized as follows:
Chapter 1 presents a literature review on the RVE concept and quantitative definitions as well as the analytical and numerical homogenization methods applicable to ROFRCs. In Chapter 2, the research objectives are introduced along with the publication strategy of the scientific articles. The two articles resulting from this work are included in Chapters 3 and 4. Chapter 3 presents a rigorous study on the validity of existing RVE quantitative definitions for ROFRCs and introduces a new definition. In Chapter 4, the predictions of the effective properties using different analytical methods are compared to that of numerical modeling using well established RVEs. Chapter 5 discusses the relationships between the articles, as

well as, complementary work performed during this project. The contributions from this thesis are finally summarized and topics for future studies are recommended.

CHAPTER 1

Literature review

1.1 Analytical homogenization

This section aims at presenting the basic equations necessary for the development of homogenization models for composites reinforced by randomly oriented inclusions. For a more thorough theoretical treatment of micromechanics and analytical homogenization models, one can refer to the works of (Mura, 1982; Nemat-Nasser and Hori, 1993; Suquet, 1997; Bornert *et al.*, 2001; Torquato, 2002; Milton, 2002), whereas a more application related and updated recollection of works in micromechanics can be found in the report by Böhm (2012).

All mathematical expressions given in this work apply to two-phase composites with matrix-inclusion microstructures, both matrix and reinforcements being assumed to be isotropically elastic. Reinforcements are taken to be ellipsoids of identical shapes, to be perfectly bonded to the matrix and to be randomly oriented and distributed.

Homogenization computes the composite's effective stiffness tensor $\mathbf{C}^*$ such that:

$$\mathbf{\Sigma} = \mathbf{C}^* : \mathbf{E}, \tag{1.1}$$

where $\mathbf{\Sigma}$ and $\mathbf{E}$ are the macroscopic stress and strain responses of the composite. Bridging between the micro- and macroscopic scales is performed by relating the microscopic fields to the macroscopic responses, such as:

$$<\boldsymbol{\varepsilon}(\mathbf{x})> = \mathbf{E}, \tag{1.2a}$$

$$<\boldsymbol{\sigma}(\mathbf{x})> = \mathbf{\Sigma}, \tag{1.2b}$$

where $\boldsymbol{\sigma}$ and $\boldsymbol{\varepsilon}$ are the local strain and stress fields, respectively, and $<.>$ denotes the volume averaging operation:

$$<\mathbf{f}(\mathbf{x})> = \frac{1}{V}\int_V \mathbf{f}(\mathbf{x})\mathrm{d}V, \tag{1.3}$$

where V is the volume of the composite that is being homogenized.

The microscopic fields can be calculated using the hereby defined localization tensors:

$$\boldsymbol{\varepsilon}(\mathbf{x}) = \mathbf{A}(\mathbf{x}) : <\boldsymbol{\varepsilon}>, \tag{1.4a}$$

$$\boldsymbol{\sigma}(\mathbf{x}) = \mathbf{B}(\mathbf{x}) : <\boldsymbol{\sigma}>. \tag{1.4b}$$

Consequently, one can obtain:

$$<\boldsymbol{\sigma}> = <\mathbf{C}(\mathbf{x}) : \mathbf{A}(\mathbf{x})> : <\boldsymbol{\varepsilon}>. \tag{1.5}$$

The knowledge of $\mathbf{A(x)}$ provides the solution for the homogenization problem. However, the exact expression of $\mathbf{A(x)}$ cannot be given analytically for general microstructures such as ROFRCs. Different assumptions and approximations are introduced in analytical homogenization models to obtain analytical expressions for $\mathbf{A(x)}$. The phase averaged strains and stresses can be related to the overall strains and stresses by the phase averaged strain and stress localization tensors (Hill, 1963):

$$<\boldsymbol{\varepsilon}>_{\mathrm{m}} = \mathbf{A}_{\mathrm{m}} : <\boldsymbol{\varepsilon}>, \tag{1.6a}$$

$$<\boldsymbol{\varepsilon}>_{\mathrm{f}} = \mathbf{A}_{\mathrm{f}} : <\boldsymbol{\varepsilon}>, \tag{1.6b}$$

where subscripts 'm' and 'f' denote the matrix and the fiber phases, respectively, $< \cdot >_{\mathrm{i}}$ is the volume average in phase 'i' and $\mathbf{A}_{\mathrm{i}}$ is the average localization within the phase. Similar relations can be obtained for the stress phase averages. The strain and stress concentration tensors can be shown to fulfill the relations (Hill, 1965):

$$c_{\mathrm{m}}\mathbf{A}_{\mathrm{m}} + c_{\mathrm{f}}\mathbf{A}_{\mathrm{f}} = \mathbf{I}, \tag{1.7}$$

where c_{m} and c_{f} are the matrix and the fibers volume fractions and $\mathbf{I}$ is the fourth order identity tensor.

Under uniform displacement and traction boundary conditions on the boundaries of V, one obtains for two-phase composites:

$$<\boldsymbol{\varepsilon}> = c_{\mathrm{m}}\langle\boldsymbol{\varepsilon}\rangle_{\mathrm{m}} + c_{\mathrm{f}}\langle\boldsymbol{\varepsilon}\rangle_{\mathrm{f}}, \tag{1.8a}$$

$$<\boldsymbol{\sigma}> = c_{\mathrm{m}}\langle\boldsymbol{\sigma}\rangle_{\mathrm{m}} + c_{\mathrm{f}}\langle\boldsymbol{\sigma}\rangle_{\mathrm{f}}. \tag{1.8b}$$

Use of Eq.1.6a to Eq.1.8b leads to:

$$\mathbf{C}^{*} = \mathbf{C}_{\mathrm{m}} + c_{\mathrm{f}}(\mathbf{C}_{\mathrm{f}} - \mathbf{C}_{\mathrm{m}}) : \mathbf{A}_{\mathrm{f}}, \tag{1.9a}$$

$$\mathbf{C}^{*-1} = {\mathbf{C}_{\mathrm{m}}}^{-1} + c_{\mathrm{f}}({\mathbf{C}_{\mathrm{f}}}^{-1} - {\mathbf{C}_{\mathrm{m}}}^{-1}) : \mathbf{B}_{\mathrm{f}}. \tag{1.9b}$$

For the special case of randomly oriented inclusions, Benveniste (1987) has obtained the

following expressions:

$$<\boldsymbol{\varepsilon}> = c_{\mathrm{m}}\langle\boldsymbol{\varepsilon}\rangle_{\mathrm{m}} + c_{\mathrm{f}}\{\langle\boldsymbol{\varepsilon}\rangle_{\mathrm{f}}\}, \tag{1.10a}$$

$$<\boldsymbol{\sigma}> = c_{\mathrm{m}}\langle\boldsymbol{\sigma}\rangle_{\mathrm{m}} + c_{\mathrm{f}}\{\langle\boldsymbol{\sigma}\rangle_{\mathrm{f}}\}, \tag{1.10b}$$

where $\{.\}$ denotes orientation averaging, such as:

$$\{\sigma_{ij}\} = \frac{\int_{-\pi}^{\pi}\int_{0}^{\pi}\int_{0}^{\pi/2} \omega_{ip}\omega_{jq}\sigma_{pq}\sin(\phi)\mathrm{d}\theta\mathrm{d}\phi\mathrm{d}\psi}{\int_{-\pi}^{\pi}\int_{0}^{\pi}\int_{0}^{\pi/2} \sin(\phi)\mathrm{d}\theta\mathrm{d}\phi\mathrm{d}\psi}, \tag{1.11a}$$

$$\{\mathrm{C}_{ijkl}\} = \frac{\int_{-\pi}^{\pi}\int_{0}^{\pi}\int_{0}^{\pi/2} \omega_{ip}\omega_{jq}\omega_{kr}\omega_{ls}\mathrm{C}_{pqrs}\sin(\phi)\mathrm{d}\theta\mathrm{d}\phi\mathrm{d}\psi}{\int_{-\pi}^{\pi}\int_{0}^{\pi}\int_{0}^{\pi/2} \sin(\phi)\mathrm{d}\theta\mathrm{d}\phi\mathrm{d}\psi}, \tag{1.11b}$$

where θ, ϕ and ψ are the Euler angles and $\boldsymbol{\omega}$ is the rotation tensor from (θ, ϕ, ψ) to (0,0,0), given explicitly in many references, see (Odegard *et al.*, 2003).

Consequently, the effective stiffness tensor for randomly oriented inclusions is given by:

$$\mathbf{C}^{*} = \mathbf{C}_{\mathrm{m}} + c_{\mathrm{f}}\{(\mathbf{C}_{\mathrm{f}} - \mathbf{C}_{\mathrm{m}}) : \mathbf{A}_{\mathrm{f}}\}. \tag{1.12}$$

Eq. 1.12 provides direct estimations of the effective stiffness tensor of composites reinforced by randomly oriented inclusions based on the knowledge of $\mathbf{A}_{\mathrm{f}}$. Such methods that provide straightforward effective properties of composites are hereby referred to as one-step methods. Expressions for $\mathbf{A}_{\mathrm{f}}$ are given in Section 1.1.1. It is also possible to homogenize composites reinforced by randomly oriented inclusions by first using Eq.1.9b for aligned inclusions followed by a second step of homogenization in which an orientation averaging procedure is performed. Two-step methods are presented in Section 1.1.2.

1.1.1 One-step methods

Dilute solution

Most mean field homogenization methods are based on the work of Eshelby (1957). His study dealt with the strain field of a homogeneous ellipsoidal inclusion (i.e., inclusion consisting of the same material as the matrix) subjected to a uniform stress-free strain and surrounded by an infinite matrix. He has shown that the resulting strain field in the con-

strained inclusion is uniform and given by:

$$\boldsymbol{\varepsilon}_{\mathrm{i}} = \mathbf{S} : \boldsymbol{\varepsilon}_{\mathrm{t}}, \tag{1.13}$$

where $\mathbf{S}$ is Eshelby's tensor, $\boldsymbol{\varepsilon}_{\mathrm{t}}$ is a uniform stress-free strain and $\boldsymbol{\varepsilon}_{\mathrm{i}}$ is the uniform strain in the constrained inclusion. Expressions for Eshelby's tensor $\mathbf{S}$ are found in Mura (1982) for several inclusions shapes, and material symmetries. For complex shapes and material symmetries, Eshelby's tensor can be numerically calculated following the methodology of Gavazzi and Lagoudas (1990).

For composites of very low volume fractions, it can be assumed that the inclusions do not have any interaction between each other. Such cases can be handled on the basis of Eshelby's theory for homogeneous inclusions, as per Eq.1.13, by replacing the heterogeneity by an equivalent homogeneous inclusions subjected to a stress-free strain (Withers *et al.*, 1989). As a result, for the Dilute (Dil) solution, $\mathbf{A}_{\mathrm{f}}$ can be given by:

$$\mathbf{A}_{\mathrm{f}}^{\mathrm{Dil}} = [\mathbf{I} + \mathbf{S} : \mathbf{C}_{\mathrm{m}}^{-1} : (\mathbf{C}_{\mathrm{f}} - \mathbf{C}_{\mathrm{m}})]^{-1}. \tag{1.14}$$

Based on Eq.1.12 and 1.14, the effective properties of dilute ROFRCs are given by:

$$\mathbf{C}^{\mathrm{Dil}} = \mathbf{C}_{\mathrm{m}} + c_{\mathrm{f}}\{(\mathbf{C}_{\mathrm{f}} - \mathbf{C}_{\mathrm{m}}) : [\mathbf{I} + \mathbf{S} : \mathbf{C}_{\mathrm{m}}^{-1} : (\mathbf{C}_{\mathrm{f}} - \mathbf{C}_{\mathrm{m}})]^{-1}\}. \tag{1.15}$$

Mori-Tanaka model

In the model of Mori and Tanaka (1973) (M-T), the inclusion fields phase averages are expressed as a function of the matrix average fields as:

$$<\boldsymbol{\varepsilon}>_{\mathrm{f}} = \mathbf{A}_{\mathrm{f}}^{\mathrm{Dil}} : <\boldsymbol{\varepsilon}>_{\mathrm{m}}, \tag{1.16a}$$

$$<\boldsymbol{\sigma}>_{\mathrm{f}} = \mathbf{B}_{\mathrm{f}}^{\mathrm{Dil}} : <\boldsymbol{\sigma}>_{\mathrm{m}}. \tag{1.16b}$$

The following localization tensor is obtained (Benveniste, 1987):

$$\mathbf{A}_{\mathrm{f}}^{\mathrm{M\text{-}T}} = \mathbf{A}_{\mathrm{f}}^{\mathrm{Dil}} : [(1 - c_{\mathrm{f}})\mathbf{I} + c_{\mathrm{f}}\{\mathbf{A}^{\mathrm{Dil}}\}]^{-1}. \tag{1.17}$$

Consequently, the effective stiffness tensor is expressed by:

$$\mathbf{C}^{\mathrm{M\text{-}T}} = \mathbf{C}_{\mathrm{m}} + c_{\mathrm{f}}\{(\mathbf{C}_{\mathrm{f}} - \mathbf{C}_{\mathrm{m}}) : \mathbf{A}_{\mathrm{f}}^{\mathrm{Dil}}\} : [c_{\mathrm{m}}\mathbf{I} + c_{\mathrm{f}}\{\mathbf{A}_{\mathrm{f}}^{\mathrm{Dil}}\}]^{-1}. \tag{1.18}$$

It should be noted that Eq.1.18 delivers non-symmetric effective elasticity tensors for many microstructures (e.g., fibers with different aspect ratios) (Ferrari, 1991; Benveniste *et al.*, 1991; Schjodt-Thomsen and Pyrz, 2001). Non-symmetric elasticity tensors are physically invalid. However, for the case presented in this study (i.e., isotropic constituents and inclusions that have the same aspect ratio), Eq. 1.18 yields symmetric effective elasticity tensors.

Self-consistent scheme

In the Self-Consistent (SC) scheme, the inclusion is immersed in the effective material. The corresponding localization tensor is given by:

$$\mathbf{A}_{\mathrm{f}}^{\mathrm{SC}} = [\mathbf{I} + \mathbf{S}^{\mathrm{SC}} : (\mathbf{C}^{\mathrm{SC}})^{-1} : (\mathbf{C}_{\mathrm{f}} - \mathbf{C}^{\mathrm{SC}})]^{-1}, \tag{1.19}$$

and $\mathbf{S}^{\mathrm{SC}}$ is Eshelby's tensor where the effective composite is the infinite media. Consequently, the effective stiffness tensor is expressed by:

$$\mathbf{C}^{\mathrm{SC}} = \mathbf{C}_{\mathrm{m}} + c_{\mathrm{f}}\{(\mathbf{C}_{\mathrm{f}} - \mathbf{C}_{\mathrm{m}}) : [\mathbf{I} + \mathbf{S}^{\mathrm{SC}} : (\mathbf{C}^{\mathrm{SC}})^{-1} : (\mathbf{C}_{\mathrm{f}} - \mathbf{C}^{\mathrm{SC}})]^{-1}\}. \tag{1.20}$$

Eq.1.20 is implicit and must be solved iteratively.

Ponte-Castañeda and Willis model

Employing the variational formulation of Hashin and Shtrikman (1962a,b), Ponte-Castañeda and Willis (1995) (PCW) developed a model to estimate the effective elastic moduli of two-phase composites. The inclusions spatial arrangement is enforced using different shapes of safety cells englobing the inclusions. For the case of randomly oriented inclusions, safety cells are spherical, as presented in Figure 1.1. For a two-phase composite consisting of an isotropic matrix and randomly oriented isotropic ellipsoidal inclusions, the effective stiffness tensor is given by:

$$\mathbf{C}^{\mathrm{PCW}} = \mathbf{C}_{\mathrm{m}} + c_{\mathrm{f}}[\mathbf{I} - c_{\mathrm{f}}\{(\mathbf{C}_{\mathrm{f}} - \mathbf{C}_{\mathrm{m}}) : \mathbf{A}_{\mathrm{f}}^{\mathrm{Dil}}\} : \mathbf{S}_{\mathrm{d}} : \mathbf{C}_{\mathrm{m}}^{-1}]^{-1} : \{(\mathbf{C}_{\mathrm{f}} - \mathbf{C}_{\mathrm{m}}) : \mathbf{A}_{\mathrm{f}}^{\mathrm{Dil}}\}, \tag{1.21}$$

where $\mathbf{S}_{\mathrm{d}}$ is Eshelby's tensor that depends on the safety ellipsoid aspect ratio. The effective properties, as per Eq.1.21, are physically valid provided that the safety cells embedding the inclusions do not interpenetrate. The range of physically valid volume fractions is limited to

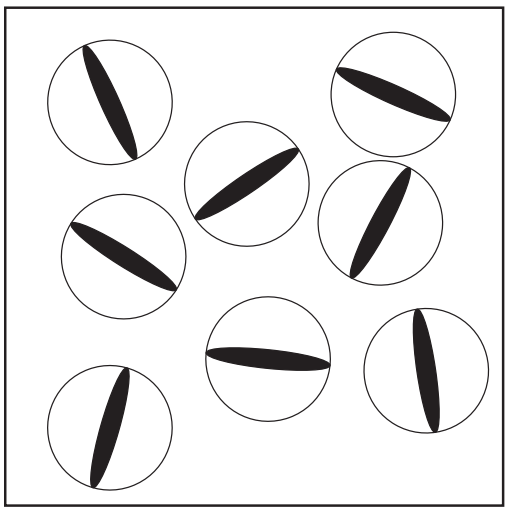

Figure 1.1 Model of PCW: randomly oriented ellipsoidal particles embedded in spherical safety cells.

$1/\rho^2$ where ρ is the aspect ratio of the fibers given by:

$$\rho = l_\mathrm{f}/d_\mathrm{f}, \tag{1.22}$$

where l_f and d_f are the fiber length and diameter, respectively. For example, the volume fraction limits are found to be only of 1% and 0.01% for fibers with an aspect ratio of 10 and 100, respectively.

Hu and Weng (2000b) compared the model of PCW to the bounds of Hashin and Shtrikman. They observed that the PCW estimations violate the rigorous bounds of Hashin and Shtrikman for volume fractions higher than the physical limit of $1/\rho^2$. It is important to notice also that the Double-Inclusion model (Hori and Nemat-Nasser, 1993) is equivalent to that of PCW for the case of randomly oriented inclusions, as demonstrated in (Hu and Weng, 2000a).

1.1.2 Two-step methods

A general two-step homogenization procedure was originally proposed by Camacho *et al.* (1990) and studied into more details by Pierard *et al.* (2004). In such methods, the RVE is first decomposed into N discrete subregions where the fibers are aligned along a unique arbitrary direction and the volume fraction in each subregion is equivalent to that of the original composite, as seen in Figure 1.2. The first step computes the properties of a subregion α ($\alpha = 1, 2, \ldots N$) using a two phase homogenization model for aligned-fiber reinforced com-

posites. Various micromechanical models for such composites are presented in the following; more models can be found in the review of Tucker III and Liang (1999). Homogenization over all subregions is performed in a second step using a second homogenization model.

First step: Subregion with Aligned fibers

Analytical homogenization models for aligned inclusions have been extensively studied in the literature (see Tucker III and Liang (1999)). Therefore, only the expressions of the effective stiffness tensors are presented in the following.
For dilute composites, the effective stiffness tensor is given by:

$$\mathbf{C}_\alpha^{\mathrm{Dil}} = \mathbf{C}_\mathrm{m} + c_\mathrm{f}(\mathbf{C}_\mathrm{f} - \mathbf{C}_\mathrm{m}) : [\mathbf{I} + \mathbf{S} : \mathbf{C}_\mathrm{m}^{-1} : (\mathbf{C}_\mathrm{f} - \mathbf{C}_\mathrm{m})]^{-1}. \tag{1.23}$$

According to the Mori-Tanaka model, the effective stiffness tensor is expressed by:

$$\mathbf{C}_\alpha^{\text{M-T}} = \mathbf{C}_\mathrm{m} + c_\mathrm{f}(\mathbf{C}_\mathrm{f} - \mathbf{C}_\mathrm{m}) : \mathbf{A}^{\mathrm{Dil}} : \left[c_\mathrm{m}\mathbf{I} + c_\mathrm{f}\mathbf{A}^{\mathrm{Dil}}\right]^{-1}. \tag{1.24}$$

In the self-consistent (SC) scheme (Hill, 1965; Budiansky, 1965), the effective stiffness tensor is given by:

$$\mathbf{C}_\alpha^{\mathrm{SC}} = \mathbf{C}_\mathrm{m} + c_\mathrm{f}(\mathbf{C}_\mathrm{f} - \mathbf{C}_\mathrm{m}) : [\mathbf{I} + \mathbf{S}_\alpha : (\mathbf{C}_\alpha^{\mathrm{SC}})^{-1} : (\mathbf{C}_\mathrm{f} - \mathbf{C}_\alpha^{\mathrm{SC}})], \tag{1.25}$$

where $\mathbf{S}_\alpha$ is Eshelby's tensor where the infinite media is the effecitve composite included in region α.

The model of Lielens *et al.* (1998) (Li) interpolates between the upper and lower Hashin-Shtrikman bounds for aligned reinforcements. The effective stiffness tensor $\mathbf{C}^{\mathrm{Li}}$ is given by:

$$\mathbf{C}_\alpha^{\mathrm{Li}} = \mathbf{C}_\mathrm{m} + c_\mathrm{f}(\mathbf{C}_\mathrm{f} - \mathbf{C}_\mathrm{m}) : \hat{\mathbf{A}}^{\mathrm{Li}} : [(1 - c_\mathrm{f})\mathbf{I} + c_\mathrm{f}\hat{\mathbf{A}}^{\mathrm{Li}}]^{-1}, \tag{1.26}$$

where

$$\hat{\mathbf{A}}^{\mathrm{Li}} = \{(1 - c^*)[\hat{\mathbf{A}}^{\mathrm{lower}}]^{-1} + c^*[\hat{\mathbf{A}}^{\mathrm{upper}}]^{-1}\}^{-1}. \tag{1.27}$$

c^* is related to the volume fraction of the particle as:

$$c^* = \frac{c_\mathrm{f} + c_\mathrm{f}^2}{2}, \tag{1.28}$$

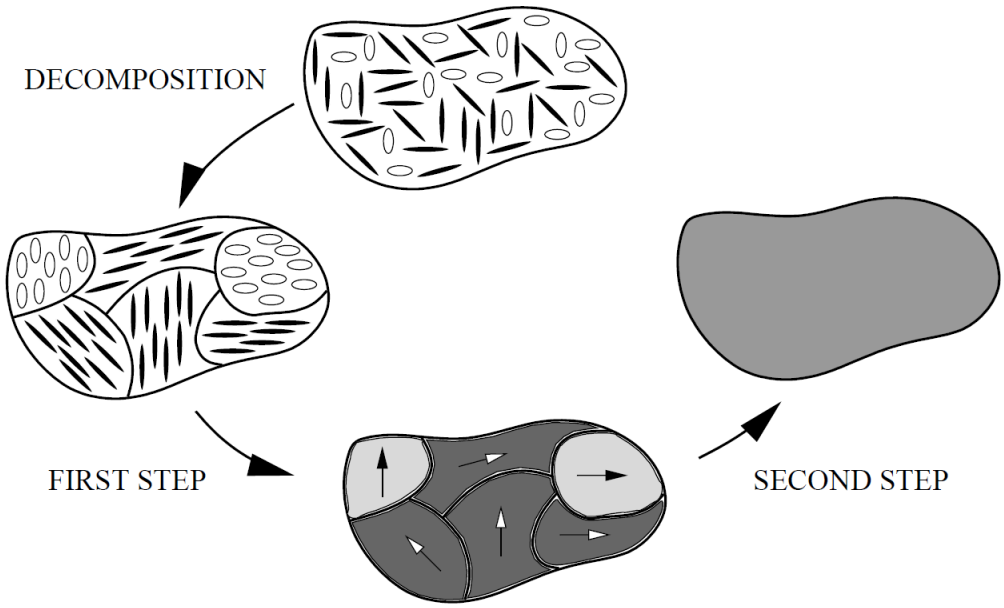

Figure 1.2 The 2-step homogenization procedure. The composite is decomposed into subregions. STEP 1: homogenization of each subregion. STEP 2: homogenization of the set of homogenized subregions (Pierard, 2006).

and $\hat{\mathbf{A}}^{\text{lower}}$ and $\hat{\mathbf{A}}^{\text{upper}}$ are expressed as:

$$\hat{\mathbf{A}}^{\text{lower}} = [\mathbf{I} + \mathbf{S}_m : (\mathbf{C}_\text{m})^{-1} : (\mathbf{C}_\text{f} - \mathbf{C}_\text{m})]^{-1}, \tag{1.29a}$$

$$\hat{\mathbf{A}}^{\text{upper}} = [\mathbf{I} + \mathbf{S}_\text{f} : (\mathbf{C}_\text{f})^{-1} : (\mathbf{C}_\text{m} - \mathbf{C}_\text{f})]^{-1}, \tag{1.29b}$$

where $\mathbf{S}_\text{f}$ is Eshelby's tensor where the infinite media has the properties of the fibers.

It has been shown by Tucker III and Liang (1999), for aligned-fiber composites, that the SC scheme overestimates the axial modulus at high volume fractions, whereas the M-T model yields the most accurate predictions for large aspect ratio fibers. They also pointed out that Lielens model may improve on the Mori-Tanaka model for higher fiber volume fractions or rigidity contrasts (Tucker III and Liang, 1999).

Second step: homogenization over all subregions

The different subregions form a multi-phase composite that can be homogenized by one of several homogenization models. For example, the overall stiffness tensor according to Voigt

model is written as:

$$\mathbf{C}^{\text{Voigt}} = \langle \mathbf{C}_\alpha \rangle = \frac{\sum_{\alpha=1}^{n} \mathbf{C}_\alpha V_\alpha}{V}, \tag{1.30}$$

where V and V_α are the volume of composite and the volume of each subregion, respectively. The effective stiffness tensor according to Reuss model is calculated as:

$$\mathbf{C}^{\text{Reuss}} = \langle \mathbf{C}_\alpha{}^{-1} \rangle^{-1} = \left(\frac{\sum_{\alpha=1}^{N} \mathbf{C}_\alpha^{-1} V_\alpha}{V} \right)^{-1}. \tag{1.31}$$

When fibers are uniformly dispersed into all possible orientations, it can be demonstrated that the volume averaging operations $<\mathbf{C}>$ and $<\mathbf{C}^{-1}>$ in Eq. (4.14) and (4.15) are equivalent to orientational averages $\{\mathbf{C}\}$ and $\{\mathbf{C}^{-1}\}$, respectively. For more particular orientation distributions (e.g., partial alignment), orientation distribution functions can be implemented in two-step homogenization approaches (Schjodt-Thomsen and Pyrz, 2001).

1.1.3 Bounds of Hashin and Shtrikman

Bounds on the macroscopic effective properties of heterogeneous materials can be obtained from a variational formulation given by Hashin and Shtrikman (1961). The Hashin and Shtrikman (1963) bounds (HS) for bulk k and shear G moduli are expressed by:

$$k^{HS} = k_{\text{m}} + c_{\text{f}} \frac{k_{\text{f}} - k_{\text{m}}}{1 + c_{\text{m}} \left(\frac{k_{\text{f}} - k_{\text{m}}}{k^* + k_{\text{f}}} \right)}, \tag{1.32a}$$

$$G^{HS} = G_{\text{m}} + c_{\text{f}} \frac{G_{\text{f}} - G_{\text{m}}}{1 + c_{\text{m}} \left(\frac{G_{\text{f}} - G_{\text{m}}}{G^* + G_{\text{f}}} \right)}, \tag{1.32b}$$

where $*$ denotes the reference material which is the fiber and the matrix for the upper and lower bounds, respectively. These bounds apply to heterogeneous materials with isotropic phases that show overall isotropic behavior. For small contrasts, the upper and lower bounds are close and produce good estimations of the effective properties. Conversely, for high contrasts and volume fractions the bounds are very distant and provide little information on the effective properties.

1.2 Numerical homogenization

In contrast to analytical methods where the local fields are approximated, numerical methods compute accurate local fields in a finite volume representation of the microstructure. Therefore, numerical homogenization is considered as an accurate homogenization method, given that the simulated volume is a RVE. However, in numerical modeling, one is often constrained to work with volumes that are smaller than the RVE. Following the terminology of Huet (1990), the properties of such volumes are referred to as "apparent properties", whereas that of the RVE are referred to as "effective properties". The apparent elastic tensor of an arbitrary volume of the composite material is such that:

$$<\boldsymbol{\sigma}> = \tilde{\mathbf{C}} : <\boldsymbol{\varepsilon}>, \tag{1.33}$$

Alternatively, the apparent elastic tensor can also be defined based on the strain energy:

$$<\boldsymbol{\sigma} : \boldsymbol{\varepsilon}> = <\boldsymbol{\varepsilon}> : \tilde{\mathbf{C}} : <\boldsymbol{\varepsilon}>. \tag{1.34}$$

The application of the so-called *Hill lemma* (Hill, 1963; Hazanov and Huet, 1994) shows that both definitions are in fact equivalent for an arbitrary volume for three different sets of boundary conditions: uniform displacement (also called kinematic or Dirichlet), uniform traction (also called static or Neumann) and mixed boundary conditions. When the volume under study is large enough (mathematically infinite), the apparent properties of random materials become equivalent to the effective properties under any set of boundary conditions, as proved by Sab (1992).

The computation of the *apparent properties* of a single given volume is described in Section 1.2.1. The RVE concept, quantitative definitions and determination methods are reviewed in Section 1.2.2.

1.2.1 Numerical homogenization of an arbitrary material volume

In a numerical homogenization approach, a three dimensional (3D) representation of the microstructure is necessary. In the following, different methodologies of 3D microstructure generation are first described. Second, different numerical methods are presented for the computation of local stress and strain fields. Different sets of boundary conditions are then presented to simulate different loadings on the microstructure. Finally, the apparent properties of the microstructure are calculated.

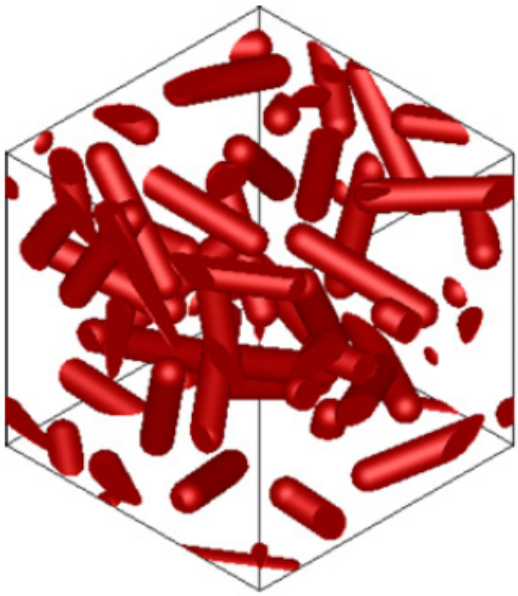

Figure 1.3 Volume generated using random sequential adsorption algorithm, including 30 randomly oriented fibers of aspect ratio 5 with 10% volume fraction (Hua and Gu, 2013).

Random microstructure generation methods

3D microstructure can be either obtained by imagery of a real microstructure sample or by a computer generated realization of the microstructure using random generation algorithms. Experimental image reconstruction techniques (Huang and Li, 2013) require expensive specialized equipments and involves destructive imaging of experimental samples. This work focuses solely on random generation methods, namely: random sequential adsorption (RSA) (Feder, 1980; Talbot *et al.*, 1991), Monte-Carlo simulations (Gusev, 1997), molecular dynamics simulations (Lubachevsky, 1990) and random walk methods (Altendorf and Jeulin, 2011a).

The random sequential adsorption (RSA) algorithm has been the most commonly used method for random microstructures generation due to its simplicity. Figure 1.3 presents a ROFRC microstructure, generated using RSA method, including 30 fibers of aspect ratio 5 at 10% volume fraction. The method consists of adding one fiber at a time into a volume while checking interferences with all other fibers. If a newly added fiber interferes with other fibers, it is removed and then repositioned randomly in the same volume. This operation is repeated until the fiber location is accepted. Methodically, non-overlapping fibers are randomly added one after another until the target volume fraction is reached. Achievable microstructures using RSA algorithm are limited to low volume fractions, also known as

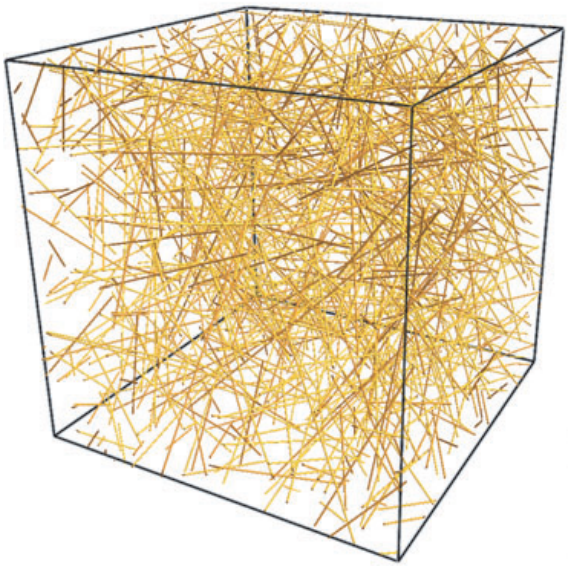

Figure 1.4 Volume generated using Monte-Carlo algorithm, including 350 randomly oriented fibers of aspect ratio 200 at 0.5% volume fraction (Lusti and Gusev, 2004).

jamming limit (Feder, 1980), due to fiber interpenetration.

In Monte-Carlo simulations, all the particles are placed at initial positions in a large volume (dilute volume fraction). At each step, the volume size is reduced and particles intersections are checked. If intersection occurs after shrinkage, the inclusions positions are randomly altered until an interference-free microstructure is obtained. Repeatedly, volume shrinkage followed by inclusions random movements are simulated. The simulation ends when the target volume fraction is attained without any overlapping. Monte-Carlo methods have also shown relatively low volume fraction jamming limits. Lusti and Gusev (2004) generated microstructures with randomly oriented fibers of aspect ratio of 100 and 200 and low volume fractions up to 1%, as presented in Figure 1.4.

Lubachevsky (1990) proposed a method based on molecular dynamics to generate random spheres or disks packings. In their algorithm, all particles are initially positioned with a null volume and each particle is assigned a randomly oriented velocity. The particles volume increases throughout the simulation and particles can collide with each other or with the cube face. This method has been able to generate very high volume fractions (74%) of spherical particles in a matrix (Ghossein and Lévesque, 2012). The method has been extended to ellipsoidal inclusions, but has been applied only for low aspect ratios of less than 5 (Donev *et al.*, 2004; Man *et al.*, 2005).

Most recent generation methods have achieved greater results by using a random-walk

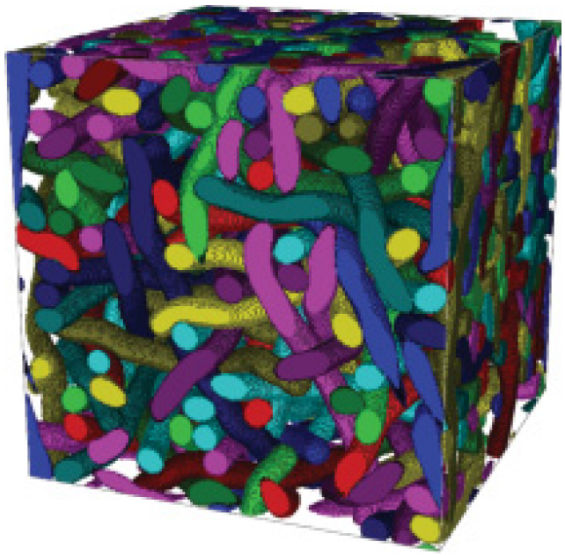

Figure 1.5 Microstructure volume generated using a random walk process, including 90 randomly oriented fibers of aspect ratio 33 with 50.35% volume fraction (Altendorf and Jeulin, 2011a).

based method as proposed by Altendorf and Jeulin (2011a). They used a random-walk process to position balls in several chains that will initially form a set of overlapping bent fibers. The balls forming the fibers are then subjected to a set of repulsive forces to separate overlapping balls and recover forces only within each balls-chain to preserve the fiber structure. Volume fractions up to 65% were achieved for randomly oriented bent fibers having an aspect ratio of 10, and up to 50% for aspect ratios of 33 as presented in Figure 1.5 (Altendorf and Jeulin, 2011a). However, such performances (e.g., high volume fractions) is limited to cases where fiber bending is permitted (Altendorf and Jeulin, 2011b).

Numerical resolution methods

Several numerical methods, such as the FE method and the FFT (Moulinec and Suquet, 1994, 1998), can be used to compute the local stress and strain fields of a given 3D microstructure. A listing of some other numerical methods can be found in Böhm (2012) and Pierard (2006). Most numerical methods require the discretization of the microstructure geometry. The discretized elements must be smaller than the intrinsic microstructure length scales in order to compute accurate local fields. Very fine discretization is necessary when a large contrast of length scales exists within the microstructure, as for the case of microstructures with very long fibers. The solution of such microstructures necessitates very large computa-

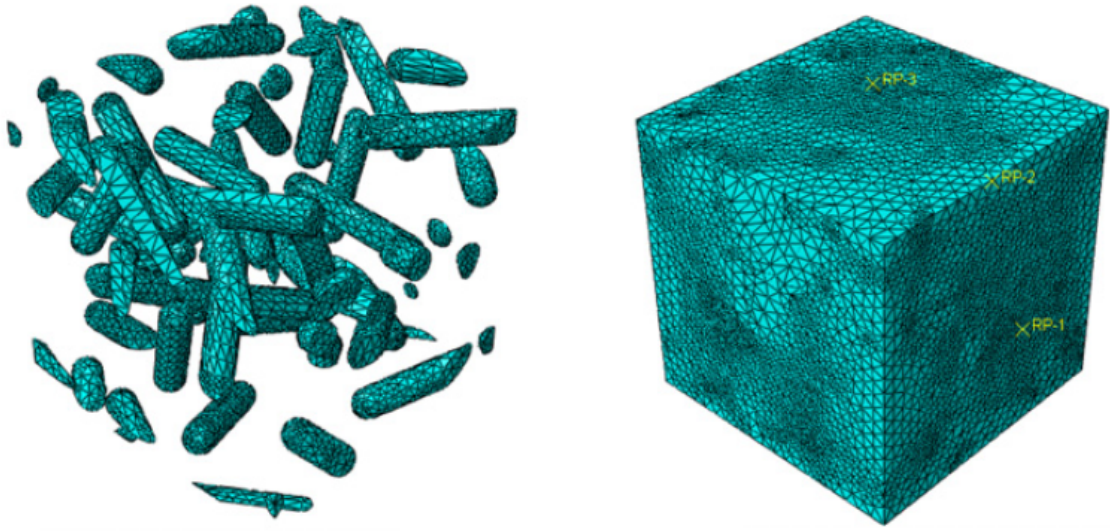

(a) (b)

Figure 1.6 a) Fiber and b) Volume meshing of a ROFRC including 30 randomly oriented fibers of aspect ratio 5 with 10% volume fraction (Hua and Gu, 2013).

tional memory to store all the numerical system, and very long processing times to perform computations over the numerical system.

The FFT solution scheme requires uniform discretization of a 3D microstructure image into equal size cubic volume elements called *voxels*. The number of voxels required to adequately represent the geometry of high aspect ratio fibers becomes very important and would lead to very large computational memory.

In contrast, the FE method allows for a non-uniform discretization of microstructure permitting different levels of mesh refinements in different parts of the microstructure. Moreover, different shapes of elements (e.g., tetrahedrons) can be used, enabling the representation of fiber circular cross-sections using very small number of elements when compared to FFT method. Figures 1.6a) and b) present the meshed particles and volume, respectively, of a ROFRC microstructure including 30 fibers of an aspect ratio of 5 at 5% volume fraction. However, by opposition to FFT based methods, FE methods require user input, which renders its automation quite challenging (Ghossein and Lévesque, 2012).

Boundary conditions

Homogenization can be performed under any set of boundary conditions. Different boundary conditions on the same material volume, that is smaller than the RVE, yield different apparent properties. By carefully choosing particular sets of boundary conditions, one can compute more accurate estimations, or even obtain rigorous bounds of the effective properties for a given volume size.

Uniform displacement boundary conditions overestimate the effective properties (Huet, 1990) and are given by:

$$\mathbf{u}(\mathbf{x}) = \mathbf{E} \cdot \mathbf{x} \quad \forall\, \mathbf{x} \in V^S \tag{1.35}$$

where $\mathbf{u}$ is the displacement vector and V^S is the surface of the volume element.

Uniform traction boundary conditions underestimate the effective properties and are such that:

$$\boldsymbol{\sigma}(\mathbf{x}) \cdot \mathbf{n} = \boldsymbol{\Sigma} \cdot \mathbf{n} \quad \forall\, \mathbf{x} \in V^S \tag{1.36}$$

where $\mathbf{n}$ is the normal vector at position $\mathbf{x}$ on V^S.

For high contrast of phases properties, the properties computed using both boundary conditions are very far apart and do not yield accurate estimations of the effective properties. On the other hand, PBCs were shown (Kanit *et al.*, 2003) to deliver more accurate estimations of the effective properties. PBCs are applied by assuming that local fields are periodic:

$$\mathbf{u}(\mathbf{x}) = \mathbf{E} \cdot \mathbf{x} + \mathbf{u}^*(\mathbf{x}) \tag{1.37}$$

where $\mathbf{u}^*$ is the periodic displacement fluctuation. It takes the same values at positions $\mathbf{x}$ and $\mathbf{x} + \mathbf{L}$, where $\mathbf{L}$ is a translation vector such that each of its components can be either 0 or L (L=edge length of V). The macroscopic strain tensor $\mathbf{E}$ can be chosen arbitrarily and is discussed in Section 1.2.1.

Periodic fields are an integral part of the FFT formulation. However, implementation of PBCs within the FE method is a more complex process. Practically, a periodic microstructure and a periodic meshing are required in order to enforce PBCs. A periodic microstructure is such that an inclusion that intersects a surface of V continues from the opposite surface (see Figure 1.3), whereas periodic meshing implies that the meshing on opposite surfaces of the cubic volume is identical. Then, PBCs can be enforced by coupling the displacements of mirror nodes on opposing surfaces:

$$\mathbf{u}(\mathbf{x_2}) - \mathbf{u}(\mathbf{x_1}) = \mathbf{E} \cdot \mathbf{x}, \tag{1.38}$$

where $\mathbf{x}_1$ and $\mathbf{x}_2$ are the coordinates of two mirror nodes located on opposite surfaces.

The PBCs requirements of microstructure periodicity and matching nodes were stated in several works as very complex processes, especially for the case of ROFRCs (Mortazavi *et al.*, 2013; Böhm *et al.*, 2002). Nguyen *et al.* (2012) have suggested overcoming these difficulties by adapting the PBCs to non-matching meshes. They have presented a new FE formulation to impose PBCs on arbitrary meshes using polynomial interpolation. However, selecting the appropriate polynomial parameters (e.g., order of Lagrange interpolation, number of segments in a spline interpolation) is not trivial to reach a given accuracy.

Computing apparent properties

Using the major and minor symmetry properties of elasticity tensors, the macroscopic constitutive behavior for a finite volume can be written in a matrix notation as:

$$\begin{bmatrix} \Sigma_{11} \\ \Sigma_{22} \\ \Sigma_{33} \\ \Sigma_{23} \\ \Sigma_{13} \\ \Sigma_{12} \end{bmatrix} = \begin{bmatrix} \tilde{\mathrm{C}}_{1111} & \tilde{\mathrm{C}}_{1122} & \tilde{\mathrm{C}}_{1133} & \sqrt{2}\tilde{\mathrm{C}}_{1123} & \sqrt{2}\tilde{\mathrm{C}}_{1131} & \sqrt{2}\tilde{\mathrm{C}}_{1112} \\ \tilde{\mathrm{C}}_{2211} & \tilde{\mathrm{C}}_{2222} & \tilde{\mathrm{C}}_{2233} & \sqrt{2}\tilde{\mathrm{C}}_{2223} & \sqrt{2}\tilde{\mathrm{C}}_{2231} & \sqrt{2}\tilde{\mathrm{C}}_{2212} \\ \tilde{\mathrm{C}}_{3311} & \tilde{\mathrm{C}}_{3322} & \tilde{\mathrm{C}}_{3333} & \sqrt{2}\tilde{\mathrm{C}}_{3323} & \sqrt{2}\tilde{\mathrm{C}}_{3331} & \sqrt{2}\tilde{\mathrm{C}}_{3312} \\ \sqrt{2}\tilde{\mathrm{C}}_{2311} & \sqrt{2}\tilde{\mathrm{C}}_{2322} & \sqrt{2}\tilde{\mathrm{C}}_{2333} & 2\tilde{\mathrm{C}}_{2323} & 2\tilde{\mathrm{C}}_{2331} & 2\tilde{\mathrm{C}}_{2312} \\ \sqrt{2}\tilde{\mathrm{C}}_{3111} & \sqrt{2}\tilde{\mathrm{C}}_{3122} & \sqrt{2}\tilde{\mathrm{C}}_{3133} & 2\tilde{\mathrm{C}}_{3123} & 2\tilde{\mathrm{C}}_{3131} & 2\tilde{\mathrm{C}}_{3112} \\ \sqrt{2}\tilde{\mathrm{C}}_{1211} & \sqrt{2}\tilde{\mathrm{C}}_{1222} & \sqrt{2}\tilde{\mathrm{C}}_{1233} & 2\tilde{\mathrm{C}}_{1223} & 2\tilde{\mathrm{C}}_{1231} & 2\tilde{\mathrm{C}}_{1212} \end{bmatrix} \begin{bmatrix} \mathrm{E}_{11} \\ \mathrm{E}_{22} \\ \mathrm{E}_{33} \\ \mathrm{E}_{23} \\ \mathrm{E}_{13} \\ \mathrm{E}_{12} \end{bmatrix}. \tag{1.39}$$

All terms of the apparent elastic tensor can be calculated by independently applying six orthogonal macroscopic deformation states $\mathbf{E}$ on V (e.g., three pure longitudinal and three pure shear deformations). Thus, six different simulations are required for each realization of the microstructure. For ROFRCs, the effective media is orientation independent, hence exhibits an isotropic behavior (Benveniste, 1987). Therefore, the bulk k and shear G moduli are sufficient to represent the effective elastic behavior of the material. The apparent bulk and shear moduli can be calculated using the isotropy projectors, resulting in the following relations:

$$\tilde{k} = \tilde{\mathrm{C}}_{iijj}/9, \tag{1.40a}$$

$$\tilde{G} = \frac{3\tilde{\mathrm{C}}_{ijij} - \tilde{\mathrm{C}}_{iijj}}{30}. \tag{1.40b}$$

It is important to note that if a small volume of the microstructure is simulated, the apparent elastic tensor is generally not isotropic. However, Kanit *et al.* (2003) demonstrated that by averaging the apparent elasticity tensors of several realizations of the microstructure, isotropy can be retrieved.

One can also choose fewer deformation states to straightforwardly compute the desired properties. To determine the apparent bulk and shear moduli of isotropic effective materials, only two cases of deformation were used by Kanit *et al.* (2003):

$$\mathbf{E}_k \equiv \begin{bmatrix} 1/3 \\ 1/3 \\ 1/3 \\ 0 \\ 0 \\ 0 \end{bmatrix}, \mathbf{E}_G \equiv \begin{bmatrix} 0 \\ 0 \\ 0 \\ 0 \\ 0 \\ 1/2 \end{bmatrix}, \tag{1.41}$$

expressed in a matrix notation. The corresponding apparent bulk and shear moduli are given by:

$$\tilde{k} = <\boldsymbol{\sigma}> : \mathbf{E}_k, \tag{1.42a}$$

$$\tilde{G} = <\boldsymbol{\sigma}> : \mathbf{E}_G. \tag{1.42b}$$

1.2.2 RVE determination

Defintion The scientific literature presents a diversity of RVE definitions, the most important being listed below:

- Hill (1963): The RVE refers to "a sample that a) is structurally entirely typical of the whole mixture on average, and b) contains a sufficient number of inclusions for the apparent overall moduli to be effectively independent of the surface values of traction and displacement, so long as these values are macroscopically uniform." While a) is a condition to the microstructure morphology, b) expresses the RVE independency of the applied boundary conditions. The latter condition has been proved Sab (1992).
- Drugan and Willis (1996): The RVE is "the smallest material volume element of the composite for which the usual spatially constant "overall modulus" macroscopic constitutive representation is a sufficiently accurate model to represent a mean constitutive response."
- Gusev (1997): The RVE is a material volume that computes the same effective properties as the bulk material.
- Ostoja-Starzewski (2006):The RVE is defined by three conditions: "(i) statistical homogeneity (stationarity) and ergodicity; (ii) Hill condition leading to admissible boundary conditions; (iii) variational principle."

Those definitions generally deal with either the morphology of the microstructure or its physical behavior, or both, as in Hill's definition. Depending on the RVE application domain,

not all of the RVE definitions should be necessarily satisfied. In the framework of homogenization, the aim is to obtain accurate effective properties. Thus, homogenization works as in (Kanit *et al.*, 2003; Kari *et al.*, 2007; Barello and Lévesque, 2008; Ghossein and Lévesque, 2012) have most often adopted the RVE defined by *a volume element that computes the same target property as the bulk material.*

For random media, a volume element is exactly representative when it contains and infinity of heterogeneities (Ostoja-Starzewski, 2002). For finite volumes, the RVE of a random medium cannot be reached exactly. In practice, a user-prescribed error tolerance is necessary in a *quantitative definition* of the RVE. In that regard, Kanit *et al.* (2003) demonstrated that a quantitative RVE is not necessarily defined by a single finite volume. It can be defined by an ensemble of r random finite volumes, including n heterogeneities each, that yields by an averaging process accurate effective properties, within a tolerance. Although it was demonstrated by Kanit *et al.* (2003) that smaller volumes can produce equally accurate results, provided that a sufficient number of realizations r is considered, a bias in the estimation of the effective properties is observed for too small volumes. Therefore, numerical RVE acceptation criteria are needed to determine the volume size (or number of fibers n) and number of random material volumes (r) that define a RVE large enough to compute accurate estimations of the effective properties, within a tolerance.

Quantitative estimates A quantitative definition of the RVE consists of a set of numerical criteria for the determination of both parameters, n and r.

In several works (Ostoja-Starzewski, 1999; Terada *et al.*, 2000), uniform displacement and traction boundary conditions were enforced to determine n such as:

$$\epsilon_n = \frac{|\bar{Z}_n^d - \bar{Z}_n^t|}{\left(\bar{Z}_{n_i}^d + \bar{Z}_{n_i}^t\right)/2} \leq \epsilon_{tol}, \tag{1.43}$$

where ϵ_{tol} is the desired tolerance, $\bar{Z}_n^d$ refers to a mean physical property (e.g., mean bulk shear modulus) computed for random material volumes including n heterogeneities each under uniform displacement boundary conditions and Z_n^t refers to that computed under uniform traction boundary conditions. For large constituent mechanical properties contrasts, the bounds are very far apart and slowly converge towards the effective properties. Periodic boundary conditions have quicker convergence rates. Figure 1.7 presents the convergence of the bulk modulus of random material volumes of a voronoï mosaic microstructure under periodic, uniform displacement and traction boundary conditions (Kanit *et al.*, 2003). It is observed that the apparent properties have converged towards the effective properties for significantly smaller volumes than uniform boundary conditions. Thus, other criteria

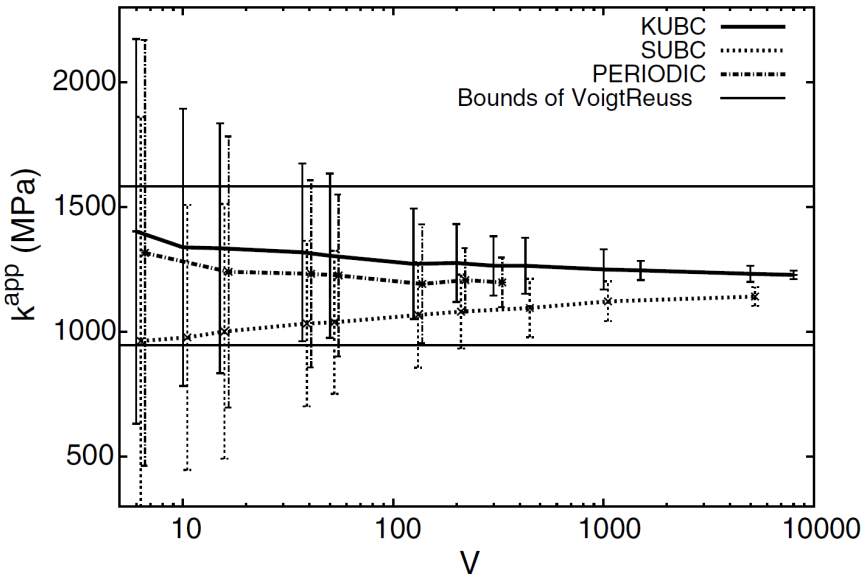

Figure 1.7 Mean bulk modulus of a voronoï mosaic composite as a function of volume size **V** measured by the number of grains included. Three different types of boundary conditions are considered: Kinematic Uniform Boundary Conditions (KUBC), Static Uniform Boundary Conditions (SUBC) and PERIODIC boundary conditions. For clarity, the errorbars are slightly shifted around each studied volume size **V** (Kanit *et al.*, 2003).

have been proposed to estimate the RVE based on the statistics of the apparent properties computed under any set of boundary conditions, rather than on the rigorous bounds under uniform boundary conditions. A list of numerical criteria found in literature for determining n is compiled in Table 1.1. It is important to note that only criteria based on physical properties (e.g., bulk and shear moduli) are presented. Several works have proposed criteria based on morphological statistics (e.g., neighbor distance) to estimate the RVE, see for example Trias *et al.* (2006).

In order to determine the number of needed random realizations, only one criterion has been proposed by Kanit *et al.* (2003) based on the confidence interval of the apparent properties:

$$\epsilon_r = \frac{2\, CI_{\bar{Z}}}{\bar{Z}} \leq \epsilon_{tol}, \tag{1.44}$$

where $\bar{Z}$ is the mean apparent property, $CI_{\bar{Z}}$ is its confidence interval and ϵ_{tol} is the user-prescribed tolerance.

Table 1.1 List of RVE acceptance criteria for determining n.

Criterion name	**Expression**		**Notes**	**References**
Convergence (stability)	$\frac{\lvert\bar{Z}^{n_1} - \bar{Z}^{n_2}\rvert}{\bar{Z}^{n_2}} \leq \epsilon_{tol}$	(1.45)	$n_2 > n_1$	(e.g., Gitman *et al.* (2007))
Deviation	$\frac{s(Z)}{\bar{Z}_n} \leq \epsilon_{tol}$	(1.46)	s: standard deviation	(e.g., Stroeven *et al.* (2004))
Hill condition	$\frac{\langle\boldsymbol{\sigma} : \boldsymbol{\varepsilon}\rangle - \langle\boldsymbol{\sigma}\rangle : \langle\boldsymbol{\varepsilon}\rangle}{\langle\boldsymbol{\sigma} : \boldsymbol{\varepsilon}\rangle} \leq \epsilon_{tol}$	(1.47)		(e.g., Ostoja-Starzewski (2006))
Mean field convergence[(a)]	$\frac{\lvert\bar{\sigma}_{ij;n_2} - \bar{\sigma_{ij;n_1}}\rvert}{\bar{\sigma}_{ij;n_2}} \leq \epsilon_{tol}$	(1.48)	$n_2 > n_1$	(e.g., Trias *et al.* (2006))
Mean field deviation[(a)]	$\frac{s(\sigma_{ij})}{\bar{\sigma}_{ij;n}} \leq \epsilon_{tol}$	(1.49)	s: standard deviation	(e.g., Trias *et al.* (2006))

[(a)] The criterion has been applied to either stress or strain fields. It has also been applied on phase (e.g., fibers, matrix) average fields instead of the whole composite (Trias *et al.*, 2006).

1.3 Works on homogenization of ROFRCs

Very few authors dealt with 3D numerical homogenization of randomly dispersed fibers in space due to its complexity. Böhm *et al.* (2002) studied the elastic and elastoplastic behavior of metal matrix composites reinforced by randomly oriented short fibers. They generated material volumes including 15 randomly oriented fibers of aspect ratio $\rho = 5$ at 15% volume fraction using the RSA generation method. The overall elastic and elastoplastic behaviors were simulated by performing FE simulations under PBCs on three random realizations, without thorough determination of the RVE. They found good agreement between the apparent elastic properties and the analytical results of the one-step model of Mori-Tanaka, the self-consistent scheme and the model of Kuster and Toksöz (1974).

Lusti and Gusev (2004) generated microstructures with 3D randomly dispersed carbon nanotubes, considered as cylindrical inclusions, of high aspect ratios (ρ = 100 and 200) limited to low volume fractions (up to 1%) using Monte-Carlo algorithms, as presented in Figure 1.4. They performed FE simulations under PBCs without determining the RVE. They also computed the apparent properties of composites reinforced by aligned nanotubes of similar volume fractions and aspect ratios, followed by an orientational averaging. They found good agreement between computed apparent properties of their 3D microstructures and that of the orientational averages of aligned-fiber composites.

Kari *et al.* (2007) generated microstructures of randomly dispersed fibers using a modified RSA algorithm. Figure 1.8 a), b) and c) present a generated microstructure of a ROFRC, its

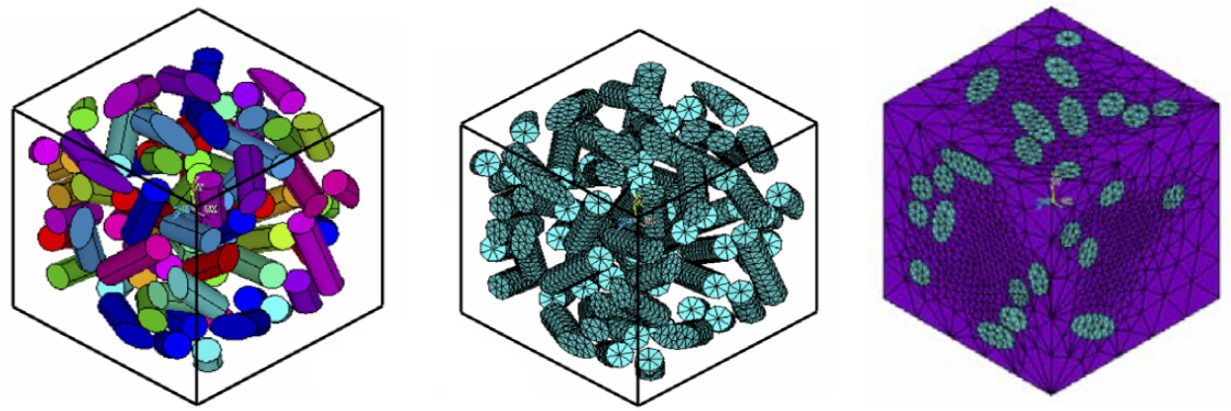

(a) (b) (c)

Figure 1.8 a) Generated microstructure of a ROFRC; b) FE meshing of the fibers and; c) FE meshing of the volume (Kari *et al.*, 2007).

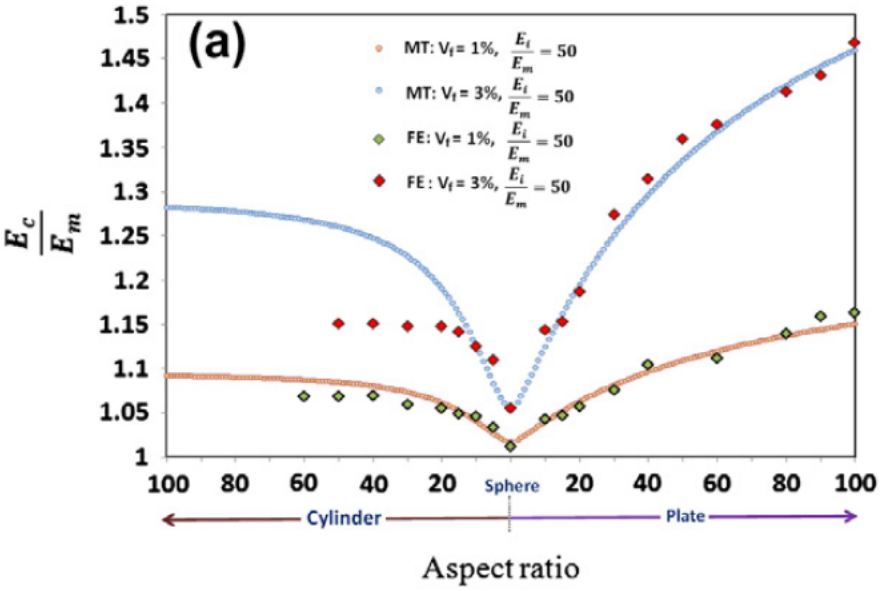

(a)

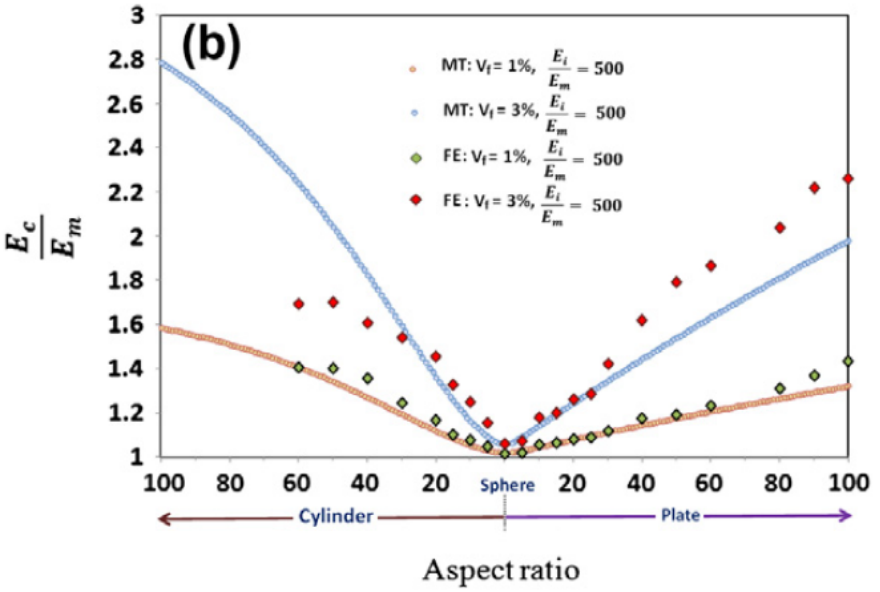

(b)

Figure 1.9 Comparison between FE and Mori–Tanaka (MT) estimates of normalized Young modulus with respect to that of the matrix, for a two-phase random composite materials for different inclusions geometries, volume fractions of 1% and 3% and different contrast in material properties of a) 50 and b) 500. (Mortazavi *et al.*, 2013).

fiber and volume meshings, respectively. Using FE simulations under PBCs, they determined the RVE for a relatively low aspect ratio of 5. They computed the effective properties of

ROFRCs with aspect ratios up to $\rho = 15$, under the assumption that the RVE determined at $\rho = 5$ is still valid. After comparing numerical results to analytical models estimates, they concluded that the SC scheme delivers best estimates of the elastic properties. They also observed that the aspect ratio of fibers in ROFRCs has no effect on the effective elastic properties.

Mortazavi *et al.* (2013) studied the effective elastic properties of composites reinforced by cylinders with aspect ratios ranging from 1/100 (i.e., platelets) up to 60 (i.e., fibers) for two low volume fractions (1% and 3%) and contrast of properties (50 and 500). A single random realization was computed for each microstructure type (i.e., volume fraction, aspect ratio) without consideration of the RVE. No indication was given on the number of inclusions represented in their material volumes. They compared the effective elastic properties to that obtained using the Mori-Tanaka model. Figure 1.9 a) and b) present the normalized effective Young modulus with respect to the aspect ratio for properties contrast of 50 and 500, respectively. They observed that Mori-Tanaka estimates were accurate for all aspect ratios and properties contrasts at a low volume fraction of 1%. It can be observed in Figure 1.9 a) that for a volume fraction of 3% and a contrast of 50, FE results deviate from Mori-Tanaka estimates. The FE results show no additional increase of the effective Young's modulus for fibers of aspect ratios larger than 20. Similar observations apply to a properties contrast of 300, however the FE deviations initiate at a larger aspect ratio.

Hua and Gu (2013) studied the effective properties of SiC reinforced metal matrix composites. They generated a single ROFRC microstructure including 30 fibers of aspect ratio

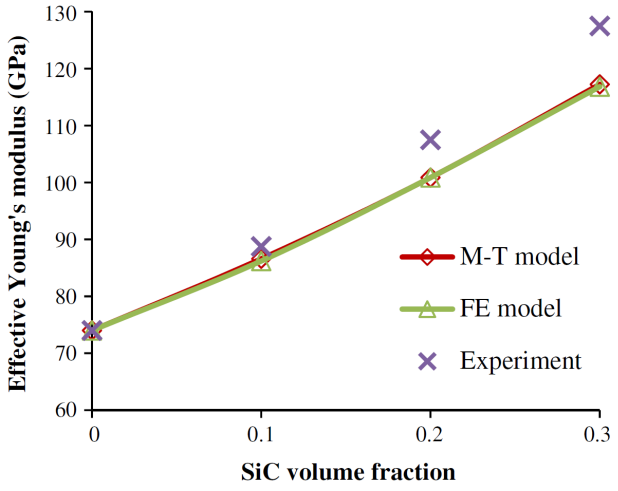

Figure 1.10 Comparisons among the M–T theory, FE model, and the experimental data. Experimental data from (Chawla *et al.*, 2006) and image from (Hua and Gu, 2013).

5 up to 30% volume fraction using RSA method, as presented in Figure 1.3. They computed the effective properties using the FE method and compared them to that of experiments and of the Mori-Tanaka model, as presented in Figure 1.10. They concluded that the model of Mori-Tanaka produces accurate estimations of the elastic properties of ROFRCs. Then, they used the Mori-Tanaka model to conduct a parametric study of the effective properties of ROFRCs for different contrasts of properties and volume fractions. They concluded that fibers with larger aspect ratios generally led to a composite with increased effective Young's modulus, as well as reduced Poisson's ratio. They also observed that for aspect ratios larger than 10, the overall material properties were almost unchanged.

It is clear from analyzing the literature that numerical challenges have limited the numerical homogenization of ROFRCs to low aspect ratios and/or low volume fractions. Most importantly, all numerical studies have been reported without a thorough determination of the appropriate RVE of the microstructure due its computational burden. Results of numerical studies without a thorough determination of the RVE are questionable. Consequently, they cannot be confidently used for the assessment of the analytical models.

CHAPTER 2

OBJECTIVES AND SCIENTIFIC APPROACH

The literature survey revealed that:

- By definition, the RVE should yield accurate effective properties that are similar to those of the macroscopic material. However, the ability of quantitative RVE definitions to deliver accurate estimations of the effective properties has not been verified yet.
- The most common RVE determination method based on convergence of apparent properties over increments of number of fibers (Gusev, 1997; Kanit *et al.*, 2003) induces very large number of computations. A more cost-efficient RVE determination method is required to facilitate the RVE determination process and reduce computational costs.
- The RVE has not been determined for ROFRCs of aspect ratio higher than 5. Moreover, the effect of inclusions aspect ratio on the RVE size has not been established yet for any type of composite.
- Several analytical models exist for predicting the elastic properties of ROFRCs. However, none of the models estimations have been rigorously verified. Thorough assessment of the analytical models is required in order to be able to use them in quick and accurate predictions of ROFRCs properties. Assessment of analytical models is usually done by comparison with numerical homogenization of the RVE.
- Numerical homogenization studies on ROFRCs were limited to low volume fractions due to challenges related to 1) low jamming limits in random generation methods and 2) dealing with very large numerical models. The random-walk process of Altendorf and Jeulin (2011a) was able to generate relatively high volume fractions of composites reinforced by randomly oriented bent fibers. However, in order to assess analytical models, only straight fibers should be considered. Improvements on random generation methods and the use of cost-reduction computation techniques are necessary to extend the range of achievable microstructures (i.e., fibers volume fractions and aspect ratios).
- Numerical homogenization has been performed for a small range of ROFRC microstructure parameters. Most studies present a single case or a small range of microstructural parameters. Accurate effective properties for a wide range of microstructure parameters can be useful for direct predictions of a given composite, but also for assessment of current and future analytical models.

2.1 Objectives

The specific objectives of this research are as follows:

1. **Assessment of existing RVE quantitative definitions and investigation of new RVE definitions**
   The objective is to assess quantitative RVE definitions by comparing their estimated effective properties to that computed from very large material volumes considered as the exact solution. The RVE were determined for ROFRCs of different aspect ratios, following different quantitative definitions of the RVE.
2. **Assessment of analytical model prediction of elastic properties**
   The objective is to compare the estimations of different analytical models to accurate results for a wide range of microstructural parameters in order to determine the best suited model for ROFRCs. The numerical results were computed using the appropriate RVE definition following the results of the first objective.

2.2 Scientific approach

Two research papers were prepared in order to achieve the two above-mentioned objectives.

2.2.1 Article 1: Assessment of existing and introduction of a new and robust efficient definition of the representative volume element

The first paper presents an examination of quantitative RVE definitions largely accepted in the literature and the proposition of several new quantitative definitions. All presented quantitative RVE definitions were applied to ROFRCs of different aspect ratios (up to 60). In order to assess the results of different RVEs, volumes including very large numbers of fibers were simulated and their effective properties were computed. The effective properties of very large volumes were compared to the corresponding estimated effective properties of the different RVE definitions.

The main findings of this paper are:

1. Current RVE quantitative definitions can produce biased RVEs yielding erroneous effective properties (i.e. effective properties that are different than those of a very large material sample). This finding questions, and could invalidate, a number of published papers related to numerical homogenization.
2. The definition of the RVE in terms of the statistical scatter of the apparent elasticity tensor, which is the basis of a newly proposed criterion, is a more robust criterion than

defining it in terms of the convergence of the apparent properties, as is widely done in the literature. Moreover, this new criterion, in addition to being more robust, requires less computations and is believed to be more efficient than current definitions.

3. Material volumes for which apparent elastic tensor exhibits isotropy yield accurate effective properties of ROFRCs, hence can be considered as RVE.

This article was submitted to the "International Journal of Solids and Structures" on February 6, 2013. This journal publishes research on the mechanics of solid materials and the mechanics of structures and has published main works on the subject of the RVE, e.g., (Ostoja-Starzewski, 1998; Terada *et al.*, 2000; Kanit *et al.*, 2003; Pelissou *et al.*, 2009). This article was written almost entirely by the author of this thesis.

2.2.2 Article 2: Evaluation of analytical homogenization models for randomly oriented and high aspect ratio fiber reinforced composites

This paper presents a rigorous assessment of existing analytical homogenization models for predicting the effective elastic properties of ROFRCs. Two categories of analytical models were considered: one-step and two-step homogenization models. The analytical estimations were compared to the results of 3D finite element simulations of RVEs determined using the new quantitative definition presented in Article 1. Comparisons were performed for a wide range of microstructural parameters: aspect ratios up to 120, contrast of properties up to 300 but the volume fractions were limited to 20% due to computational limitations. More than 2500 random microstructures were simulated in the course of this study.

The main findings of this paper are:

1. None of the current analytical models produces accurate estimations of the effective properties of ROFRCs with very long fibers (aspect ratio over 100). For relatively short fibers (aspect ratio under 100) and low volume fractions (up to 5%), the analytical models deliver accurate estimations.
2. The two-step Lielens/Voigt analytical model is the best suited model for the widest range of ROFRC microstructural parameters.
3. It was also demonstrated that one can accurately estimate the effective properties of ROFRCs with very long fibers (mathematically infinite) with that of fibers with an aspect ratio of approximately 100. This finding can be applied in the modeling of advanced composites (e.g. nanocomposites) that are impossible to model using current computational resources.

This article was submitted to "Composites Part B: Engineering" on February 20, 2013. This journal publishes research on the mechanics and the material aspects of composites

and has recently published several studies on the effective properties of ROFRCs (Mortazavi *et al.*, 2013; Hua and Gu, 2013). The work described in this article was led by the author of this thesis and was performed in part in collaboration with Maryam Pahlavanpour, a PhD candidate under the supervision of prof. Martin Lévesque, who assisted in generating the analytical models results. This article was written almost entirely by the author of this thesis.

CHAPTER 3

ARTICLE 1: Assessment of existing and introduction of a new and robust efficient definition of the representative volume element

H. Moussaddy, D. Therriault, M. Lévesque (2013). Submitted to: "*International Journal of Solids and Structures*".

3.1 Abstract

Accurate numerical homogenization necessitates the thorough determination of the Representative Volume Element (RVE). This paper demonstrates that common techniques, based on studying the convergence rate of the effective properties with respect to the volume element size, are invalid for a certain range of microstructures and yield erroneous estimates of their effective properties. Different RVE determination methods were tested for the case of composites reinforced by randomly oriented and high aspect ratio fibers. Following the failure of traditional RVE determination methods, we proposed a new RVE determination criterion that is not based on the average property stability, but its statistical variations. Our new proposed criterion has been shown to be more accurate than other criteria in computing the effective properties of composites for aspect ratios up to 60. Moreover, the proposed criterion does not necessitate a convergence study over the volume element size, hence reducing considerably the RVE determination cost. Finally, our work questions the validity of many published works dealing with composites including heterogeneities of high aspect ratios.

3.2 Introduction

Three-dimensional (3D) numerical homogenization can deliver accurate effective properties for composites with arbitrary microstructures. Several authors have studied specific microstructures, such as randomly dispersed spheres (Ghossein and Lévesque, 2012) or aligned fibers (Tucker III and Liang, 1999), using 3D numerical homogenization methods based on the Finite Element (FE) and Fast Fourier Transforms (FFT). However, only a few works on Randomly Oriented Fiber Reinforced Composites (ROFRCs) are reported in the literature and are limited, due to computational challenges, to low volume fractions (e.g., Lusti and Gusev (2004) up to 1%, Mortazavi *et al.* (2013) at 1% and 3%) and low fibers aspect ratios $\mathrm{AR} = l_{fiber}/d_{fiber}$ where l_{fiber} is the fiber length and d_{fiber} is the fiber radius (e.g., $\mathrm{AR} = 5$ in Böhm *et al.* (2002), $\mathrm{AR} \leq 15$ in Kari *et al.* (2007)). Most importantly, most ROFRCs

numerical studies were conducted without a rigorous determination of the Representative Volume Element (RVE). In the sequel, the "apparent properties" refer to the properties of an arbitrary volume element, whereas "effective properties" refer to that of the RVE.

The RVE determination is of paramount importance to numerical homogenization methods since it ensures accurate estimations of the effective properties. The RVE is classically defined as a volume of the material large enough to represent the material macroscopic behavior, i.e. a volume that yields the same effective properties as the bulk composite. The volume of the material is hereby quantified by the number of heterogeneities/fibers that are represented within. Larger volume elements include larger number of heterogeneities. The process of establishing the RVE is traditionally based on the criterion of apparent property stability, within a tolerance, when incrementing the number of heterogeneities in the composite volume (Gusev, 1997; Kanit *et al.*, 2003). However, no studies have verified the validity of this method for the case of heterogeneities with high aspect ratios (AR>10). The RVE determination process generally requires the numerical homogenization of a large number of random microstructure realizations (i.e., 3D virtual images of ROFRC microstructures) for a series of volumes with an incrementing number of heterogeneities (e.g., number of fibers represented in the ROFRC virtual image) (Kanit *et al.*, 2003). The high computational cost of the RVE determination process for ROFRCs has lead many authors to ignore the elementary RVE concept in their studies (Böhm *et al.*, 2002; Kari *et al.*, 2007; Lusti and Gusev, 2004; Mortazavi *et al.*, 2013). As a result, one could question the accuracy of the results in most of the published papers dealing with ROFRCs.

The objective of this paper is to rigorously study the RVE determination process for the case of ROFRCs with different aspect ratios. Different methods of RVE determination were tested through a series of FE numerical simulations of a ROFRC with 5% volume fraction of fibers and for different aspect ratios. The validity of the different RVE determination methods was assessed by comparing their corresponding effective properties to those of very large volumes. To the authors' knowledge, the RVE determination has neither been rigorously analyzed nor even attempted, yet, for ROFRCs.

The challenges for each step of a numerical homogenization process are first reviewed. In Section 3.4, several RVE determination criteria and methods are presented. Section 3.5 describes briefly the numerical simulations and the parameters used in this study. Section 3.6 contains a comparison between the results of different RVE determination methods. Finally, the main conclusions of this work are listed in Section 3.7.

3.3 Background

Most numerical homogenization studies follow the methodology described below. First, a 3D image of a random microstructure is generated (Section 3.3.1). Then, the 3D image is discretized following the technique of FE or FFT (Section 3.3.2). Boundary conditions are then enforced on the model (Section 3.3.3), followed by the computation of the microstructure apparent properties (Section 3.3.4). Several techniques can help reducing the computational cost of the numerical homogenization process (Section 3.3.5). Finally, the RVE is determined by analyzing the numerical results of several random microstructures (Section 3.3.6).

3.3.1 Random microstructure generation

The first step in numerical homogenization of ROFRCs is to generate a 3D image of a microstructure where the fibers are randomly positioned and oriented. Different methods are commonly used for constructing random microstructure volumes, namely: random sequential adsorption (RSA) (Feder, 1980; Talbot *et al.*, 1991), Monte-Carlo simulations (Gusev, 1997), molecular dynamics simulations (Ghossein and Lévesque, 2012; Lubachevsky, 1990), random-walk methods (Altendorf and Jeulin, 2011a) and experimental image reconstruction techniques (Huang and Li, 2013). The RSA algorithm (Feder, 1980; Talbot *et al.*, 1991), presented herein, has been the most commonly used method for random microstructures generation due to its simplicity. Among the other above-mentioned methods, only the random-walk method has been shown recently to generate more compact packings for ROFRCs (Altendorf and Jeulin, 2011a). However, the method is limited to bended fibers only, which are not desired in our case since this work aims at comparing the computed effective properties with that estimated from micromechanical analytical models (e.g., Mori and Tanaka (1973)) that assume straight fibers.

The RSA method consists of sequentially adding fibers into a volume, while checking for contact interferences with all previously generated fibers, until the target volume fraction is reached. If a newly added fiber overlaps with another fiber, it is removed and then repositioned randomly in the same volume. This repositioning operation is repeated until the new fiber location is free from interferences. However, achievable microstructures by RSA are limited to low volume fractions, due to fiber interpenetration, also known as the jamming limit (Feder, 1980). The RSA process becomes even more complicated for high aspect ratio fibers because they have more probability to interfere with each other. This can be observed in the percolation theory where it is predicted that longer and randomly oriented fibers have an increased probability of forming a connected network (Sandler *et al.*, 2003). This explains partially why ROFRCs efforts have been limited to low aspect ratios. Kari *et al.* (2007) pro-

posed a modification to the original RSA scheme to overcome the jamming limit by adding smaller fibers to fill-up the volume after reaching the jamming limit at a given initial fiber size. However, discrepancies in aspect ratios and sizes of fibers in the same microstructure induce very refined discretizations of microstructures, increasing substantially the computational cost. Therefore, there is still a need to improve the RSA method for randomly oriented straight fibers in order to extend the range of achievable volume fractions and aspect ratios. An original modification to the RSA scheme is proposed in Appendix where a displacement is imposed on added fibers that interfere with existing fibers.

3.3.2 Numerical solution methods and geometry discretization

The FE and the FFT methods are among the most used numerical methods to estimate the effective properties of composite microstructures. The latter has been reported by (Moulinec and Suquet, 1994, 1998) and has been recently used in a study on the effective properties of sphere reinforced composites (Ghossein and Lévesque, 2012). The FFT method requires uniform discretization of a three dimensional microstructure image into equal size cubic volumes (i.e., voxels) in order to enjoy the computational efficiency of FFT. The principal advantage of this method is that it avoids the meshing difficulties usually associated with FE and can be fully automated, by opposition to FE where user input is required in most cases. However, the number of voxels required to represent adequately the geometry of high aspect ratio fibers becomes very important and leads to very large computational costs. The FE allows for a non-uniform distribution of elements (i.e., free meshes) permitting different levels of mesh refinements in different parts of the microstructure. Moreover, different types and shapes of elements can be used to accurately represent the fiber circular cross-section. When the meshing is complete, boundary conditions are enforced on the meshing as described next.

3.3.3 Boundary conditions

For an infinitely large volume, the effective properties are independent of the applied boundary conditions (Hill, 1963; Sab, 1992). Therefore, regardless of the enforced boundary conditions, all apparent properties should converge to the effective properties when increasing the number of heterogeneities. The main criterion that should be driving the choice of boundary conditions is the convergence rate of the apparent properties towards the effective properties. It has been demonstrated (Kanit *et al.*, 2003) that periodic boundary conditions converge towards the effective properties for smaller volumes than uniform tractions or displacements. By definition, periodic boundary conditions are implemented into FFT methods (Moulinec and Suquet, 1998). However, the implementation of periodic boundary conditions

into FE models is more challenging. Periodic boundary conditions application in FE packages can be achieved through the elimination method using Multiple-Point Constraints (MPC). In order to exactly meet the periodicity of the displacement field, the microstructure must be periodic and the meshes on opposite faces of the volume element must be identical. Following the meshing, all matching nodes displacements are coupled through the periodic boundary conditions equation:

$$\mathbf{u}_{(\mathbf{x_2})} - \mathbf{u}_{(\mathbf{x_1})} = \mathbf{E} \cdot (\mathbf{x}_2 - \mathbf{x}_1), \tag{3.1}$$

where $\mathbf{u}_{(\mathbf{x}_i)}$ is the displacement vector of the node at location $\mathbf{x}_i$, $\mathbf{x}_1$ and $\mathbf{x}_2$ are the coordinates of two matching nodes on opposite faces of the cubic volume and $\mathbf{E}$ is the applied macroscopic strain (set by the user). The reader is referred to (Barello and Lévesque, 2008) for a more detailed discussion on periodic boundary conditions implementation in numerical homogenization problems. Following the boundary conditions enforcement, the numerical model is solved and the apparent elastic properties are consequently determined as described in the next section.

3.3.4 Computation of the elastic properties

The apparent elastic tensor $\widetilde{\mathbf{C}}$ of a volume element is computed through:

$$\mathbf{\Sigma} = \widetilde{\mathbf{C}} : \mathbf{E}, \tag{3.2}$$

where $\mathbf{\Sigma}$ is the macroscopic stress tensor. $\mathbf{\Sigma}$ and $\mathbf{E}$ are defined as :

$$\mathbf{\Sigma} = \langle \boldsymbol{\sigma}(\mathbf{x}) \rangle_V \tag{3.3a}$$

$$\mathbf{E} = \langle \boldsymbol{\varepsilon}(\mathbf{x}) \rangle_V \tag{3.3b}$$

where $\boldsymbol{\sigma}$ and $\boldsymbol{\varepsilon}$ are the local stress and strain fields, respectively. Angle brackets $\langle . \rangle$ indicate an averaging over the volume V as

$$\langle \boldsymbol{\sigma}(\mathbf{x}) \rangle_V = \frac{1}{V} \int_V \boldsymbol{\sigma}(\mathbf{x}) \, \mathrm{d}V. \tag{3.4}$$

For discretized elements, angle brackets $\langle . \rangle$ indicate a volume averaging of the discrete field:

$$\langle \boldsymbol{\sigma}_i \rangle_V = \frac{1}{V} \sum V_i \, \boldsymbol{\sigma}_i, \tag{3.5}$$

where V_i and σ_i are the volume and stress attributed to the i^{th} finite element (or integration point).

In order to show explicitly how the effective elastic tensor $\widetilde{\mathbf{C}}$ is calculated, the modified Voigt (Mandel) notation is used by which Eq.3.2 becomes:

$$\begin{bmatrix} \Sigma_{11} \\ \Sigma_{22} \\ \Sigma_{33} \\ \sqrt{2}\Sigma_{12} \\ \sqrt{2}\Sigma_{13} \\ \sqrt{2}\Sigma_{23} \end{bmatrix} = \begin{bmatrix} \widetilde{\mathrm{C}}_{1111} & \widetilde{\mathrm{C}}_{1122} & \widetilde{\mathrm{C}}_{1133} & \sqrt{2}\widetilde{\mathrm{C}}_{1112} & \sqrt{2}\widetilde{\mathrm{C}}_{1113} & \sqrt{2}\widetilde{\mathrm{C}}_{1123} \\ \widetilde{\mathrm{C}}_{2211} & \widetilde{\mathrm{C}}_{2222} & \widetilde{\mathrm{C}}_{2233} & \sqrt{2}\widetilde{\mathrm{C}}_{2212} & \sqrt{2}\widetilde{\mathrm{C}}_{2213} & \sqrt{2}\widetilde{\mathrm{C}}_{2223} \\ \widetilde{\mathrm{C}}_{3311} & \widetilde{\mathrm{C}}_{3322} & \widetilde{\mathrm{C}}_{3333} & \sqrt{2}\widetilde{\mathrm{C}}_{3312} & \sqrt{2}\widetilde{\mathrm{C}}_{3313} & \sqrt{2}\widetilde{\mathrm{C}}_{3323} \\ \sqrt{2}\widetilde{\mathrm{C}}_{1211} & \sqrt{2}\widetilde{\mathrm{C}}_{1222} & \sqrt{2}\widetilde{\mathrm{C}}_{1233} & 2\widetilde{\mathrm{C}}_{1212} & 2\widetilde{\mathrm{C}}_{1213} & 2\widetilde{\mathrm{C}}_{1223} \\ \sqrt{2}\widetilde{\mathrm{C}}_{1311} & \sqrt{2}\widetilde{\mathrm{C}}_{1322} & \sqrt{2}\widetilde{\mathrm{C}}_{1333} & 2\widetilde{\mathrm{C}}_{1312} & 2\widetilde{\mathrm{C}}_{1313} & 2\widetilde{\mathrm{C}}_{1323} \\ \sqrt{2}\widetilde{\mathrm{C}}_{2311} & \sqrt{2}\widetilde{\mathrm{C}}_{2322} & \sqrt{2}\widetilde{\mathrm{C}}_{2333} & 2\widetilde{\mathrm{C}}_{2312} & 2\widetilde{\mathrm{C}}_{2313} & 2\widetilde{\mathrm{C}}_{2323} \end{bmatrix} \begin{bmatrix} \mathrm{E}_{11} \\ \mathrm{E}_{22} \\ \mathrm{E}_{33} \\ \sqrt{2}\mathrm{E}_{12} \\ \sqrt{2}\mathrm{E}_{13} \\ \sqrt{2}\mathrm{E}_{23} \end{bmatrix}. \tag{3.6}$$

In order to obtain all the terms of the apparent elasticity tensor $\widetilde{\mathbf{C}}$, each FE model can be solved 6 times using 6 orthogonal deformation states, namely:

$$\mathrm{E}^1 = \begin{bmatrix} \varepsilon \\ 0 \\ 0 \\ 0 \\ 0 \\ 0 \end{bmatrix};\ \mathrm{E}^2 = \begin{bmatrix} 0 \\ \varepsilon \\ 0 \\ 0 \\ 0 \\ 0 \end{bmatrix};\ \mathrm{E}^3 = \begin{bmatrix} 0 \\ 0 \\ \varepsilon \\ 0 \\ 0 \\ 0 \end{bmatrix};\ \mathrm{E}^4 = \begin{bmatrix} 0 \\ 0 \\ 0 \\ \varepsilon\sqrt{2} \\ 0 \\ 0 \end{bmatrix};\ \mathrm{E}^5 = \begin{bmatrix} 0 \\ 0 \\ 0 \\ 0 \\ \varepsilon\sqrt{2} \\ 0 \end{bmatrix};\ \mathrm{E}^6 = \begin{bmatrix} 0 \\ 0 \\ 0 \\ 0 \\ 0 \\ \varepsilon\sqrt{2} \end{bmatrix}. \tag{3.7}$$

Each deformation state is applied separately on the non-deformed FE model. By implementing 3.7 in 3.6, each deformation state results in a single column of the apparent elastic tensor $\widetilde{\mathbf{C}}$ in its matrix notation. Consequently, all 6 columns of the apparent elasticity tensor can be calculated. Conversely, if tractions based boundary conditions were to be applied, six orthogonal states of applied tractions would be needed to determine the 36 terms of the compliance tensor $\widetilde{\mathbf{S}}$ in its matrix notation. It should be noted that for infinitely large volume elements, at most 21 constants need to be determined due to the symmetry of the stress and strain tensors.

It is well established that a random orientation distribution of fibers should lead to isotropic effective properties (Benveniste, 1987). Therefore, only two elastic parameters are sufficient to describe the effective behavior of the composite. Assuming the isotropy of the volume element, the apparent bulk modulus $\widetilde{k}$ and shear modulus $\widetilde{G}$ can be calculated from $\widetilde{\mathbf{C}}$ using the isotropy projectors resulting in the following equations expressed using the Einstein summation convention:

$$\widetilde{k} = \frac{\widetilde{\mathrm{C}}_{iijj}}{9}, \tag{3.8a}$$

$$\widetilde{G} = \frac{3\,\widetilde{\mathrm{C}}_{ijij} - \widetilde{\mathrm{C}}_{iijj}}{30}. \tag{3.8b}$$

It should be noted that only two loading cases are required to estimate $\widetilde{k}$ and $\widetilde{G}$. However, we performed the 6 load cases, stated in Eq.3.7, required to obtain the full stiffness tensor in order to study its deviation from isotropy (see Section 3.3.4).

3.3.5 FE computation techniques

ROFRCs discretized microstructures usually require large FE models with a very high number of degrees of freedom (DOF). With 15 randomly oriented fibers of aspect ratio 5 and a volume fraction of 15%, Böhm *et al.* (2002) obtained a 130,000 nodes FE model (390,000 DOF). The number of DOF substantially increases for higher aspect ratios of fibers. The computational memory required for the solution of the corresponding FE models cannot be handled by typical workstation computers and classical solving methods. However, specific techniques can reduce the memory requirements and computational time of the FE computations. One important technique to significantly reduce the computational cost is the use of iterative solvers. Iterative solvers such as the Krylov subspace methods (e.g. pre-conditioned conjugate gradient) can significantly reduce the memory required as well as the computational time when compared to the direct sparse solver. These types of solvers are most efficient when used for block-like structures with high number of DOF (i.e., over a million) (ABAQUS Analysis User's Manual, 2010), as for the case of ROFRC volume elements. Most commercial FE packages (e.g., Abaqus/Standard v6.10, ANSYS v13.0) have iterative solvers already implemented but must be specified by the user. However, certain element types, contact or non-linearity of material properties or geometries can lead to ill-conditioned models which will slowly or even fail to converge.

Another important aspect of large model computation is parallelization. Thread-based-parallelization can be utilized to parallelize independent tasks and loops. Moreover, Message Passing Interface (MPI) based parallelization in domain decomposition methods (Farhat *et al.*, 1994; Farhat and Roux, 1991; Lenhardt and Rottner, 1999) can be utilized in parallelizing the model on a computer cluster. FE Tearing and Interconnecting method (FETI) (Farhat *et al.*, 1994; Farhat and Roux, 1991) is a domain decomposition method which breaks down the model into subdomains that share only interfaces. Forces and displacements at the interfaces of subdomains are determined iteratively in an automated process without any user intervention. The N subdomains are solved in N different processes that communicate through the MPI. The combination of iterative solvers and parallelization schemes can help widen the range of achievable volume fractions and fibers aspect ratios for ROFRCs. However, not every combination of parallelization scheme and solver is possible. For more information about FE solvers and parallelization, the reader is referred to (Farhat and Roux, 1994).

3.3.6 RVE determination

RVE definitions

The validity of the numerical homogenization relies on the notion of the RVE. As originally described by Hill (1963) and later by others (Drugan and Willis, 1996; Ostoja-Starzewski, 1998; Sab, 1992), the "theoretical RVE" refers to a sample that is large enough 1) to include a sampling of all microstructural heterogeneities that occur in the composite and 2) to deliver effective properties that are independent of boundary conditions. The theoretical RVE definition is simple in its physical meaning but remains challenging to determine in practice. A more practical RVE definition is found in the framework of homogenization in which a "numerical RVE" is defined as the smallest volume element that has the same target property/behavior as the full scale material (Gusev, 1997; Kanit *et al.*, 2003). While the theoretical RVE is specific for the microstructure under study (e.g., volume fraction, contrast of properties, heterogeneities shapes, dispersion and orientation), the numerical RVE is in addition specific to the targeted property/behavior (e.g., bulk modulus, shear modulus, thermal properties) (Gitman *et al.*, 2007; Harper *et al.*, 2012; Kanit *et al.*, 2003; Pelissou *et al.*, 2009). The numerical RVE definition is more interesting than that of a theoretical RVE from a practical standpoint. Numerical RVE should result in smaller volumes while still satisfying the homogenization primary objective of having accurate effective properties.

Numerical RVE determination

A numerical RVE is usually characterized by the number of represented heterogeneities in the volume. The number of heterogeneities that are required in a RVE is estimated through the verification of specific criteria. Those RVE determination criteria should, necessarily, be able to identify a RVE with accurate properties and, ideally, with the smallest volume element as possible. Selecting appropriate RVE criteria is not trivial. Inadequately selected criteria can lead either to a volume smaller than the RVE, hence yielding erroneous results, or to a very large RVE that induces prohibitively large computational costs.

The first numerical RVE criteria reported in the literature relied on the stability of the apparent properties of volume elements over increments of the number of heterogeneities in the volume (Gusev, 1997). Gusev (1997) used this determination criterion to determine the RVE of randomly dispersed spheres reinforced composites. Later on, Kanit *et al.* (2003) have presented an algorithm to determine the RVE defined not only by its number of represented heterogeneities, but also by the number of random realizations of the volume element required to have confidence in the results. In Kanit *et al.* (2003), it is shown that by performing a certain number of realizations with fewer heterogeneities, it is possible to obtain the same

property as that of a single and larger RVE and with the same accuracy. However, this was shown to be untrue for small volume sizes, as there is a bias caused by deterministic size effects (e.g., boundary effects) which cannot be eliminated through ensemble averaging (Kanit *et al.*, 2003). Hence the numerical RVE is defined as the representative ensemble of realizations, with the fewest number of heterogeneities , which yields by average the composite effective properties, within a given tolerance.

Several determination criteria have been used in the literature (Ghossein and Lévesque, 2012; Gitman *et al.*, 2007; Kanit *et al.*, 2003; Moussaddy *et al.*, 2011; Pelissou *et al.*, 2009; Salmi *et al.*, 2012; Trias *et al.*, 2006) to determine RVE parameters (n_{RVE}, r_{RVE}). To the author's knowledge, only one criterion was used, under several forms, to determine the number realizations required r_{RVE} (Ghossein and Lévesque, 2012; Gitman *et al.*, 2007; Moussaddy *et al.*, 2011; Pelissou *et al.*, 2009). The criterion aims at the determination of the ensemble size r of realizations that will give satisfactory confidence in the average properties. Precisely, the criterion ensures that the ensemble of realizations average property should be representative, within a tolerance, of the average of the whole statistical population of possible microstructures at that number of heterogeneities. In contrast, several different criteria were used to determine the number of heterogeneities in the RVE n_{RVE}. The first, and most commonly used, criterion is that of effective property stability over increments of number of heterogeneities in the volume (Barello and Lévesque, 2008; Ghossein and Lévesque, 2012; Gusev, 1997; Kari *et al.*, 2007; Pelissou *et al.*, 2009; Trias *et al.*, 2006). The only difference from the early definition of the criterion, used by Gusev (1997), is that the stability criterion is applied to the ensemble average properties and not to a single volume element for each volume size. Another criterion was based on increasing the number of heterogeneities until the bounds of effective properties, issued from uniform displacement and uniform traction boundary conditions, are close within a tolerance (Salmi *et al.*, 2012). Even though this criterion is the only one to provide exact bounds and errors for the effective properties, uniform displacement and traction boundary conditions are too distant apart for high contrasts of constituents' properties. It was demonstrated in Salmi *et al.* (2012) that uniform displacement and traction boundary conditions converge faster for a free-form volume element, whose side does not intersect with heterogeneities, than for a cubic volume element which intersects heterogeneities. Whether the refined bounds converge quicker than periodic boundary conditions or not is left for future studies since the generation of free form VE for the microstructures studied herein would require significant amount of work. A third criterion to determine n_{RVE} is that of enforcing that the variation/deviation of the targeted property over all realizations is within a tolerance of their average (Salmi *et al.*, 2012; Trias *et al.*, 2006). Indeed, very low scattering of the effective properties would be observed if an arbitrarily large number of heterogeneities

were included in the volume. Other RVE size determination criteria were developed based on geometrical and statistical properties of the realizations (Trias *et al.*, 2006), but are not directly related to the effective properties and, hence, are not included in this study.

The process of determining the RVE parameters is therefore usually done using a two-fold convergence. First the number of realizations is incremented until satisfying the first criterion and determining r_{RVE}. Second, the volume size is incremented until satisfaction of the second criterion and determining n_{RVE}. This process usually leads to a very large number of FE models to evaluate, among which only one set will be defined as the RVE. Furthermore, no studies have verified the validity of the different criteria results, especially for the case of heterogeneities with high aspect ratios. For example, the stability criterion verifies only the convergence rate of the targeted property over size increments without any indication on the effective properties accuracy. There might be cases where the property converges very slowly over size increments and the numerical stability criterion is not strict enough to ensure that the property of interest has effectively stabilized. As a result, premature convergence towards false results is possible. In this study, an attempt was made to evaluate the accuracy of the stability criterion, but also to suggest and assess the robustness of new methods of RVE determination.

3.4 RVE determination methods

Several RVE determination methods were tested to determine both RVE parameters (n_{RVE}, r_{RVE}). Each method consists of an algorithm involving two RVE determination criteria. In the following, the determination criteria are first presented, followed by the listing of the general algorithm for all determination methods.

3.4.1 Determination criteria

Two groups of determination criteria were tested to compute the RVE parameters (n_{RVE}, r_{RVE}). The first group lists the number of realizations r_{RVE} determination criteria, while the second group lists number of fibers n_{RVE} determination criteria. While the bulk modulus is studied below for illustration purposes, the criteria can be applied to any elastic property.

Ensemble size criteria

An ensemble size criterion aims at ensuring that the ensemble of realizations is large enough to have confidence in the ensemble average apparent properties. Two criteria are used: the confidence interval criterion and the ensemble isotropy criterion.

Confidence criterion: This criterion has been used under different forms in several RVE determination studies (Ghossein and Lévesque, 2012; Kanit *et al.*, 2003; Moussaddy *et al.*, 2011). The criterion states that the ensemble size is satisfactory if the confidence interval relative error is within a certain tolerance, namely:

$$\zeta_{\text{con}} = \frac{I_{\tilde{k}}^{95\%} \Big/ 2}{\overline{k}_n^r} \leq tol, \tag{3.9}$$

where $I_{\tilde{k}}^{95\%}$ is the 95% confidence interval of the apparent bulk moduli, *tol* is the fixed tolerance, and $\overline{k}_n^r$ represents the arithmetic averaging of the apparent bulk moduli over the r realizations with n fibers each.

Ensemble isotropy criterion: This criterion imposes the condition that the ensemble average properties should have the same material symmetry as the full scale material, which is isotropy in our case. Using this criterion, individual realizations should not be necessarily isotropic, but the average stiffness tensor of the representative ensemble of realizations should be. The average stiffness tensor isotropy should always be true for an arbitrarily large ensemble of realizations since the theoretical orientation averaging of the stiffness or compliance tensor of even a single fiber composite over all orientations exhibits isotropic behavior. Several isotropy indices can be found (Bucataru and Slawinski, 2009; Ranganathan and Ostoja-Starzewski, 2008) in the literature but none of them provides a percentage error measurement. It is therefore not trivial to define a range in which the isotropy index provides an acceptable isotropy. Moreover, these indices collapse the whole elasticity matrix into one single index value. This operation can be practical in most cases, but may lead to inaccurate isotropy measurements.

A new isotropy error is hereby proposed that computes an error for each non-zero term of the stiffness matrix. For a single random microstructure, the isotropy error matrix is given

by:

$$\Lambda = \begin{bmatrix} \frac{\widetilde{\mathrm{C}}_{11}-\mathrm{C}_{11}^{(\widetilde{k}^r,\widetilde{G}^r)}}{\mathrm{C}_{11}^{(\widetilde{k}^r,\widetilde{G}^r)}} & \frac{\widetilde{\mathrm{C}}_{12}-\mathrm{C}_{12}^{(\widetilde{k}^r,\widetilde{G}^r)}}{\mathrm{C}_{12}^{(\widetilde{k}^r,\widetilde{G}^r)}} & \frac{\widetilde{\mathrm{C}}_{13}-\mathrm{C}_{13}^{(\widetilde{k}^r,\widetilde{G}^r)}}{\mathrm{C}_{13}^{(\widetilde{k}^r,\widetilde{G}^r)}} & 0 & 0 & 0 \\ \frac{\widetilde{\mathrm{C}}_{21}-\mathrm{C}_{21}^{(\widetilde{k}^r,\widetilde{G}^r)}}{\mathrm{C}_{21}^{(\widetilde{k}^r,\widetilde{G}^r)}} & \frac{\widetilde{\mathrm{C}}_{22}-\mathrm{C}_{22}^{(\widetilde{k}^r,\widetilde{G}^r)}}{\mathrm{C}_{22}^{(\widetilde{k}^r,\widetilde{G}^r)}} & \frac{\widetilde{\mathrm{C}}_{23}-\mathrm{C}_{23}^{(\widetilde{k}^r,\widetilde{G}^r)}}{\mathrm{C}_{23}^{(\widetilde{k}^r,\widetilde{G}^r)}} & 0 & 0 & 0 \\ \frac{\widetilde{\mathrm{C}}_{31}-\mathrm{C}_{31}^{(\widetilde{k}^r,\widetilde{G}^r)}}{\mathrm{C}_{31}^{(\widetilde{k}^r,\widetilde{G}^r)}} & \frac{\widetilde{\mathrm{C}}_{32}-\mathrm{C}_{32}^{(\widetilde{k}^r,\widetilde{G}^r)}}{\mathrm{C}_{32}^{(\widetilde{k}^r,\widetilde{G}^r)}} & \frac{\widetilde{\mathrm{C}}_{33}-\mathrm{C}_{33}^{(\widetilde{k}^r,\widetilde{G}^r)}}{\mathrm{C}_{33}^{(\widetilde{k}^r,\widetilde{G}^r)}} & 0 & 0 & 0 \\ 0 & 0 & 0 & \frac{\widetilde{\mathrm{C}}_{44}-\mathrm{C}_{44}^{(\widetilde{k}^r,\widetilde{G}^r)}}{\mathrm{C}_{44}^{(\widetilde{k}^r,\widetilde{G}^r)}} & 0 & 0 \\ 0 & 0 & 0 & 0 & \frac{\widetilde{\mathrm{C}}_{55}-\mathrm{C}_{55}^{(\widetilde{k}^r,\widetilde{G}^r)}}{\mathrm{C}_{55}^{(\widetilde{k}^r,\widetilde{G}^r)}} & 0 \\ 0 & 0 & 0 & 0 & 0 & \frac{\widetilde{\mathrm{C}}_{66}-\mathrm{C}_{66}^{(\widetilde{k}^r,\widetilde{G}^r)}}{\mathrm{C}_{66}^{(\widetilde{k}^r,\widetilde{G}^r)}} \end{bmatrix}, \tag{3.10}$$

and for an ensemble of r realizations, the isotropy error matrix is expressed by:

$$\Lambda^{\mathrm{r}} = \begin{bmatrix} \frac{\overline{\mathrm{C}}_{11}^{\mathrm{r}}-\mathrm{C}_{11}^{(\overline{k}^r,\overline{G}^r)}}{\mathrm{C}_{11}^{(\overline{k}^r,\overline{G}^r)}} & \frac{\overline{\mathrm{C}}_{12}^{\mathrm{r}}-\mathrm{C}_{12}^{(\overline{k}^r,\overline{G}^r)}}{\mathrm{C}_{12}^{(\overline{k}^r,\overline{G}^r)}} & \frac{\overline{\mathrm{C}}_{13}^{\mathrm{r}}-\mathrm{C}_{13}^{(\overline{k}^r,\overline{G}^r)}}{\mathrm{C}_{13}^{(\overline{k}^r,\overline{G}^r)}} & 0 & 0 & 0 \\ \frac{\overline{\mathrm{C}}_{21}^{\mathrm{r}}-\mathrm{C}_{21}^{(\overline{k}^r,\overline{G}^r)}}{\mathrm{C}_{21}^{(\overline{k}^r,\overline{G}^r)}} & \frac{\overline{\mathrm{C}}_{22}^{\mathrm{r}}-\mathrm{C}_{22}^{(\overline{k}^r,\overline{G}^r)}}{\mathrm{C}_{22}^{(\overline{k}^r,\overline{G}^r)}} & \frac{\overline{\mathrm{C}}_{23}^{\mathrm{r}}-\mathrm{C}_{23}^{(\overline{k}^r,\overline{G}^r)}}{\mathrm{C}_{23}^{(\overline{k}^r,\overline{G}^r)}} & 0 & 0 & 0 \\ \frac{\overline{\mathrm{C}}_{31}^{\mathrm{r}}-\mathrm{C}_{31}^{(\overline{k}^r,\overline{G}^r)}}{\mathrm{C}_{31}^{(\overline{k}^r,\overline{G}^r)}} & \frac{\overline{\mathrm{C}}_{32}^{\mathrm{r}}-\mathrm{C}_{32}^{(\overline{k}^r,\overline{G}^r)}}{\mathrm{C}_{32}^{(\overline{k}^r,\overline{G}^r)}} & \frac{\overline{\mathrm{C}}_{33}^{\mathrm{r}}-\mathrm{C}_{33}^{(\overline{k}^r,\overline{G}^r)}}{\mathrm{C}_{33}^{(\overline{k}^r,\overline{G}^r)}} & 0 & 0 & 0 \\ 0 & 0 & 0 & \frac{\overline{\mathrm{C}}_{44}^{\mathrm{r}}-\mathrm{C}_{44}^{(\overline{k}^r,\overline{G}^r)}}{\mathrm{C}_{44}^{(\overline{k}^r,\overline{G}^r)}} & 0 & 0 \\ 0 & 0 & 0 & 0 & \frac{\overline{\mathrm{C}}_{55}^{\mathrm{r}}-\mathrm{C}_{55}^{(\overline{k}^r,\overline{G}^r)}}{\mathrm{C}_{55}^{(\overline{k}^r,\overline{G}^r)}} & 0 \\ 0 & 0 & 0 & 0 & 0 & \frac{\overline{\mathrm{C}}_{66}^{\mathrm{r}}-\mathrm{C}_{66}^{(\overline{k}^r,\overline{G}^r)}}{\mathrm{C}_{66}^{(\overline{k}^r,\overline{G}^r)}} \end{bmatrix}, \tag{3.11}$$

where $\mathbf{C}^{(\widetilde{k},\widetilde{G})}$ is the isotropic stiffness matrix recalculated from the apparent elastic properties $\widetilde{k}$ and $\widetilde{G}$ and $\mathbf{C}^{(\overline{k},\overline{G})}$ is the isotropic stiffness matrix recalculated from the average apparent elastic properties $\overline{k}$ and $\overline{G}$.

The criterion dictates that the maximum term of the isotropy error matrix should be lower than a fixed tolerance:

$$\zeta_{\mathrm{iso}} = \max\left(|\Lambda^r|\right) \ \leq \ tol, \tag{3.12}$$

where $\max\left(|\Lambda^r|\right)$ indicates the maximum value of the matrix components.

Volume size criteria

Stability criterion: The property stability criterion is the most commonly used RVE determination criterion. It aims at the determination of the point of convergence of the target

property when the number of heterogeneities is increased. Thus, we propose a generalized form of the stability criterion for an arbitrary increment of the number of fibers represented. To reach stability, the criterion states that the convergence rate of the bulk modulus should be within a certain tolerance:

$$\delta_{\text{stab}} = \frac{\left|\overline{k}_{n_2}^{r_2} - \overline{k_{n_1}^{r_1}}\right|}{\overline{k}_{n_2}^{r_2}} \times \left(\frac{\Delta n}{n_2 - n_1}\right) \leq tol, \tag{3.13}$$

where n_2 is larger than n_1, and Δn indicates the chosen reference step size. The ratio between Δn and $n_2 - n_1$ is hereby proposed to generalize the stability criterion for an arbitrary choice of volumes n_1 and n_2. The criterion's ability to determine accurately the RVE value depends on the choice of the tolerance value and of the reference volume step size Δn. Even though this criterion works well for microstructures with randomly dispersed spheres (Ghossein and Lévesque, 2012; Gusev, 1997), or grains (Kanit *et al.*, 2003), the microstructure of ROFRCs with high aspect ratios fibers were not tested and should provide more insight into the problems that can be faced.

Deviation criterion: The standard deviation of the target property is an indicator of the scatter in the ensemble of realizations. When the number of fibers increases, lower property variations should be observed. Theoretically, no variations should be observed when the RVE is reached since the latter is typical of the whole microstructure. In this perspective, the RVE can be identified by fixing a maximum deviation tolerance for an ensemble of realizations:

$$\delta_{\text{dev}} = \frac{s_n^r}{\overline{k}_n^r} \leq tol, \tag{3.14}$$

where s_n^r is the standard deviation of the target property for an ensemble r with n fibers in each volume.

Averaging variations criterion (new): All previous criteria were based on the arithmetic mean of the apparent target property for the ensemble. The arithmetic mean value of the apparent properties of the realizations was considered as the overall ensemble property. Here we consider the arithmetic and harmonic means of the stiffness tensor:

$$\overline{\mathbf{C}} = \frac{1}{r}\sum_{i=1}^{r} \tilde{\mathbf{C}}_i, \tag{3.15a}$$

$$\underline{\mathbf{C}} = \left(\frac{1}{r}\sum_{i=1}^{r} \tilde{\mathbf{C}}_i^{-1}\right)^{-1}. \tag{3.15b}$$

where $\tilde{\mathbf{C}}_i$ is the apparent elastic tensor of the i^{th} realization. The corresponding bulk moduli are given by:

$$\bar{k} = \frac{\overline{\mathrm{C}}_{iijj}}{9}, \tag{3.16a}$$

$$\bar{\bar{k}} = \frac{\underline{\mathrm{C}}_{iijj}}{9}. \tag{3.16b}$$

It can be demonstrated that the result of Eq.3.16a is equivalent to the arithmetic mean of $\tilde{k}$ evaluated by $\left[\frac{1}{r}\sum_{i=1}^{r}\tilde{k}^i\right]$, hence the arithmetic mean symbol $\bar{k}$ is used. However, Eq.3.16b is different than the harmonic mean of $\tilde{k}$ evaluated by $\left[\frac{r}{\sum_{i=1}^{r}\frac{1}{\tilde{k}^i}}\right]$.

The estimation of the average properties of the ensemble is taken as the average of both means:

$$\widehat{k}^r = \frac{\overline{k}^r + \overline{\overline{k}}^r}{2} \tag{3.17}$$

By construction, we have that:

$$\overline{\overline{k}}^r \leq \widehat{k}^r \leq \overline{k}^r \tag{3.18}$$

Equality in Eq.3.18 can only be obtained when all realizations lead to identical properties. This new criterion states that the RVE is obtained when the difference between the ensemble average properties $\widehat{k}^r$ and any of $\overline{k}^r$ or $\overline{\overline{k}}^r$ is within a certain tolerance of their mean:

$$\delta_{\mathrm{av}} = \left(\frac{\widehat{k}^r - \overline{\overline{k}}^r}{\widehat{k}^r}\right) = \left(\frac{\widehat{k}^r - \overline{k}^r}{\widehat{k}^r}\right) \leq tol \tag{3.19}$$

Isotropy criterion (new): This last criterion investigates if a single isotropic microstructure can provide accurate estimations of the effective properties. For this purpose, particular isotropic microstructures, within a tolerance, were searched for among all generated volume elements. The criterion states:

$$\delta_{\mathrm{iso}} = \max\left(|\Lambda|\right) \ \leq \ tol, \tag{3.20}$$

where Λ is calculated using Eq.3.10. The RVE consists of the smallest volume element which satisfies Eq.3.20.

Determination algorithm

Each RVE determination Method (M) was formed by combining an ensemble size criterion with a volume size criterion. Table 3.1 lists all methods that were used in this study. For all methods involving two criteria, the main algorithm is:

1. Set the microstructure parameters: volume fraction, aspect ratio, elastic properties of

constituents, tolerance and initial number of fibers represented in the volume element.

2. Generate and solve random realizations until Criterion A is satisfied.
3. If Criterion B is satisfied, the RVE is found; Else, increase the number of fibers and repeat from step 2.

It is important to note that only $M_{\zeta_{con}\,\delta_{stab}}$ and $M_{\zeta_{iso}\,\delta_{stab}}$, including the stability criterion based on the convergence rate of the effective properties, necessarily require sequential increments of the number of fibers. However, an incremental approach was conducted for all methods in order to determine the smallest RVE possible. The estimated smallest RVE, for all methods, would have the least accurate effective properties. Such an approach will help conduct a more rigorous analysis of the validity of the different methods.

As for $M_{\delta_{iso}}$, all generated volumes were individually tested to find isotropic microstructures, as per Eq.3.20. The RVE size was considered as the volume element with the fewest fibers that satisfies the isotropy criterion δ_{iso}. The objective of $M_{\delta_{iso}}$ is not to test another determination criterion, but rather to investigate if a single isotropic microstructure is equivalent to a RVE, within a tolerance.

3.5 Numerical method

3.5.1 Numerical simulation

More than 1200 periodic microstructures were generated in MATLABR-2009a using a new modified RSA scheme presented in Appendix. Figure 3.1 presents a microstructure

Table 3.1 The RVE determination methods.

	Determination of r		**Determination of n**		**RVE**
Methods	Criterion A	Name	Criterion B	Name	Effective property
$M_{\zeta_{con}\,\delta_{stab}}$	$\zeta_{con} \leq tol$	Confidence	$\delta_{stab} \leq tol$	Stability	$\overline{k}^{r_1}_{n_1}$ in Eq.3.13
$M_{\zeta_{iso}\,\delta_{stab}}$	$\zeta_{iso} \leq tol$	Ensemble isotropy			
$M_{\zeta_{con}\,\delta_{dev}}$	$\zeta_{con} \leq tol$	Confidence	$\delta_{dev} \leq tol$	Deviation	$\overline{k}^{r}_{n}$
$M_{\zeta_{iso}\,\delta_{dev}}$	$\zeta_{iso} \leq tol$	Ensemble isotropy			
$M_{\zeta_{con}\,\delta_{av}}$	$\zeta_{con} \leq tol$	Confidence	$\delta_{av} \leq tol$	Averaging	$\widehat{k}^{r}_{n}$
$M_{\zeta_{iso}\,\delta_{av}}$	$\zeta_{iso} \leq tol$	Ensemble isotropy			
$M_{\delta_{iso}}$	NA	NA	$\delta_{iso} \leq tol$	Isotropy	$\widetilde{k}$

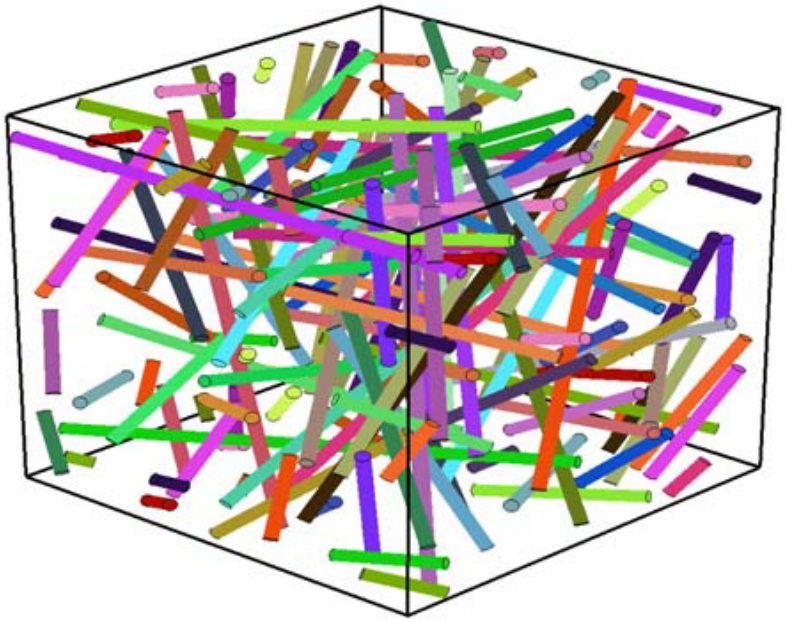

Figure 3.1 Generated microstructure using the modified RSA method with 50 randomly oriented fibers having an aspect ratio of 50 and 5% volume fraction.

generated using the modified RSA scheme containing 50 randomly oriented fibers of aspect ratio 50 with a 5% volume fraction. The geometries were meshed in ANSYS v12.0 using 10 nodes tetrahedron elements and solved in Abaqus/Standard v.6.10 under 6 different cases of displacement based periodic boundary conditions as stated in Eq.3.7, resulting in a total of more than 7200 FE analyses. FE models contained more than 12 million nodes for volumes containing 40 fibers with an aspect ratio of 60. Computations were performed on an IBM X server 7145-AC1 with 1.5 TB RAM and parallelized over 6 to 12 XEON X7550 cores.

3.5.2 Material properties

A high contrast of elastic properties of 300, for the bulk and shear moduli of the fibers over that of the matrix, was fixed in order to submit the RVE determination methods to a rigorous case typical of nanocomposite materials. The constituent properties, listed in Table

Table 3.2 Materials properties in GPa.

	Bulk modulus	Shear modulus
Matrix	1.67	0.77
Fibers	500	231

3.2, are similar to those of an epoxy matrix reinforced by single-walled carbon nanotube bundles (Liu *et al.*, 2005).

3.6 Results and discussions

3.6.1 Convergence of the RVE

Figures 3.2 a) and b) show the evolution of the ensemble mean bulk and shear moduli, respectively, for two aspect ratios of 20 and 30 and several number of fibers as a function of the number of realizations in the ensemble. The apparent properties shown in Figures 3.2 a) and b) were computed using Eq.3.15a. The properties in all figures are normalized with respect to that of the matrix, while the number of fibers represented in a volume is denoted by n and the fibers aspect ratio by AR. The bulk and shear moduli in Figures 3.2 a) and b) show similar trends. The confidence interval for all microstructures narrows as more realizations are included in the average properties. Volumes with fewer fibers are shown to have more scattering (i.e., larger confidence intervals) and usually required more realizations to satisfy the confidence criterion of Eq.3.9. For very few fibers in the volume (e.g., AR20n1 or AR30n10), it can be observed that the mean apparent properties, even after several realizations, are still distant apart from that observed for larger numbers of fibers (e.g., AR20n30 or AR30n30). This is a reproduction of the bias that (Kanit *et al.*, 2003) have observed for small volumes, once again showing the importance of determining effectively the RVE.

Figures 3.3 a) and b) show the evolution of the normalized mean bulk and shear moduli, respectively, for increasing number of fibers. Each point represents not a single realization but the ensemble of realizations that were computed. The solid lines with downward pointing triangles represent the arithmetic mean elastic properties obtained using Eq.3.16a and the dashed lines with empty circles represent the harmonic mean elastic properties computed using Eq.3.16b. Both means get closer to each other as the number of fibers increases. For AR < 20, the means quickly stabilize; however for higher AR the curves show a lower convergence rate and required larger volumes to stabilize. The higher the aspect ratio, the more difficult it was to generate microstructures with a high number of fibers. Usually, the last point of each curve in Figure 3.3 was the largest number of fibers that was practically possible to generate/mesh/solve with the available methods and computational resources.

3.6.2 Ensemble size criteria analysis

This section analyzes and compares the ensemble isotropy criterion ζ_{iso} and the confidence criterion ζ_{iso}. To test both criteria, we introduce the ensemble mean property error with

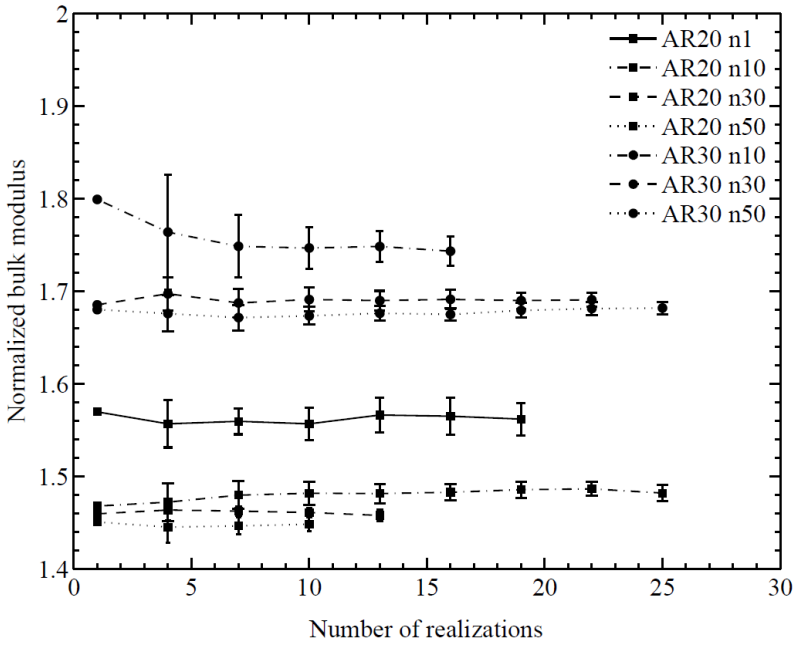

(a)

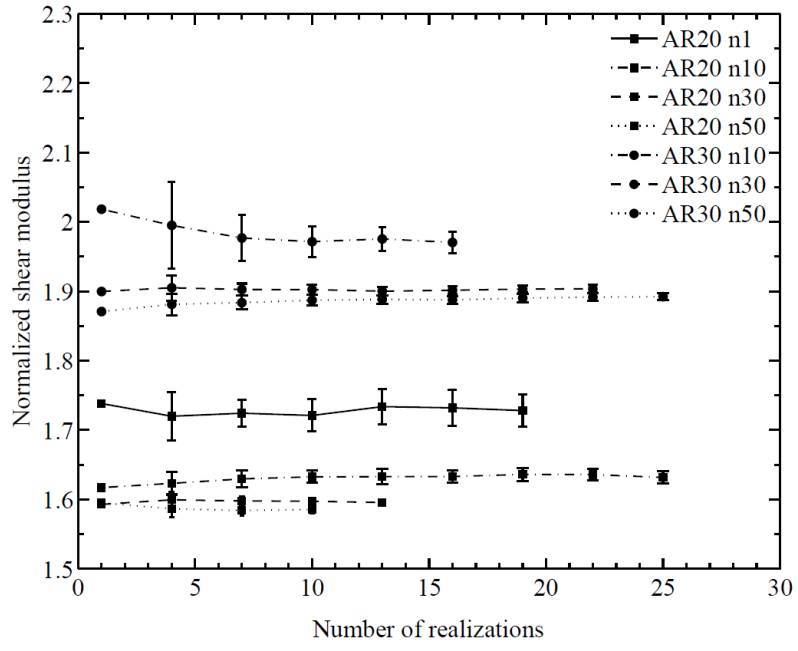

(b)

Figure 3.2 Normalized average apparent properties with respect of that of the matrix as a function of the number of realizations for fiber Aspect Ratios (AR) 20 and 30 and different number of fibers (n) ranging from 1 to 50. a) Normalized bulk modulus; b) Normalized shear modulus. The error bars represent a 95% confidence interval on the mean value.

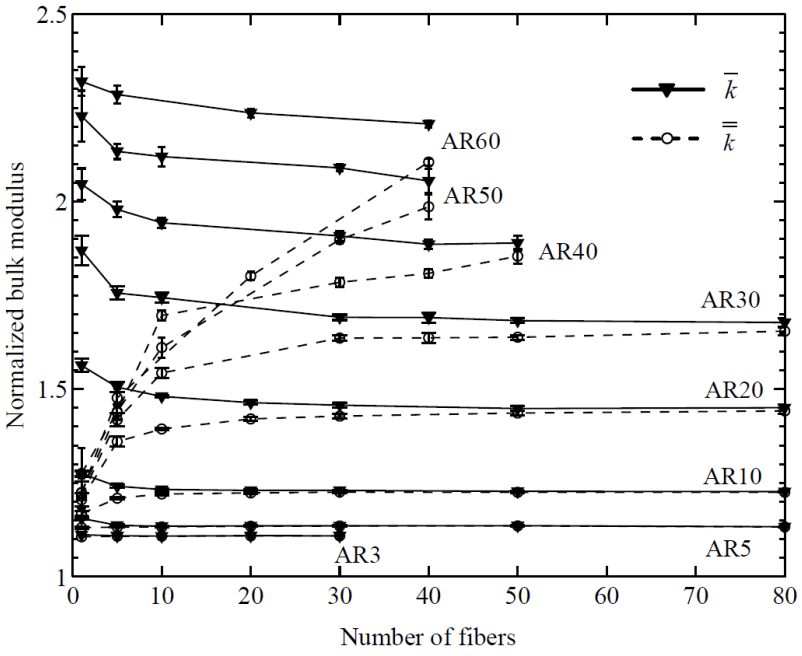

(a)

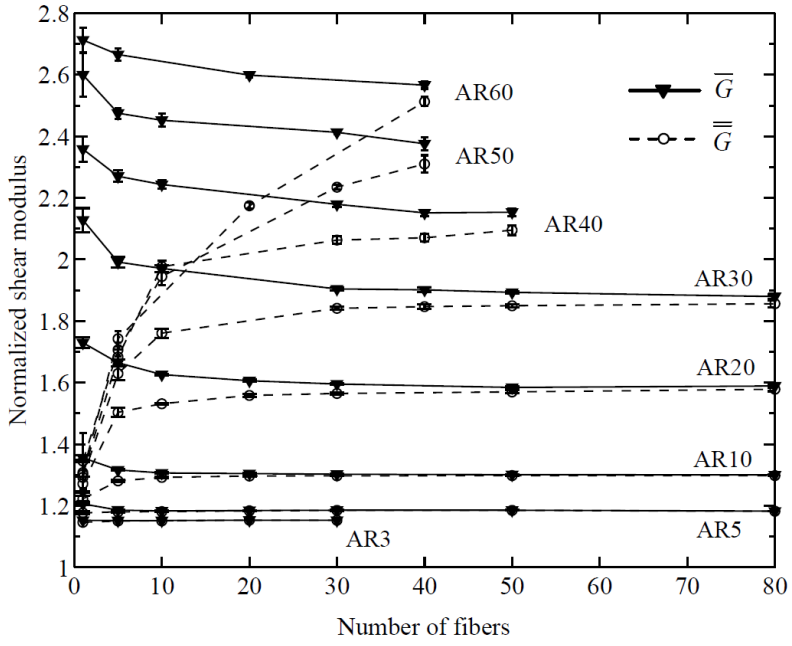

(b)

Figure 3.3 Normalized average apparent properties with respect of that of the matrix as a function of the number of fibers for different Aspect Ratios (AR). a) Normalized bulk modulus; b) Normalized shear modulus. The error bars represent a 95% confidence interval on the mean value.

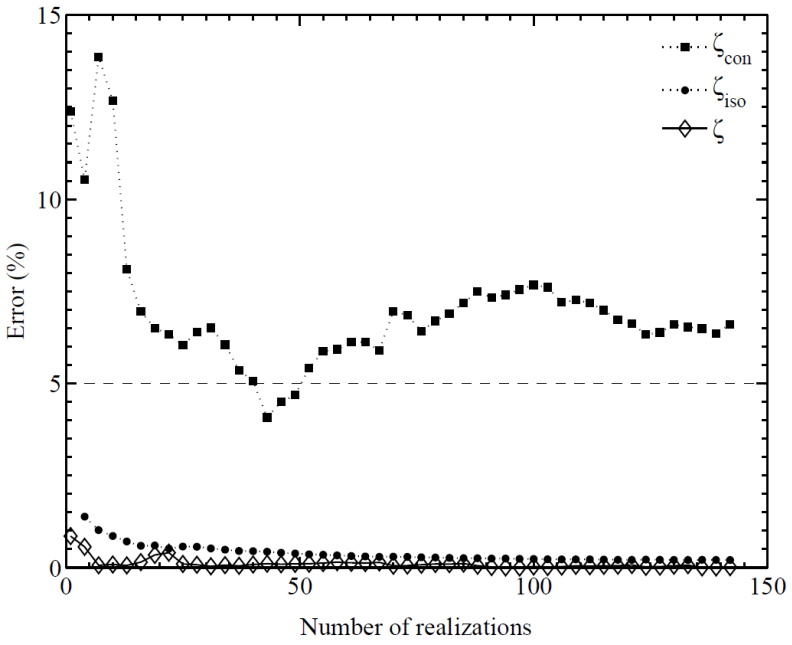

Figure 3.4 Evolution of the ensemble number of realizations criteria errors ζ_{con}, ζ_{iso} and ζ expressed in Eq.3.9, 3.10 and 3.21, respectively, as a function of the number of realizations in the ensemble for 10 fibers of aspect ratio 20. The dashed line represents the tolerance threshold of 5%.

respect to that of the whole population of possible microstructures that have the same number of fibers:

$$\zeta = \frac{\left|\overline{k}^{r} - \overline{k}^{r_{tot}}\right|}{\overline{k}^{r_{tot}}}, \tag{3.21}$$

where r_{tot} is very large. Therefore, ζ provides a rigorous comparison basis for the ensemble size criteria, namely, the confidence criterion ζ_{con} and the isotropy criterion ζ_{iso}. Figure 3.4 shows the evolution of ensemble number of realizations criteria errors ζ_{con} and ζ_{iso} computed using Eq.3.9 and 3.13, respectively, and the mean property error ζ using Eq.3.21 as a function of the number of realizations for microstructures with 10 fibers of aspect ratio 20 at 5% volume fraction and for r_{tot}=150 (i.e., 150 realizations were computed). The confidence criterion ζ_{con} is close to the mean property error ζ, both around 1% even for a low number of realizations. The ensemble isotropy criterion yields larger error values. Most importantly, the isotropy error ζ_{iso} does not vanish when increasing the ensemble's number of realizations. Same trends were observed for other aspect ratios. This indicates that the ensemble isotropy criterion ζ_{iso} is too strict and cannot always determine ensemble sizes. It is concluded that this criterion

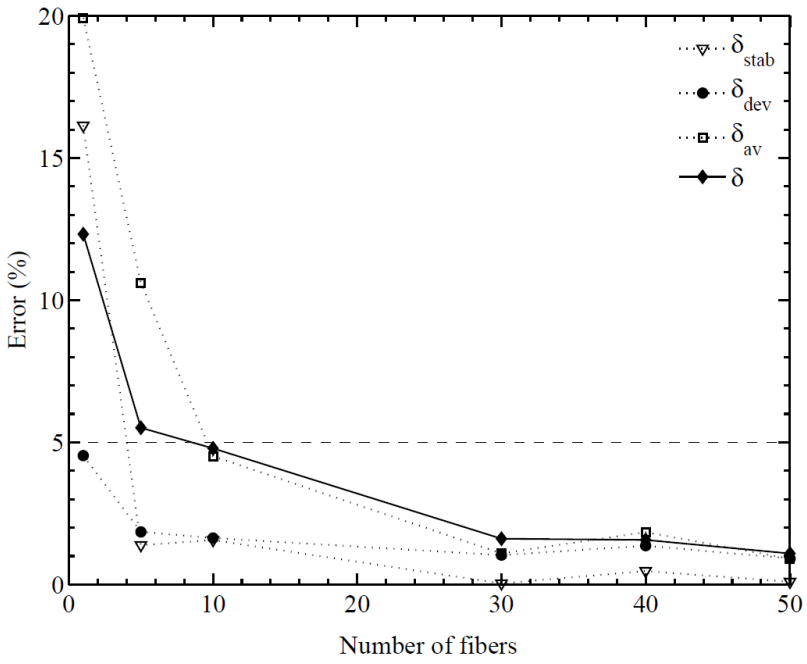

Figure 3.5 Evolution of the volume size criteria errors δ_{stab}, δ_{dev}, δ_{av} and δ expressed in Eq.3.13, 3.14, 3.19 and 3.22, respectively, as a function of the number of fibers represented for AR = 30. The dashed line represents the tolerance threshold of 5%.

is not ideal for the smallest RVE ensemble size determination.

3.6.3 Volume size criteria analysis

To analyze the property stability criterion δ_{stab}, the deviation criterion δ_{dev} and the averaging variations criterion δ_{av}, we introduce the effective property error with respect to the 'exact' effective properties of very large volumes:

$$\delta = \frac{\left|\overline{k}_n - \overline{k}_{n_{\max}}\right|}{\overline{k}_{n_{\max}}}, \tag{3.22}$$

where $n_{\max}$ indicates the largest volume size that was computed for a given aspect ratio, with enough realizations to satisfy the confidence criterion ζ_{con}. For AR $\leq$ 30, volume elements containing $n_{\max} = 80$ fibers were simulated and very low scattering of the effective properties was observed and both arithmetic and harmonic means were almost identical, as seen in Figure 3.3. We hereby assume that those largest volume sizes of $n_{\max} = 80$ simulated for AR $\leq$ 30 provide an accurate estimation of the effective properties. The results of those largest volume sizes are referred to as 'exact properties' and are used to validate the estimated effective properties of all methods listed in Table 3.1. Figure 3.5 shows the

volume size criteria δ_{stab}, δ_{dev} and δ_{av} computed with Eq.3.13, 3.14 and 3.19 and the effective property error δ computed with Eq.3.22 where $n_{\max} = 80$ at different volume sizes n for AR = 30. For each volume size, all errors have been computed using the same ensemble of realizations that satisfied the confidence criterion ζ_{con}. For the stability criterion in Eq.3.13, the number of fibers step was taken as $\Delta n = 10$. In Figure 3.5, the deviation criterion δ_{dev} was lower than the 5% tolerance threshold even for the smallest volume size including only one single fiber. In contrast, the effective property error δ is larger and is over the 5% tolerance threshold for the smallest volume size. This observation suggests that the deviation criterion δ_{dev} determines biased RVEs. Herein, a biased RVE designates a RVE which has effective properties errors that exceed the prefixed tolerance. The stability criterion δ_{stab} shows good agreement with the effective property error δ only for the smallest volume size. However, the stability criterion δ_{stab} decreases very quickly with increasing volume sizes. For volume sizes above one single fiber, effective property errors δ are exceedingly larger suggesting that the stability criterion δ_{stab} determines biased RVEs. The only criterion that is shown to be able to generate non-biased RVEs is the proposed averaging variation criterion δ_{av}. The averaging variation criterion shows very good agreement with the effective property error. A similar trend was observed for all aspect ratios AR$\leq$30.

3.6.4 RVE parameters

Following the RVE determination methods listed in Table 3.1, the RVE parameters (n_{RVE}, r_{RVE}) were determined, for $tol = 5\%$, and are listed in Tables 3.3 and 3.4 for the bulk and shear moduli, respectively. Other tolerance values were tested and are presented in

Table 3.3 RVE volume sizes n and number of realizations r for the bulk modulus at different aspect ratios for various determination Methods (M) with 5% tolerance. The last column indicates how many isotropic realizations were found over the ensemble size. When no RVE parameters are given, the RVE was not found.

	$M_{\zeta_{\text{con}}\,\delta_{\text{stab}}}$		$M_{\zeta_{\text{iso}}\,\delta_{\text{stab}}}$		$M_{\zeta_{\text{con}}\,\delta_{\text{dev}}}$		$M_{\zeta_{\text{iso}}\,\delta_{\text{dev}}}$		$M_{\zeta_{\text{con}}\,\delta_{\text{av}}}$		$M_{\zeta_{\text{iso}}\,\delta_{\text{av}}}$		$M_{\delta_{\text{iso}}}$	
AR	n	r	n	r	n	r	n	r	n	r	n	r	n	r/r_{tot}
3	1	5	1	5	1	5	1	5	1	5	1	5	1	2/30
5	5	5	5	5	1	5	1	6	1	5	1	6	5	2/20
10	5	5	5	5	1	5	1	13	1	5	5	5	10	3/27
20	5	5	–	–	1	5	10	38	5	5	20	26	–	–
30	5	5	–	–	1	6	–	–	10	5	–	–	–	–
40	10	5	–	–	1	9	–	–	30	5	–	–	–	–
50	5	5	–	–	5	5	–	–	30	5	–	–	–	–
60	1	7	–	–	1	7	–	–	40	5	–	–	–	–

Section 3.6.6. The same microstructure realizations were used for all determination methods investigated. It is observed in Tables 3.3 and 3.4 that $M_{\delta_{iso}}$ based on microstructure isotropy criterion δ_{iso}, as well as all methods that include the ensemble isotropy criterion ζ_{iso}, i.e. $M_{\zeta_{iso}\,\delta_{stab}}$, $M_{\zeta_{iso}\,\delta_{dev}}$ and $M_{\zeta_{iso}\,\delta_{av}}$, have not been able to find RVEs for AR > 20. Moreover, the results in Figures 3.3 a) and b) suggest that for an aspect ratio of 30, for example, the RVE should be reached as the property is seen to have converged. This confirms that the ensemble isotropy criterion ζ_{iso} and the single microstructure isotropy criterion are too strict. The last column in Table 3.3 shows the number of isotropic realizations found over the total number of realizations computed at that particular volume size. It can be concluded that finding isotropic realizations using δ_{iso} is not a trivial process. In contrast, the methods including the confidence criterion ζ_{con}, i.e. $M_{\zeta_{con}\,\delta_{stab}}$, $M_{\zeta_{con}\,\delta_{dev}}$ and $M_{\zeta_{con}\,\delta_{av}}$, reach the RVE for all volume sizes. It is also observed that $M_{\zeta_{con}\,\delta_{av}}$, including the averaging variation criterion delivers the largest RVE sizes, whereas $M_{\zeta_{con}\,\delta_{dev}}$ generally yielded smallest RVEs containing one single fiber.

3.6.5 Effective properties

Tables 3.5 and 3.6 present for all methods the estimated effective bulk and shear moduli, respectively. Also included in Tables 3.5 and 3.6 are the 'exact properties' determined using the larger number of fibers $n_{max} = 80$ for ARs up to 30. The errors of the estimated effective properties of the different methods with respect to the 'exact properties' are also presented in Tables 3.5 and 3.6.

For all methods that include the ensemble isotropy criterion ζ_{iso}, i.e. $M_{\zeta_{iso}\,\delta_{stab}}$, $M_{\zeta_{iso}\,\delta_{dev}}$

Table 3.4 RVE volume sizes n and number of realizations r for the shear modulus at different aspect ratios for various determination Methods (M) with 5% tolerance. The last column indicates how many isotropic realizations were found over the ensemble size. When no RVE parameters are given, the RVE was not found.

	$M_{\zeta_{con}\,\delta_{stab}}$		$M_{\zeta_{iso}\,\delta_{stab}}$		$M_{\zeta_{con}\,\delta_{dev}}$		$M_{\zeta_{iso}\,\delta_{dev}}$		$M_{\zeta_{con}\,\delta_{av}}$		$M_{\zeta_{iso}\,\delta_{av}}$		$M_{\delta_{iso}}$	
AR	n	r	n	r	n	r	n	r	n	r	n	r	n	r/r_{tot}
3	1	5	1	5	1	5	1	5	1	5	1	5	1	2/30
5	5	5	5	5	1	5	1	6	1	5	1	6	5	2/20
10	5	5	5	5	1	5	1	13	1	5	5	5	10	3/27
20	5	5	–	–	1	5	10	38	5	5	20	26	–	–
30	5	5	–	–	1	6	–	–	10	5	–	–	–	–
40	10	5	–	–	5	5	–	–	30	5	–	–	–	–
50	5	5	–	–	5	5	–	–	30	5	–	–	–	–
60	–	–	–	–	1	15	–	–	40	5	–	–	–	–

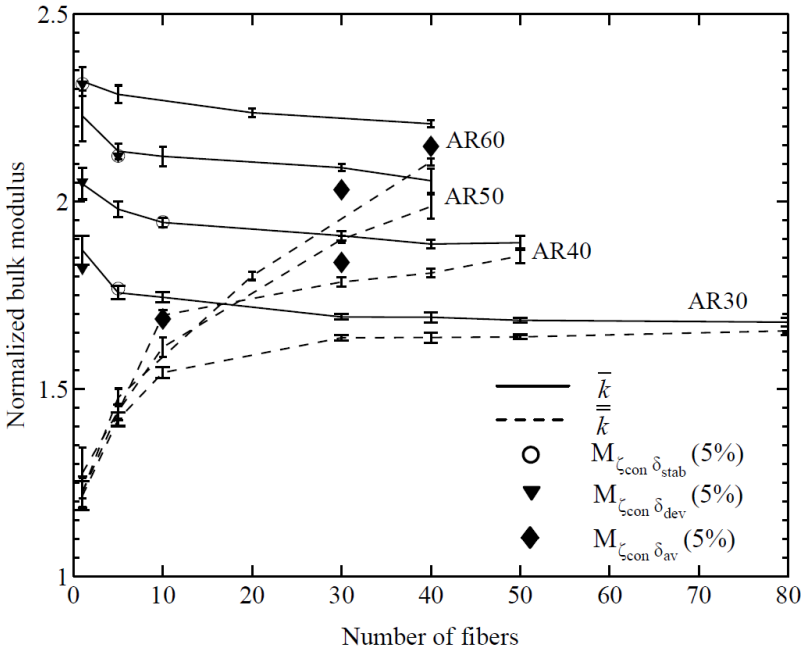

(a)

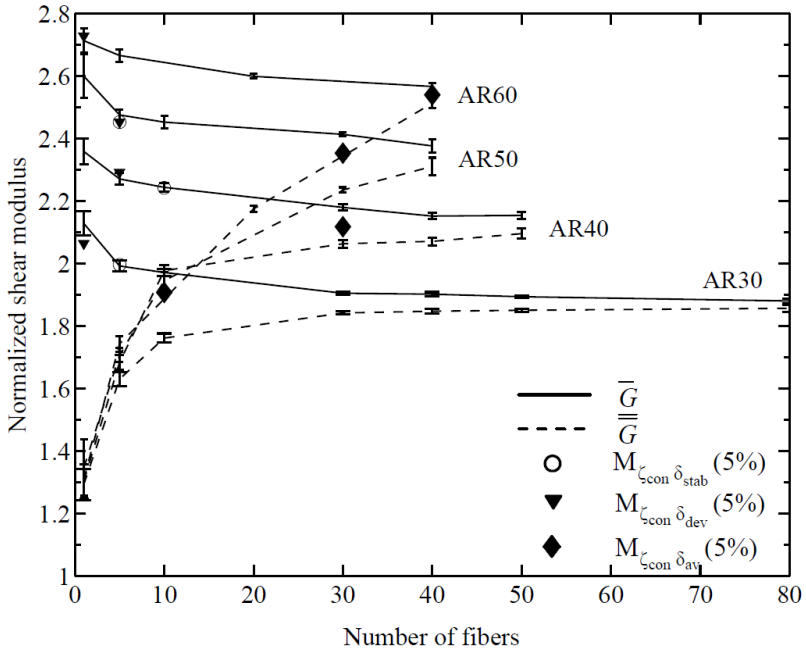

(b)

Figure 3.6 Normalized properties with respect of that of the matrix as a function of the number of fibers and the RVE results using methods $M_{\zeta_{con}\,\delta_{stab}}$, $M_{\zeta_{con}\,\delta_{dev}}$ and $M_{\zeta_{con}\,\delta_{av}}$ at 5% tolerance. a) Normalized bulk modulus; b) Normalized shear modulus. The error bars represent a 95% confidence interval on the mean value.

and $M_{\zeta_{iso}\,\delta_{av}}$, whenever the RVE was found, the corresponding effective properties are relatively accurate (error under 5%), with the lowest errors found when combined with the averaging criterion δ_{av} in $M_{\zeta_{iso}\,\delta_{av}}$ (1% error or lower).

As for methods that include the confidence criterion ζ_{con}, $M_{\zeta_{con}\,\delta_{stab}}$ and $M_{\zeta_{con}\,\delta_{dev}}$ based on the stability criterion δ_{stab} and the deviation criterion δ_{dev}, respectively, produce errors, with respect to 'exact properties', that increase with higher aspect ratio values. The errors reach 6% and 10% at AR= 30 for $M_{\zeta_{con}\,\delta_{stab}}$ and $M_{\zeta_{con}\,\delta_{dev}}$, respectively. In contrast, RVE volume sizes determined as per $M_{\zeta_{con}\,\delta_{av}}$ show very low errors (1% or lower) for aspect ratios up to 30.

The realizations which were found to satisfy the isotropy criterion δ_{iso} provided exceedingly accurate effective properties with practically zero errors with respect to 'exact properties', as seen in Tables 3.5 and 3.6. This indicates that for the case of ROFRCs under study, whenever an isotropic realization is found, it can serve as an accurate RVE.

To assess the estimated effective properties for AR=30, they are compared with FE results for all the number of fibers simulated as in Figures 3.6 a) and b) for the bulk and shear moduli, respectively. It can be seen in Figures 3.6 a) and b) that, for $M_{\zeta_{con}\,\delta_{stab}}$ and $M_{\zeta_{con}\,\delta_{dev}}$, the determined RVEs for all aspect ratios show a bias. The stability criterion δ_{stab} induced bias in $M_{\zeta_{con}\,\delta_{stab}}$ can be explained by the fact that the effective properties of ROFRCs with high aspect ratios of fibers have a low converging rate, lower than the 5% tolerance, with increasing number of fibers. However, the stability criterion is expected, in principle, to identify accurate RVEs if the tolerance was arbitrarily small. Therefore, to be able to identify the real RVE using the properties stability criterion, a convergence study has also to be performed on the choice of tolerance. The choice of tolerance values is discussed in the following section. Also

Table 3.5 RVE effective normalized bulk modulus at different aspect ratios for various determination Methods (M) with 5% tolerance. When no properties are given, the RVE was not found. The errors are computed in respect to the 'exact' results (final column).

	$M_{\zeta_{con}\,\delta_{stab}}$	$M_{\zeta_{iso}\,\delta_{stab}}$	$M_{\zeta_{con}\,\delta_{dev}}$	$M_{\zeta_{iso}\,\delta_{dev}}$	$M_{\zeta_{con}\,\delta_{av}}$	$M_{\zeta_{iso}\,\delta_{av}}$	$M_{\delta_{iso}}$	**Exact**
AR	k/k_m *er.*	k/k_m *er.*	k/k_m *er.*	k/k_m *er.*	k/k_m *er.*	k/k_m *er.*	k/k_m *er.*	k/k_m
3	1.11 0%	1.11 0%	1.11 0%	1.11 0%	1.11 0%	1.11 0%	1.11 0%	1.11
5	1.14 0%	1.14 0%	1.15 1%	1.15 2%	1.14 0%	1.14 0%	1.13 0%	1.13
10	1.24 2%	1.24 2%	1.27 4%	1.27 4%	1.22 0%	1.22 0%	1.22 0%	1.23
20	1.51 5%	– –	1.56 7%	1.48 2%	1.46 1%	1.44 1%	– –	1.45
30	1.77 6%	– –	1.82 9%	– –	1.69 1%	– –	– –	1.68
40	1.94 –	– –	2.03 –	– –	1.84 –	– –	– –	–
50	2.12 –	– –	2.12 –	– –	2.03 –	– –	– –	–
60	2.31 –	– –	2.31 –	– –	2.15 –	– –	– –	–

seen in Figures 3.6 a) and b), $M_{\zeta_{con}\,\delta_{av}}$ is the only method to provide realistic estimations of effective properties for all aspect ratios.

Another substantial benefit of $M_{\zeta_{con}\,\delta_{av}}$ is that it does not necessarily require a series of computations on subsequent volumes sizes to determine the RVE. If the first guess volume size satisfies Eq.3.13, there is no need for incrementing the volume size. In contrast, the methods based on the stability criterion require a series of computations for increasing volume sizes. Therefore, $M_{\zeta_{con}\,\delta_{av}}$ helps reducing the computational time of the whole RVE determination process.

3.6.6 Tolerance analysis

The real errors of the estimated effective properties of all methods are that which are calculated with respect to the 'exact properties'. Even though the different tolerance definitions have different meanings than that of the real error, it would be very useful that a method estimates effective properties yielding errors, with respect to the exact results, which are equal or lower than the initial tolerance value. Such a method would ensure that the real errors of effective properties estimations are lower than the chosen tolerance value. To analyze the effect of tolerance choice, $M_{\zeta_{con}\,\delta_{stab}}$, $M_{\zeta_{con}\,\delta_{dev}}$ and $M_{\zeta_{con}\,\delta_{av}}$ were performed for tolerances varying from 1% to 5%. Figure 3.7 presents the estimated effective properties errors, with respect to the 'exact properties', using the three RVE determination methods ($M_{\zeta_{con}\,\delta_{stab}}$, $M_{\zeta_{con}\,\delta_{dev}}$ and $M_{\zeta_{con}\,\delta_{av}}$) for fibers aspect ratio of 30. The dashed line represents the case of equality between the tolerance and the error value. An appropriate RVE determination method should yield errors lower or equal to the tolerance value. $M_{\zeta_{con}\,\delta_{stab}}$ and

Table 3.6 RVE effective normalized shear modulus at different aspect ratios for various determination Methods (M) with 5% tolerance. When no properties are given, the RVE was not found. The errors are computed in respect to the 'exact' results (final column).

	$M_{\zeta_{con}\,\delta_{stab}}$		$M_{\zeta_{iso}\,\delta_{stab}}$		$M_{\zeta_{con}\,\delta_{dev}}$		$M_{\zeta_{iso}\,\delta_{dev}}$		$M_{\zeta_{con}\,\delta_{av}}$		$M_{\zeta_{iso}\,\delta_{av}}$		$M_{\delta_{iso}}$		**Exact**
AR	G/G_m	*er.*	G/G_m	*er.*	G/G_m	*er.*	G/G_m	*er.*	G/G_m	*er.*	G/G_m	*er.*	G/G_m	*er.*	G/G_m
3	1.15	0%	1.15	0%	1.15	0%	1.15	0%	1.15	0%	1.15	0%	1.15	0%	1.15
5	1.18	0%	1.18	0%	1.20	1%	1.20	2%	1.19	0%	1.19	0%	1.18	0%	1.18
10	1.32	2%	1.32	2%	1.35	4%	1.36	4%	1.29	1%	1.29	0%	1.30	0%	1.30
20	1.66	5%	–	–	1.72	8%	1.63	2%	1.59	0%	1.58	0%	–	–	1.59
30	2.00	6%	–	–	2.06	10%	–	–	1.91	1%	–	–	–	–	1.88
40	2.24	–	–	–	2.29	–	–	–	2.12	–	–	–	–	–	–
50	2.45	–	–	–	2.45	–	–	–	2.35	–	–	–	–	–	–
60	–	–	–	–	2.73	–	–	–	2.54	–	–	–	–	–	–

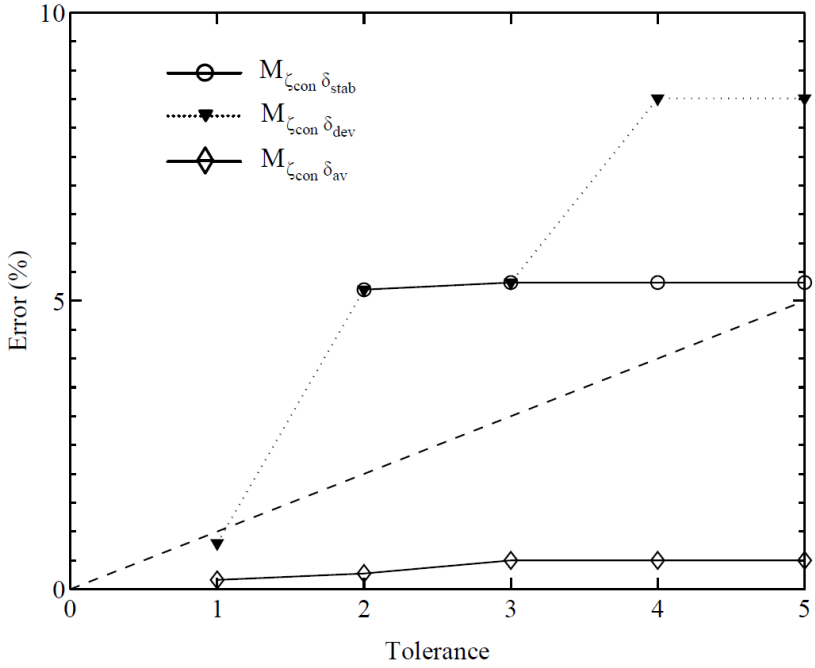

Figure 3.7 Relative errors of the effective bulk modulus of RVEs determined using methods $M_{\zeta_{con}\,\delta_{stab}}$, $M_{\zeta_{con}\,\delta_{dev}}$ and $M_{\zeta_{con}\,\delta_{av}}$ with respect to the 'exact properties', for different values of tolerance and for AR=30. The dashed line represents the desired tolerance.

$M_{\zeta_{con}\,\delta_{dev}}$ show errors larger than the tolerance value. The $M_{\zeta_{con}\,\delta_{av}}$, based on the confidence and averaging variation criteria, is the only method to show acceptable errors for all tolerance choices.

3.6.7 RVE size correlation

Here we attempt to investigate the existence of a correlation between any RVE related parameter (e.g. RVE edge length) and geometrical parameters of the microstructure (e.g. aspect ratio of fibers). Any correlation could provide a firsthand tool for a quick estimation of the RVE size without performing any FE computations. Harper *et al.* (2012) determined the RVEs of randomly oriented carbon fiber composites simplified in 2D representations using an embedded cell FE approach. They observed that the results always converged at the same RVE edge length which is about 4 times larger than the fiber length (tested for three aspect ratios: 1.8, 3.6 and 7.1 and two volume fractions: 30% and 50%). Figure 3.8 shows the RVE edge length normalized with respect to the fiber edge length as a function of the aspect ratio. All results are those of the RVEs determined using $M_{\zeta_{con}\,\delta_{av}}$ for both bulk and shear moduli for a tolerance of 5%. The RVE normalized edge length is shown to be constant for aspect ratios

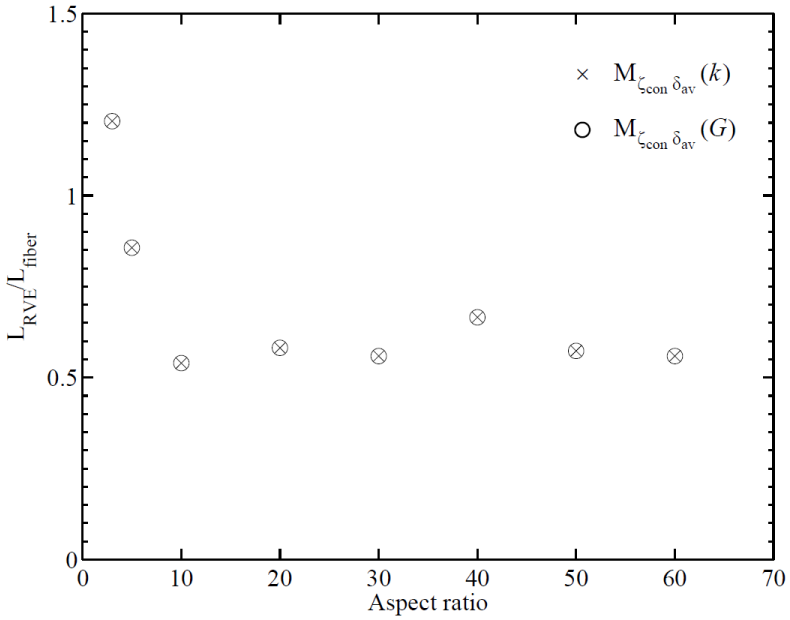

Figure 3.8 Correlation between the RVE edge length $\mathbf{L}_{RVE}$ with respect to the length of the fibers represented $\mathbf{L}_{fiber}$ as a function of the fibers aspect ratio. Represented RVEs data were determined using $M_{\zeta_{con}\,\delta_{av}}$ at 5% tolerance for bulk and shear moduli.

of 10 or larger. However, the RVE normalized edge length value (around 0.5) is strictly lower than the normalized RVE length value of 4 that was stated by (Harper *et al.*, 2012). This finding, based on 3D simulations and rigorous RVE determination, can provide guidelines to estimate the RVE size for a specified aspect ratio without any computation, reducing further the RVE determination computational costs. It should be noted, however, that this value is restricted to the mechanical properties simulated. It is expected that lower contrasts between the constituents' properties or lower volume fractions should lead to smaller RVE sizes.

3.7 Conclusions

Several RVE determination methods have been presented and tested for the determination of both RVE parameters (n_{RVE}, r_{RVE}). The RVE was determined using different criteria separated in two sub-categories: ensemble size criteria and volume size criteria. The most important conclusions of the study are summarized in the following:

1. The property stability criterion, which is the most commonly used criterion for RVE determination, as well as the standard deviation criterion are inappropriate for determining RVEs of ROFRCs with high aspect ratios of fibers.

2. Single microstructures that yield isotropic elasticity tensors, within a tolerance, yield accurate effective properties. However, it becomes very difficult to obtain isotropic microstructures for high aspect ratios. This criterion could be added as an exit condition into a RVE determination algorithm in order to reduce further the computational time if, by chance, a realization meeting this criterion was obtained.
3. The newly proposed averaging criterion computes accurate estimations of ROFRCs effective properties, within a given tolerance. Moreover, the averaging criterion does not necessitate the computation of the apparent properties at different volume sizes to study the convergence, as the stability criterion does. This reduces substantially the computational cost related to the RVE determination process.
4. The RVE edge length was found to be around half the fiber length for aspect ratios larger than 10, allowing firsthand quick estimations of RVE sizes.

The above-mentioned findings have two major impacts on existing and future works:

1. The validity of all studies relying on the property stability criterion is under question. In fact, the criterion was also not assessed, to the author's knowledge, for other types of microstructures.
2. ROFRCs RVE determination cost is reduced due to the new proposed criterion and to the RVE size firsthand estimation, hence guiding the way towards numerical homogenization of high cost microstructures such as nanocomposites with very high aspect ratio reinforcements.

However, in order to achieve higher volume fractions, and especially larger aspect ratios, further advancements should be made in the microstructure generation method. In addition, cost-efficient mesh-free techniques should be sought for solving volume elements containing fibers of larger aspect ratios that are impossible to solve with the current computational resources.

3.8 Acknowledgment

The work of Hadi Moussaddy was funded by the National Science and Engineering research Council of Canada (NSERC). Most of the computations were performed on supercomputers financed by the Canadian Foundation for Innovation (CFI) and the NSERC. These computers are hosted by the Fluid Dynamics Laboratory (LADYF) of École Polytechnique de Montréal.

APPENDIX - Modified RSA

We propose an extension for the RSA algorithm in order to facilitate the generation of higher volume fractions and aspect ratios in random packings of straight fibers. In this modified algorithm, fibers are considered as straight cylinders having the same aspect ratio and same dimensions. A single modification to the RSA classical scheme is implemented when overlapping occurs, i.e. when the distance between a newly generated fiber *f2* and an existing fiber *f1* is less than the fixed minimum distance e between two accepted fibers.

Let the minimum distance vector from the first fiber *f1* axis to the newly generated fiber *f2* axis be noted v_{12}. The second fiber *f2* is translated following the v_{12} direction to satisfy the minimum distance requirement. The vector of translation $\mathbf{d}$ is expressed by:

$$\mathbf{d} = e \ \frac{\mathbf{v}_{12}}{\|\mathbf{v}_{12}\|} \tag{A.1}$$

Following the translation, the distances between the translated fiber *f2* and all other existing fibers axes are verified. If the minimum distance is not satisfied, the fiber *f2* is removed, and a new random fiber position and orientation are generated. Using this algorithm with a zero inter-fiber minimum distance, volume fractions up to 38% and 29% were generated for ROFRCs with aspect ratios 10 and 30, respectively. Figure 3.1 shows an example of a ROFRC generated using the modified RSA method. The microstructure contains 50 randomly oriented fibers of aspect ratio 50 at 5% volume fraction. The microstructure is periodic, meaning that a fiber that crosses one surface of the volume penetrates back from the opposite surface. This condition is imperative in order to obtain identical FE meshes on opposite sides and, consequently, to apply periodic boundary conditions as expressed in Eq.3.1.

CHAPTER 4

ARTICLE 2: Evaluation of analytical homogenization models for randomly oriented and high aspect ratio fiber reinforced composites

H. Moussaddy, M. Pahlavanpour, D. Therriault, M. Lévesque (2013). Submitted to: "*Composites Part B: Engineering*".

4.1 Abstract

The elastic properties of Randomly Oriented Fiber Reinforced Composites (ROFRC) were determined using 1) analytical micromechanical models and 2) Finite Element (FE) homogenization of the Representative Volume Element (RVE). Accurate effective elastic properties of ROFRCs were computed through a rigorous RVE determination process involving the FE computation of more than 2500 three-dimensional (3D) microstructures. The FE computations were performed for different volume fractions, fibers aspect ratios and properties of constituents. The FE accurate results were compared to analytical models such as that of Mori-Tanaka, in order to assess the accuracy of the latter. It was determined that the two-step Lielens/Voigt model provides more accurate estimations for most studied cases up to an aspect ratio of approximately 90. These findings allow the future utilization of the appropriate analytical model for very quick and accurate calculation of effective properties. For fiber aspect ratios higher than 90, no model provided accurate estimations of the bulk and shear moduli. Furthermore, the stiffness saturation aspect ratio was determined to be approximately 90. The latter finding is also of a major impact since it creates the possibility for the numerical study of composites with very high aspect ratios fibers that are currently impossible to solve in regard to their computational cost.

4.2 Introduction

Numerous micromechanical analytical models have been reported in the literature for predicting the mechanical properties of Randomly Oriented Fiber Reinforced Composites (ROFRC) (Benveniste, 1987; Schjodt-Thomsen and Pyrz, 2001; Pierard *et al.*, 2004). Thanks to their relative low computational costs, analytical models can be very useful in many applications. However, their accuracy at predicting the elastic properties of ROFRCs has not been rigorously evaluated yet, especially for fibers with high aspect ratios $\rho > 5$, $\rho = l_f/d_f$,

where l_f is the fiber length and d_f its diameter. On the other hand, numerical homogenization techniques, like the Finite Element (FE) method, can deliver accurate effective properties of composite microstructures, provided that Representative Volume Elements (RVE) are simulated. The determination of the RVE is a complex process that induces very high computational costs, especially for high fibers aspect ratios. Recently, Moussaddy *et al.* (2013) analyzed the RVE determination process for ROFRCs and demonstrated that traditional RVE determination techniques are invalid. They proposed a new RVE determination method that was successful at determining accurate elastic properties of ROFRCs with less computational costs (tested at 5% volume fraction for $\rho \leq 60$).

The numerical results of appropriately determined RVEs can be used to assess the accuracy of analytical models. The assessment of analytical models has been conducted for composites reinforced by aligned fibers using FE numerical method (Tucker III and Liang, 1999) and for spheres reinforced composites using a numerical scheme based on the Fast Fourier Transforms (FFT) (Ghossein and Lévesque, 2012), among other studies. In contrast, very few works have compared the analytical models predictions to that of numerical simulations for ROFRCs. Several studies have been limited to a low fibers aspect ratio of 5 (Böhm *et al.*, 2002; Hua and Gu, 2013; Kari *et al.*, 2007) and found good agreement between numerical results and the predictions of the Mori-Tanaka model and self-consistent scheme. Other studies dealt with high aspect ratios for very low volume fractions ($\rho \leq 60$ and volume fractions up to 3% in (Mortazavi *et al.*, 2013) and $\rho \leq 200$ and volume fractions up to 1% in (Lusti and Gusev, 2004)). However, the RVE was not determined in those works, and the important scattering in the results observed in some cases (Mortazavi *et al.*, 2013) questions the validity of these results. Moreover, all those studies (Böhm *et al.*, 2002; Hua and Gu, 2013; Kari *et al.*, 2007; Mortazavi *et al.*, 2013; Lusti and Gusev, 2004) did not cover a wide range of fibers volume fraction, aspect ratio nor stiffness.

The objective of this work is to assess the accuracy of the analytical models reported in literature for ROFRCs, with regard to their elastic moduli estimations. The assessment is conducted by comparing the analytical models elastic moduli predictions to that of FE simulations using rigorously determined RVEs. The work is preformed for a wide range of fibers aspect ratios, volume fractions and contrasts of properties (elastic properties fibers/matrix).

Section 4.3 reviews the analytical models for predicting the elastic properties of ROFRCs. The methodology for FE homogenization and the RVE determination process are presented in Section 4.4. The analytical models estimations are compared to the computed FE results in Section 4.5. Section 4.6 discusses the results and identifies the application ranges and accuracies of the tested models. Finally, Section 4.7 concludes this work.

4.3 Analytical models

The analytical models studied in this work are categorized as *one-* and *two-step* models. In one-step models, the overall properties of ROFRCs are calculated in a single homogenization step whereas a combination of two models are sequentially used in the second approach.

4.3.1 One-step methods

Benveniste (Benveniste, 1987) used the Mori-Tanaka (M-T) method to describe composites with randomly oriented inclusions. The stiffness tensor is evaluated with the orientational average as:

$$\mathbf{C}^{\text{M-T}} = \mathbf{C}_\text{m} + c_\text{f}\{(\mathbf{C}_\text{f} - \mathbf{C}_\text{m}) : \mathbf{T}\} : [c_\text{m}\mathbf{I} + c_\text{f}\{\mathbf{T}\}]^{-1}, \tag{4.1}$$

where $\mathbf{C}$ and c denote the stiffness tensor and the volume fraction, respectively. Subscripts 'm' and 'f' represent the matrix and fiber, respectively, and curly brackets $\{.\}$ stand for orientation averaging. Tensor $\mathbf{T}$ is given by:

$$\mathbf{T} = [\mathbf{I} + \mathbf{S}_\text{m} : \mathbf{C}_\text{m}^{-1} : (\mathbf{C}_\text{f} - \mathbf{C}_\text{m})]^{-1} \tag{4.2}$$

where $\mathbf{S}_\text{m}$ is Eshelby's tensor (Eshelby, 1957).

The so-called *Dilute* (Dil) estimation for low volume fraction composites is expressed as:

$$\mathbf{C}^{\text{Dil}} = \mathbf{C}_\text{m} + c_\text{f}(\mathbf{C}_\text{f} - \mathbf{C}_\text{m}) : \{\mathbf{T}\} \tag{4.3}$$

Similarly, the Self-Consistent (SC) scheme (Hill, 1965; Budiansky, 1965) for randomly oriented inclusions is expressed by:

$$\mathbf{C}^{\text{SC}} = \mathbf{C}_\text{m} + c_\text{f}(\mathbf{C}_\text{f} - \mathbf{C}^{\text{SC}}) : \{\mathbf{T}^{\text{SC}}\} \tag{4.4}$$

where $\mathbf{T}^{\text{SC}}$ is given by:

$$\mathbf{T}^{\text{SC}} = [\mathbf{I} + \mathbf{S}^{\text{SC}} : \mathbf{C}^{\text{SC}-1} : (\mathbf{C}_\text{f} - \mathbf{C}^{\text{SC}})]^{-1} \tag{4.5}$$

Eq.4.4 is an implicit problem that is iteratively solved since the elastic tensor of the composite $\mathbf{C}^{\text{SC}}$ and Eshelby's tensor $\mathbf{S}^{\text{SC}}$ are initially unknown.

The only other explicit one step methods for ROFRCs are, to the author's knowledge, the model of Ponte-Castañeda and Willis (1995) and the double inclusion method (Hori and Nemat-Nasser, 1993). It has been proved that both models are equivalent for ROFRCs (Hu and Weng, 2000a). However, their analytical estimates have a limited range of allowable

volume fractions ($c_\mathrm{f} \leq 1/\rho^2$) due to assumptions on the composites microstructure (Ponte-Castañeda and Willis, 1995). Consequently, the allowable volume fractions are found to be limited under 1% and 0.01% for fibers with aspect ratios of 10 and 100, respectively, which is unpractical for the purpose of this work. When exceeding the volume fraction limit, the Ponte-Castañeda and Willis estimates have been shown to lie outside the Hashin-Shtrikman bounds (Hu and Weng, 2000b).

4.3.2 Two-step methods

The two-step homogenization approach has been originally suggested by Camacho *et al.* (1990) and later on studied by Pierard *et al.* (2004). In two-step methods, the RVE is decomposed into a number of discrete subregions α ($\alpha = 1, 2, \ldots n$) where the fibers are aligned along an arbitrary direction. The homogenized elastic tensor of each subregion, $\mathbf{C}_\alpha$, is calculated in a first step and homogenization over all subregions is performed in a second step, as illustrated in Fig. 4.1.

First step: homogenization of each subregion

Each subregion is considered as a two-phase aligned fiber composite. The overall elasticity tensor of a subregion, $\mathbf{C}_\alpha$, is computed from:

$$\mathbf{C}_\alpha = \mathbf{C}_\mathrm{m} + c_\mathrm{f}[(\mathbf{C}_\mathrm{f} - \mathbf{C}_\mathrm{m})] : \mathbf{A}, \tag{4.6}$$

where $\mathbf{A}$ denotes the strain-localization tensor.

The first given expression of $\mathbf{A}$ is that for dilute composites as (Eshelby, 1957):

$$\mathbf{A}^\mathrm{Dil} = \mathbf{T}. \tag{4.7}$$

In the Mori-Tanaka model, $\mathbf{A}$ is given by:

$$\mathbf{A}^\mathrm{M\text{-}T} = \mathbf{T} : [c_\mathrm{m}\mathbf{I} + c_\mathrm{f}\mathbf{T}]^{-1}, \tag{4.8}$$

In the SC scheme (Hill, 1965; Budiansky, 1965), the strain-localization tensor is expressed as:

$$\mathbf{A}^\mathrm{SC} = [\mathbf{I} + \mathbf{S}_\alpha : {\mathbf{C}_\alpha}^{-1} : (\mathbf{C}_\mathrm{f} - \mathbf{C}_\alpha)], \tag{4.9}$$

where $\mathbf{S}_\alpha$ is Eshelby's tensor where the infinite media is the effective composite.

Lielens *et al.* (1998) proposed a model (Li) that interpolates between the upper and lower

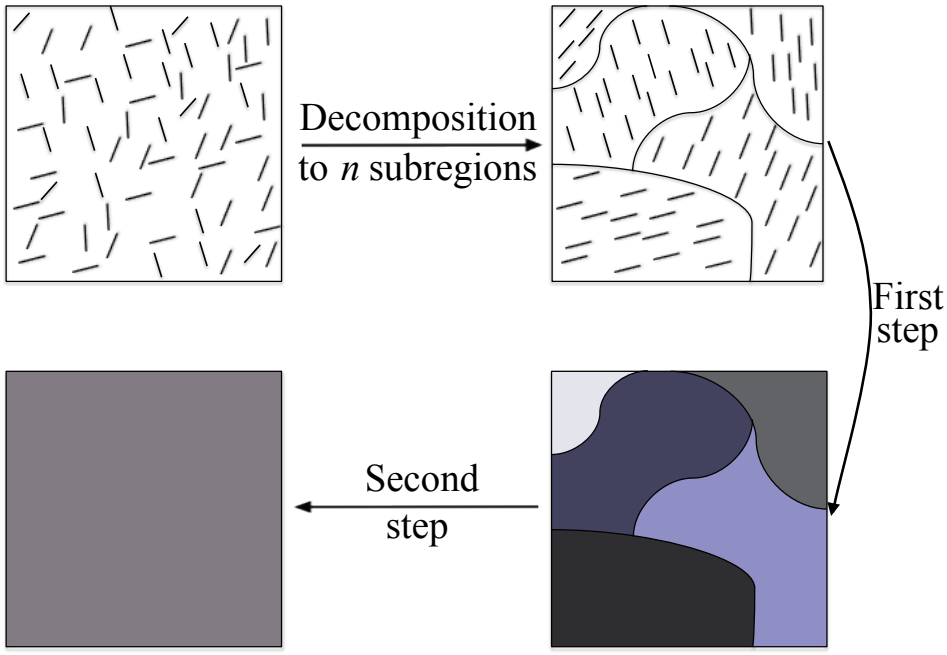

Figure 4.1 Two-step method: Decomposition of RVE to a set of subregions. Each subregion is individually homogenized in the first step. In the second step, homogenization is performed over all the subregions.

Hashin-Shtrikman bounds for aligned reinforcements and reads as:

$$\mathbf{A}^{\mathrm{Li}} = \hat{\mathbf{A}}^{\mathrm{Li}}[(1 - c_{\mathrm{f}})\mathbf{I} + c_{\mathrm{f}}\hat{\mathbf{A}}^{\mathrm{Li}}]^{-1}, \tag{4.10}$$

where

$$\hat{\mathbf{A}}^{\mathrm{Li}} = \{(1 - c^*)[\hat{\mathbf{A}}^{\mathrm{lower}}]^{-1} + c^*[\hat{\mathbf{A}}^{\mathrm{upper}}]^{-1}\}^{-1}, \tag{4.11}$$

and c^* is related to the reinforcements volume fraction as:

$$c^* = \frac{c_{\mathrm{f}} + c_{\mathrm{f}}^2}{2}. \tag{4.12}$$

$\hat{\mathbf{A}}^{\mathrm{lower}}$ and $\hat{\mathbf{A}}^{\mathrm{upper}}$ are expressed as:

$$\hat{\mathbf{A}}^{\mathrm{lower}} = [\mathbf{I} + \mathbf{S}_m : (\mathbf{C}_{\mathrm{m}})^{-1} : (\mathbf{C}_{\mathrm{f}} - \mathbf{C}_{\mathrm{m}})]^{-1}, \tag{4.13a}$$

$$\hat{\mathbf{A}}^{\mathrm{upper}} = [\mathbf{I} + \mathbf{S}_{\mathrm{f}} : (\mathbf{C}_{\mathrm{f}})^{-1} : (\mathbf{C}_{\mathrm{m}} - \mathbf{C}_{\mathrm{f}})]^{-1}, \tag{4.13b}$$

where $\mathbf{S}_{\mathrm{f}}$ is Eshelby's tensor where the infinite media has the properties of the fibers.

Tucker III and Liang (1999) reported that the SC model overestimates the axial modulus

at high volume fractions and that the M-T model delivers the most accurate predictions for large aspect ratio fibers. They also pointed out that Lielens model may improve on the M-T model for higher fiber volume fractions or rigidity contrasts (Tucker III and Liang, 1999).

Second step: homogenization of all subregions

Subregions form a multi-phase composite that can be homogenized by one of several homogenization models. For example, the overall stiffness tensor according to Voigt model is written as

$$\mathbf{C}^{\text{Voigt}} = \frac{\sum_{\alpha=1}^{N} \mathbf{C}_\alpha V_\alpha}{V}, \tag{4.14}$$

where V and V_α are the volume of composite and the volume of each subregion, respectively, and $\mathbf{C}_\alpha$ is the effective elastic tensor of a subregion calculated using one of the models for aligned inclusions enumerated in Section 4.3.2. The effective stiffness tensor according to Reuss model is calculated as

$$\mathbf{C}^{\text{Reuss}} = \left(\frac{\sum_{\alpha=1}^{N} \mathbf{C}_\alpha^{-1} V_\alpha}{V} \right)^{-1}. \tag{4.15}$$

For uniform random orientation of inclusions, it can be proved that Eq.4.14 and 4.15 are equivalent to the orientation averages $\{\mathbf{C}_\alpha\}$ and $\{\mathbf{C}_\alpha^{-1}\}$, respectively.

Two-step methods are noted herein by "1st method/2nd method" and are listed in the following: M-T/Voigt, M-T/Reuss, Li/Voigt, Li/Reuss, SC/Voigt, SC/Reuss, Dil/Voigt and Dil/Reuss.

One-step M-T (Eq.4.1) and two-step M-T/Voigt (Eq.4.6, 4.8 and 4.14) have been used in literature under the name of Mori-Tanaka without specifying which of the two models has been used. The current study brings forth clarifications to the differences between the two methods and identifes the models best suited for ROFRCs. It can be proven that the one-step Dilute model in Eq.4.3 and the two-steps model of Dil/Voigt are mathematically equivalent, hence have the exact same estimations. Therefore, only Dil/Voigt is mentioned in the sequel to distinguish it from the two-step method of Dil/Reuss.

4.3.3 Bounds: Hashin-Shtrikman

The Hashin-Shtrikman (HS) bounds (Hashin and Shtrikman, 1963) for bulk k and shear G moduli of isotropic materials are expressed by:

$$k^{\mathrm{HS}} = k_{\mathrm{m}} + c_{\mathrm{f}} \frac{k_{\mathrm{f}} - k_{\mathrm{m}}}{1 + c_{\mathrm{m}} \left(\frac{k_{\mathrm{f}} - k_{\mathrm{m}}}{k^* + k_{\mathrm{f}}} \right)}, \tag{4.16a}$$

$$G^{\mathrm{HS}} = G_{\mathrm{m}} + c_{\mathrm{f}} \frac{G_{\mathrm{f}} - G_{\mathrm{m}}}{1 + c_{\mathrm{m}} \left(\frac{G_{\mathrm{f}} - G_{\mathrm{m}}}{G^* + G_{\mathrm{f}}} \right)}, \tag{4.16b}$$

where $*$ denotes the reference material which is the fiber and the matrix for the upper and lower bounds, respectively.

4.4 Numerical homogenization

In the sequel, "effective properties" refer to the homogenized properties of the RVE whereas "apparent properties" refer to those of any given volume of the microstructure. Numerical homogenization is usually performed through two distinct, but related, procedures: a) the computation of the "apparent properties" of a given microstructure (Section 4.4.1) and b) the determination of the RVE and its "effective properties" using a series of microstructures' apparent properties (Section 4.4.2).

4.4.1 Single microstructure homogenization method

Four steps, as schematized in Figure 4.2, were needed in order to compute the apparent properties of a single random microstructure: 1. random microstructure generation; 2. volume meshing; 3. enforcement of boundary conditions and; 4. computation of the apparent properties.

Microstructure generation

Fibers were assumed to be cylinders of circular cross-section. A random fiber generator in a periodic cubic cell was developed with MATLAB. The generation algorithm was based on the modified RSA scheme proposed by Moussaddy *et al.* (2013). The generated volumes were periodic, i.e., every fiber that crossed a surface of the cubic cell penetrated back from the opposite surface. The method consisted of sequentially adding fibers into a volume, while checking for contact interferences with all previously generated fibers, until the target volume fraction was reached. When verifying fiber interferences, a minimum distance of 2.5 times the

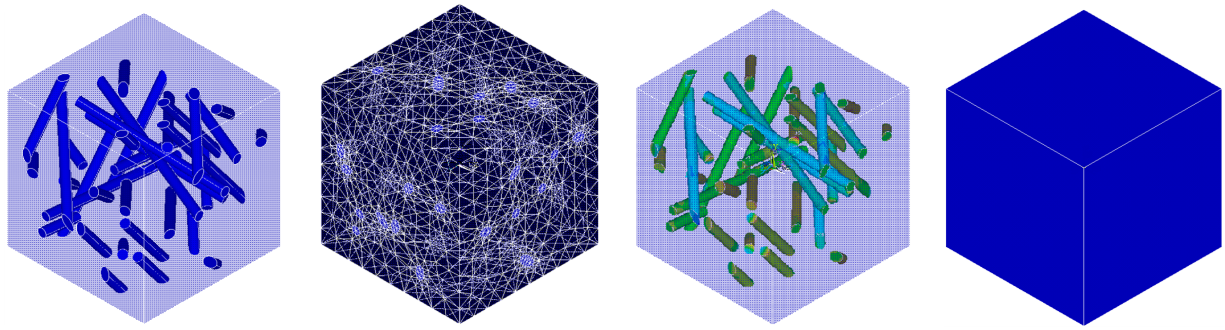

(a) (b) (c) (d)

Figure 4.2 Numerical homogenization process: a) microstructure generation; b) meshing; c) FE solution under PBCs and; d) calculation of apparent properties.

radius was imposed between two fiber axes in order to adequately mesh the space between them. If a newly added fiber interfered with another fiber, the position of the new fiber was translated just enough to respect the inter-fiber distance limit. If the translation resulted in interferences with other fibers, the new fiber was removed and repositioned randomly in the same volume. This operation was repeated until the new fiber location was free from interferences. Figure 4.3(a) shows a periodic volume generated with the developed MATLAB script.

Meshing

The generated microstructures were transferred to ANSYS FE package for meshing. In order to apply periodic boundary conditions (PBC) (see Section 4.4.1), homologous nodes on opposite surfaces had to match each other perfectly. The external surfaces of the cubic volume located at $x = 0$, $y = 0$ and $z = 0$ were first meshed using triangular surface elements, and the meshing was copied to the homologous surfaces using the "MSHCOPY" command. Afterwards, the volumes of all fibers and matrix were meshed with 10 nodes tetrahedron elements. A mesh size convergence study was conducted and is not presented in this paper for brevity. Meshing the fibers with tetrahedron elements with a maximum edge length equivalent to the fiber radius and that of the matrix with an edge length of 1/10 of the cube's edge length were required. ANSYS Parametric Design Language (APDL) was used in scripts to automate the meshing process. Figure 4.3(b) shows a periodic volume meshed with 50 fibers having an aspect ratio of 50 and a volume fraction of 5%.

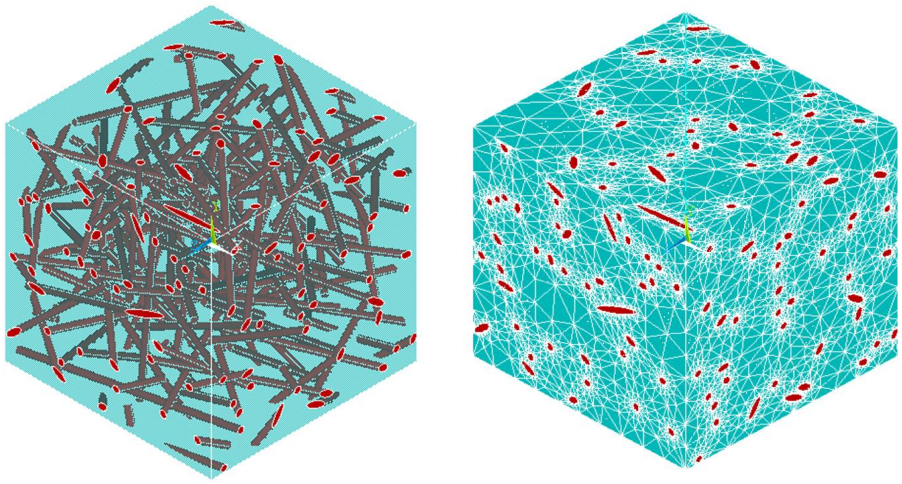

(a) (b)

Figure 4.3 Generated microstructure including 50 fibers with an aspect ratio of 50 at 5% volume fraction. a) Generated volume. b) Corresponding meshing.

Periodic boundary conditions

All FE models were transferred to ABAQUS/Standard FE package and solved under PBCs. In order to impose PBCs, each surface node displacement was coupled to its mirror node on the opposite surface according to:

$$\mathbf{u_{(x_2)}} - \mathbf{u_{(x_1)}} = \mathbf{E} \cdot (\mathbf{x_2} - \mathbf{x_1}), \tag{4.17}$$

where $u_{(x_i)}$ is the displacement vector of the node located at x_i, x_1 and x_2 are two homologous nodes on opposite surfaces and E is the applied strain. Readers are referred to (Moussaddy *et al.*, 2013; Barello and Lévesque, 2008) for a more detailed description on the PBCs application methodology. Once the PBCs were applied, the FE models were solved in ABAQUS Standard v. 6.10 using the iterative solver option, parallelising on 3 to 10 XEON X7550 cores and using from 30 Gb to 600 Gb RAM memory per model.

Calculation of apparent properties

The apparent elasticity tensor is such that:

$$\langle \boldsymbol{\sigma} \rangle = \tilde{\mathbf{C}} \colon \mathbf{E}, \tag{4.18}$$

where $\tilde{\mathbf{C}}$ is the apparent elasticity tensor, $\boldsymbol{\sigma}$ is the local stress field and $\langle\cdot\rangle$ represents volume averaging. Six orthogonal states of deformation were applied according to the methodology of (Moussaddy *et al.*, 2013) in order to obtain all the terms of the apparent elasticity tensor $\tilde{\mathbf{C}}$.

Following the determination of the apparent elastic tensor $\tilde{\mathbf{C}}$, the apparent elastic bulk and shear moduli $\tilde{k}$ and $\tilde{G}$, respectively, were calculated as:

$$\tilde{k} = \frac{\tilde{\mathrm{C}}_{iijj}}{9}, \tag{4.19a}$$

$$\tilde{G} = \frac{3\tilde{\mathrm{C}}_{ijij} - \tilde{\mathrm{C}}_{ijij}}{30}. \tag{4.19b}$$

4.4.2 RVE determination

The RVE is defined herein following the work of Kanit *et al.* (2003) as an ensemble of random finite volumes (i.e., realizations) of the microstructure that yield, in average, the effective properties of the composite. The RVE is described using two parameters: the number of realizations and the volume size (i.e., the number of fibers included in the volume element of each realization). The determination of the RVE parameters was performed according to two RVE determination criteria, one for each parameter. Following our findings in (Moussaddy *et al.*, 2013), the confidence criterion was applied for determining the number of realizations, whereas the averaging variation criterion was applied to determine the number of fibers included in the volume.

The confidence criterion is expressed by:

$$\frac{CI^{95\%}}{2\bar{Z}} \leq \epsilon_r, \tag{4.20}$$

where Z refers to the targeted property being either the bulk k or shear G modulus, ϵ_r is a fixed tolerance, $CI^{95\%}$ and $\bar{Z}$ represent the 95% confidence interval and the arithmetic mean of the apparent moduli over the r realizations of the ensemble, respectively.

The averaging criterion of Moussaddy *et al.* (2013) consists of computing the average properties of the ensemble of realizations using the arithmetic and harmonic means:

$$\overline{\mathbf{C}} = \frac{1}{r}\sum_{i=1}^{r} \tilde{\mathbf{C}}_i, \tag{4.21a}$$

$$\underline{\mathbf{C}} = \left(\frac{1}{r}\sum_{i=1}^{r} \tilde{\mathbf{C}}_i^{-1}\right)^{-1}. \tag{4.21b}$$

The corresponding elastic moduli $\bar{Z}$ and $\bar{\bar{Z}}$ are computed using Eq.4.19 with either of Eq.4.21a or 4.21b, respectively. The estimation of the overall properties of the ensemble of realizations was considered as the average of both means:

$$\hat{Z} = \frac{\bar{Z} + \bar{\bar{Z}}}{2} \tag{4.22}$$

The criterion states that the RVE is obtained when the difference between the ensemble overall properties and any of both means $\bar{Z}$ and $\bar{\bar{Z}}$ is within a certain tolerance ϵ_{RVE}:

$$\frac{|\hat{Z} - \bar{Z}|}{\hat{Z}} = \frac{|\hat{Z} - \bar{\bar{Z}}|}{\hat{Z}} \leq \epsilon_n. \tag{4.23}$$

In most cases, $\epsilon_n = \epsilon_r = 1\%$. If Eq.4.23 was not satisfied after reaching the maximum volume size possible with the available computational resources, the tolerance values were loosened to 5% or to 10% to find a RVE.

4.5 Results

The elastic properties of ROFRCs have been evaluated for a wide range of fibers aspect ratios, volume fractions and contrast of properties. More than 2500 microstructures were generated, meshed and computed in order to determine RVEs and their corresponding accurate effective properties. Whenever the FE results are given, the corresponding RVE criteria tolerance are jointly specified. All previously described analytical models (see Section 4.3) have been evaluated, namely: the M-T model, the SC scheme, the two-step methods of M-T/Voigt, M-T/Reuss, Li/Voigt, Li/Reuss, SC/Voigt, SC/Reuss, Dil/Voigt, Dil/Reuss and the HS bounds. In this work, the contrast of properties indicates the ratio of the elastic moduli of the fibers with respect to that of the matrix, i.e. $k_{\text{f}}/k_{\text{m}}{=}G_{\text{f}}/G_{\text{m}}$.

4.5.1 Aspect ratio study

Figures 4.4(a-d) present the effective elastic moduli of ROFRCs at (a,b) 2% and (c,d) 5% volume fractions as a function of the fibers aspect ratio for a contrast of 300. All results have been normalized with respect to the matrix properties. The FE curves stop at the highest aspect ratio that was technically achievable with the modified RSA method and the available computational resources. The apparent scattering in the FE results is due to the non-zero RVE determination tolerance. Figures 4.4(a-d) also includes all analytical models. All analytical models estimates were found to lie within the HS bounds. However, the upper HS bound was very high due to the high contrast of properties and does not

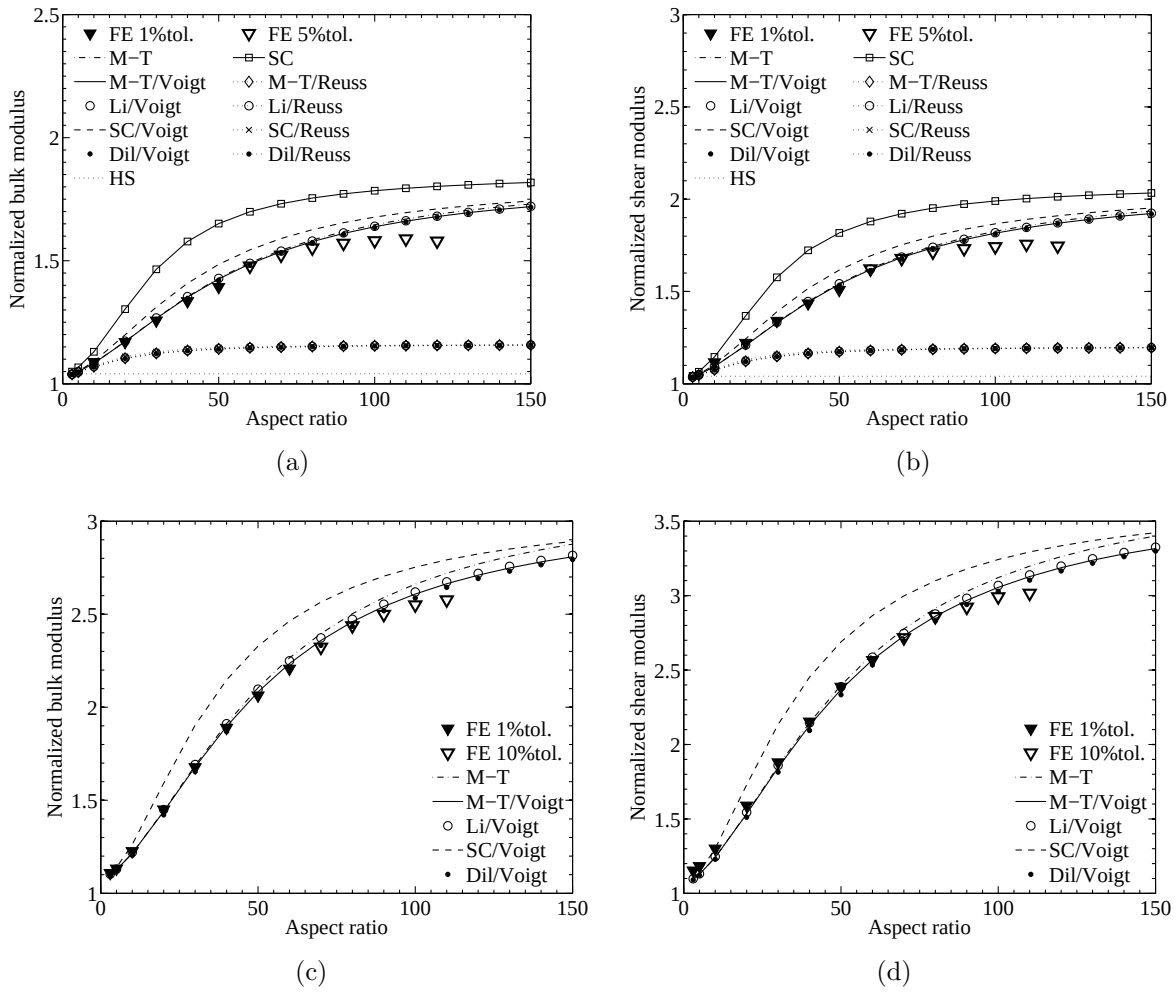

Figure 4.4 Normalized a) bulk and b) shear moduli of ROFRCs at 2% volume fraction and contrast of properties of 300 as a function of the fibers aspect ratio. Normalized c) bulk and d) shear moduli of ROFRCs at 5% volume fraction and contrast of properties of 300 as a function of the fibers aspect ratio.

appear in the figures. Moreover, the methods including the Reuss model produced results that were further from the FE results than their Voigt counterpart. The one-step SC scheme considerably overestimates the FE results. In the sequel, only the most accurate models, which were found to be: M-T, M-T/Voigt,Li/Voigt, SC/Voigt and Dil/Voigt models, are presented for the sake of clarity. The errors associated with each model were also computed and are presented in Section 4.6.

Figures 4.4(a) and 4.4(c) at 2% and 5% volume fractions, respectively, show that the M-T, Li/Voigt, M-T/Voigt and Dil/Voigt analytical models provide the best bulk modulus predictions. However, at 2% volume fraction and for aspect ratios higher than 90, the few

FE results presented in Figure 4.4(a) show very little changes in the bulk modulus when increasing the fibers aspect ratios. The analytical models do not have the same change in slope and, consequently, none of the models delivers accurate predictions for fibers aspect ratios over 100. The same conclusions can be drawn at 5% volume fraction. However, the bulk modulus has not reached the plateau yet for the highest computed aspect ratio (ρ =110), as seen in Figure 4.4(c). The exact same behaviours are observed for the shear modulus in Figures 4.4(b) and 4.4(d). It is important to note that M-T and M-T/Voigt models yield very similar results for relatively low aspect ratios (up to 50 as seen in Figure 4.4(c)), but they start diverging for higher aspect ratios.

4.5.2 Volume fraction study

Figures 4.5(a,b), 4.5(c,d) and 4.5(e,f) present the effective elastic properties of ROFRCs for fibers aspect ratios of 5, 10 and 20, respectively, as a function of the fibers volume fraction for a contrast of 300. For low volume fractions (up to 5%), all analytical models provide accurate estimates for the bulk shear modulus. For higher volume fractions, the model of Li/Voigt produces the most accurate bulk modulus predictions for all three aspect ratios and shear modulus predictions for aspect ratios of 10 and 20. The SC/Voigt model yields the best shear modulus predictions for an aspect ratio of 5, as also found by Kari *et al.* (2007), but considerably oversestimates the effective properties for all other cases. The models of M-T, M-T/Voigt and Dil/Voigt underestimate the effective properties for volume fractions over 5%. As expected, the Dil/Voigt model shows the lowest dependency on volume fraction. This is due to the Dilute model assumption of non-interaction between inclusions which is true only for very low volume fractions.

4.5.3 Contrast of properties study

Figures 4.6(a,b), 4.6(c,d) and 4.6(e,f) present the effective elastic properties of 5% volume fraction ROFRCs for fibers aspect ratios of 5, 10 and 20, respectively, as a function of the fibers/matrix contast of elastic moduli. For all three aspect ratios, the models of Li/Voigt, M-T/Voigt and M-T provide the most accurate estimates for the bulk modulus for all contrasts of properties under study, as seen in Figures 4.6(a), 4.6(c) and 4.6(e). However, all models underestimate the effective shear modulus for an aspect ratio of 5, as as seen in Figure 4.6(b), whereas the SC/Voigt model and that of Li/Voigt yield accurate predictions for aspect ratios of 10 (see Figure 4.6(d)) and 20 (see Figure 4.6(f)), respectively.

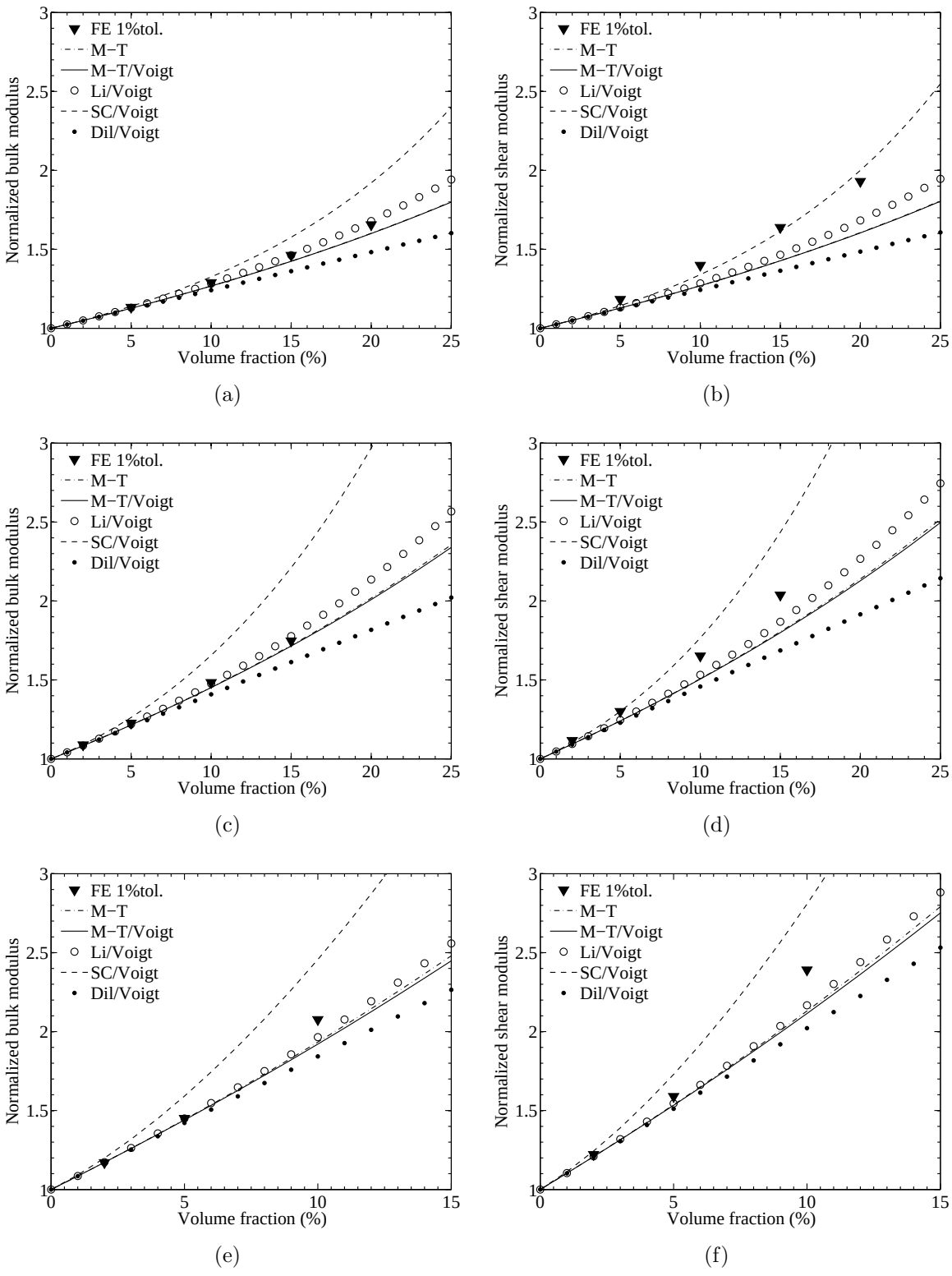

Figure 4.5 Normalized bulk modulus and normalized shear modulus of ROFRCs with fibers of aspect ratio (a,b) 5, (c,d) 10 and (e,f) 20 as a function of the fibers volume fraction for a contrast of of 300.

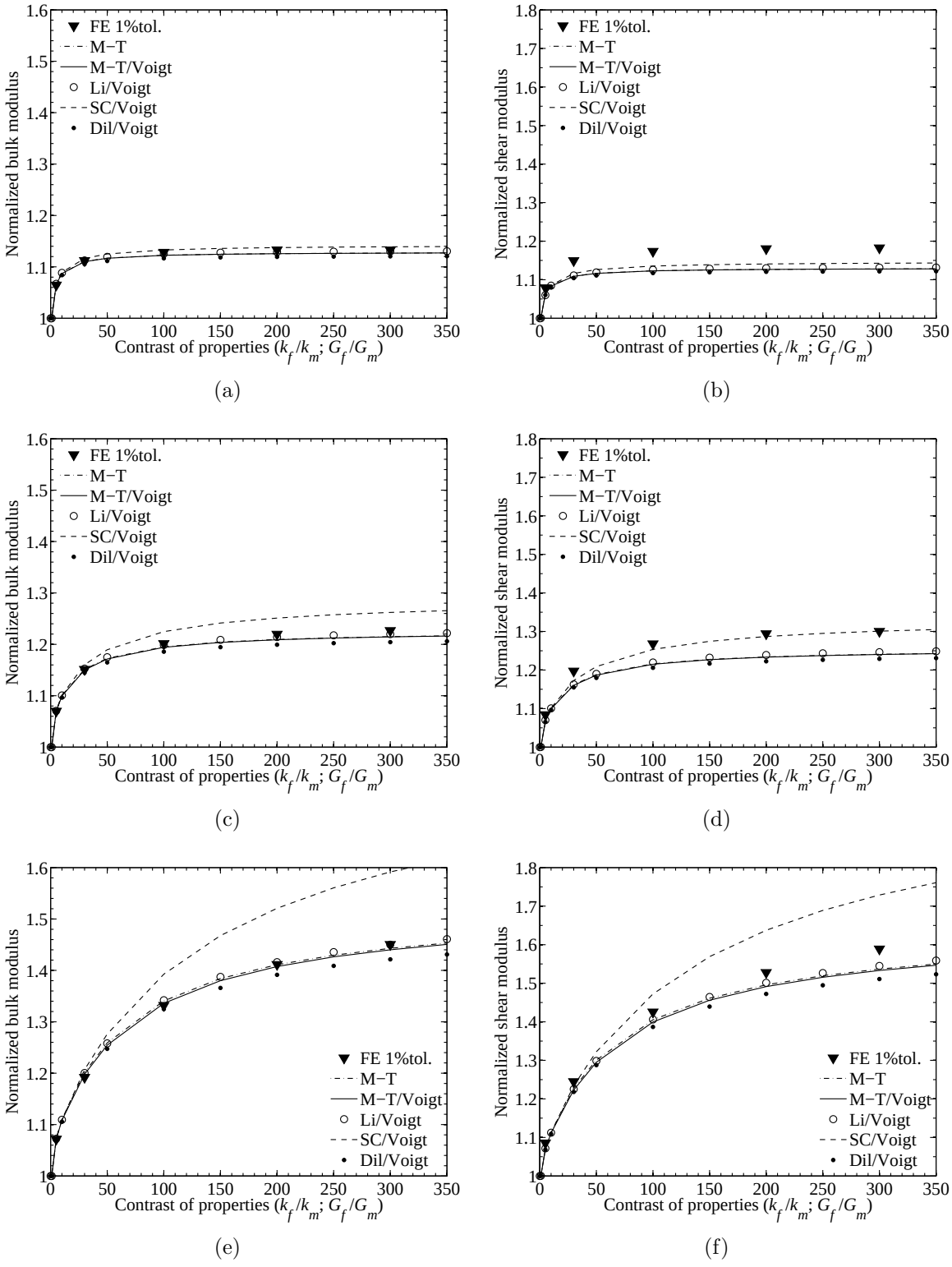

Figure 4.6 Normalized bulk modulus and normalized shear modulus of ROFRCs with fibers of aspect ratio (a,b) 5, (c,d) 10 and (e,f) 20 as a function of the properties contrast at a volume fraction of 5%.

4.6 Discussion

In the following, the errors of each analytical model are computed and analyzed in order to determine the best suited one for accurate predictions of ROFRCs effective properties. The computed error values over the ranges of parameters (i.e., aspect ratios, volume fractions and properties contrasts) allow determining the range of validity of each model based on the choice of tolerance, hereby chosen at 5%. Two-step Dil/Voigt model computed effective properties very close to that of M-T/Voigt and Li/Voigt for small volume fractions (2% and 5%) and it diverges from both models as well as FE results for higher volume fractions. Therefore, the Dil/Voigt model is not included in the following discussion.

4.6.1 Bulk modulus

Figure 4.7(a) presents the errors for the bulk modulus estimates of the analytical models with respect to the FE effective results as a function of the fibers aspect ratio for a volume fraction of 2%. It is observed that the SC/Voigt scheme errors increase quickly for increasing aspect ratio and are not well suited for predicting the effective bulk modulus for high aspect ratios. The models of M-T, M-T/Voigt and Li/Voigt have the smallest errors. However, the errors reach approximately 5% for an aspect ratio of 110 while continuously increasing. This decrease in models accuracy for high aspect ratios can be explained by the plateau observed for FE results and not for analytical models for aspect ratios over 90, as seen in Figure 4.4(a). The fibers aspect ratio at which stiffening saturation is observed is of major importance to numerical modeling. The saturation aspect ratio can be practically used for the modeling of composites with higher aspect ratios (e.g. carbon nanotubes with an aspect ratio of approximately 1000), which are currently impossible to solve due to computational limits.

Figures 4.8(a-d) present the bulk modulus errors of the models of M-T, M-T/Voigt, Li/Voigt and SC/Voigt, respectively, as a function of the volume fraction and for fibers aspect ratios of 5, 10 and 20 with a contrast of properties of 300. In the range of aspect ratios studied, it is observed that higher volume fractions induce larger errors, especially for the model of SC/Voigt. On the other hand, the models of M-T, M-T/Voigt and Li/Voigt have less dependency on the volume fraction, Li/Voigt being the most accurate model. However, they both show more important discrepencies for the highest aspect ratio (20) and the highest corresponding volume fraction (10%).

As for the effect of the contrast of properties, Figures 4.9(a-d) present the bulk modulus errors of the models of M-T, M-T/Voigt, Li/Voigt and SC/Voigt, respectively, as a function of the properties contrast for fibers aspect ratios of 5, 10 and 20 at a volume fraction of 5%. Once again, it is observed that the models of M-T, M-T/Voigt and Li/Voigt produce the

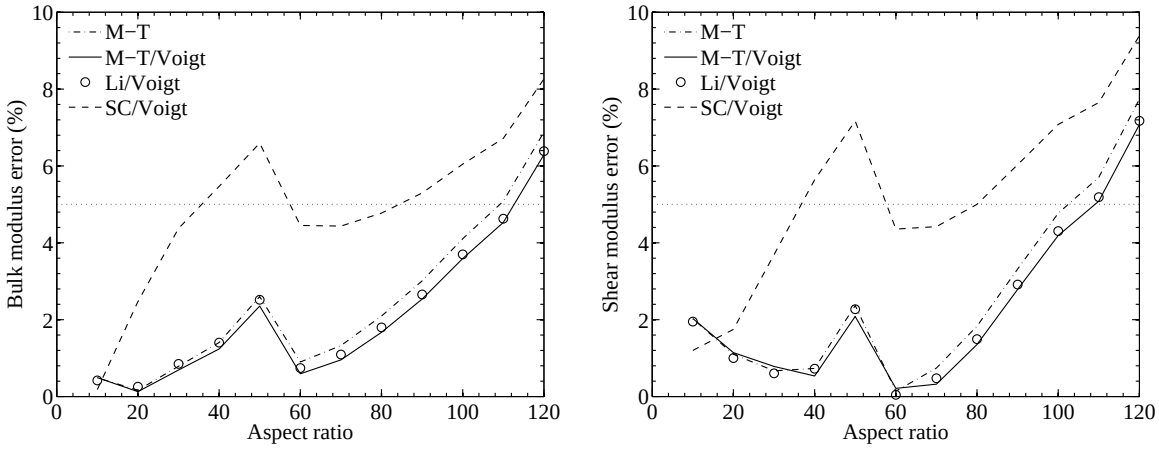

Figure 4.7 a) Bulk modulus errors and b) shear modulus errors of the anlytical estimates with respect to the numerical results for ROFRCs at 2% volume fraction and contrast of properties of 300 as a function of the fibers aspect ratio. The dotted line presents a 5% error tolerance.

smallest errors and exhibit little dependency on the properties contrast. This observation can be extrapolated to higher contrasts ratios since the FE results, as well as the models of M-T, M-T/Voigt and Li/Voigt, have practically reached the properties contrast saturation limit, as seen in Figures 4.6(a), 4.6(c) and 4.6(e).

Based on the results presented above, it is concluded that the models of M-T, M-T/Voigt and Li/Voigt provide the most accurate estimations of the effective bulk modulus of ROFRCs for aspect ratios up to 100 (validated for volume fractions up to 5%). No analytical model provides accurate estimations for larger aspect ratios. The accuracy of all three models, i.e. M-T, M-T/Voigt and Li/Voigt, practically is not affected by the properties contrast. The model of Li/Voigt is best suited for bulk modulus predictions at higher volume fractions (validated for volume fractions up to 20% and aspect ratios up to 20).

4.6.2 Shear modulus

Figure 4.7(b) presents the errors for the shear modulus estimates of the analytical models with respect to the FE effective results as a function of the fibers aspect ratio for a volume fraction of 2%. The errors are very similar to the bulk modulus errors in that the SC/Voigt scheme produces the largest errors wheras the M-T, M-T/Voigt and Li/Voigt models produce accurate estimations of the shear modulus up to an aspect ratio of 100. Above this aspect ratio, none of the models could deliver accurate estimations (i.e., models have errors higher

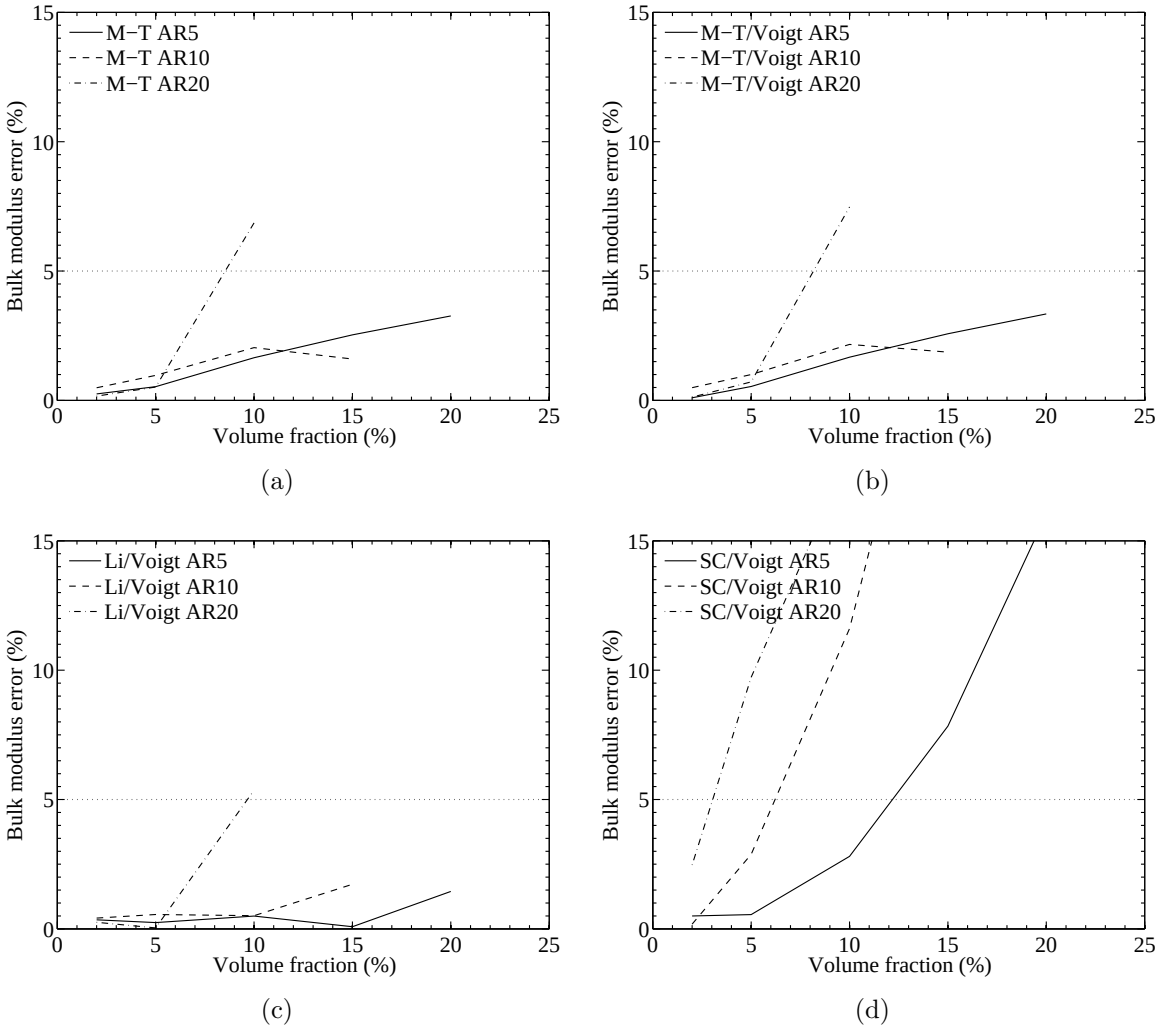

Figure 4.8 Bulk modulus errors for the models of a) M-T, b) M-T/Voigt, c) Li/Voigt and d) SC/Voigt with respect to the numerical results for ROFRCs for fibers aspect ratios of 5, 10 and 20 and contrast of properties of 300 as a function of the fibers volume fraction. The dotted line presents a 5% error tolerance.

than 5%). The inaccuracy of shear modulus estimations for high aspect ratios is also due to the plateau observed for FE results for aspect ratios over 90, as seen in Figure 4.4(b).

Figures 4.10(a-d) present the shear modulus errors for the analytical models of M-T, M-T/Voigt, Li/Voigt and SC/Voigt, respectively, as a function of the volume fraction and for fibers aspect ratios of 5, 10 and 20 with a contrast of properties of 300. Within the range of aspect ratios studied, it is observed that all analytical methods induce large errors for volume fractions higher than 5%, except for the SC/Voigt scheme for a low aspect ratio of 5. Therefore, none of the methods provide accurate estimations (i.e., errors lower than 5%) for

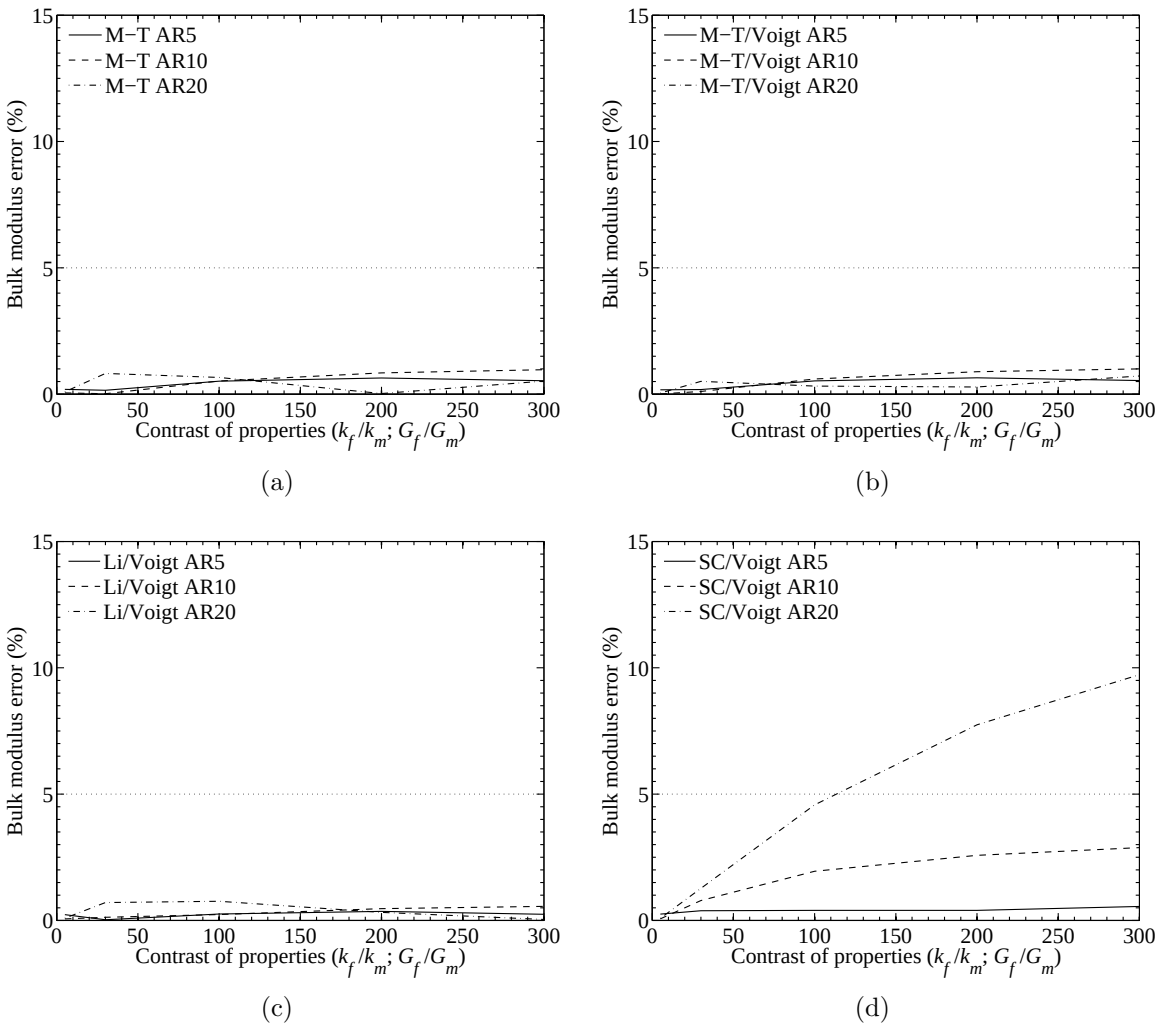

Figure 4.9 Bulk modulus errors for the models of a) M-T, b) M-T/Voigt, c) Li/Voigt and d) SC/Voigt with respect to the numerical results for ROFRCs at 5% volume fraction for fibers with aspect ratios of 5, 10 and 20 as a function of the contrast of properties. The dotted line presents a 5% error tolerance.

high volume fractions.

As for the effect of the contrast of properties, Figures 4.11(a-d) present the shear modulus errors for the models of M-T, M-T/Voigt, Li/Voigt and SC/Voigt, respectively, as a function of the contrast of properties for fibers aspect ratios of 5, 10 and 20 at a volume fraction of 5%. It is observed that the model of SC/Voigt computes the highest errors at high properties contrast, especially for higher fibers aspect ratios. The other three analytical models show small errors even at high contrasts.

Based on the results presented above, it is concluded that the models of M-T, M-T/Voigt

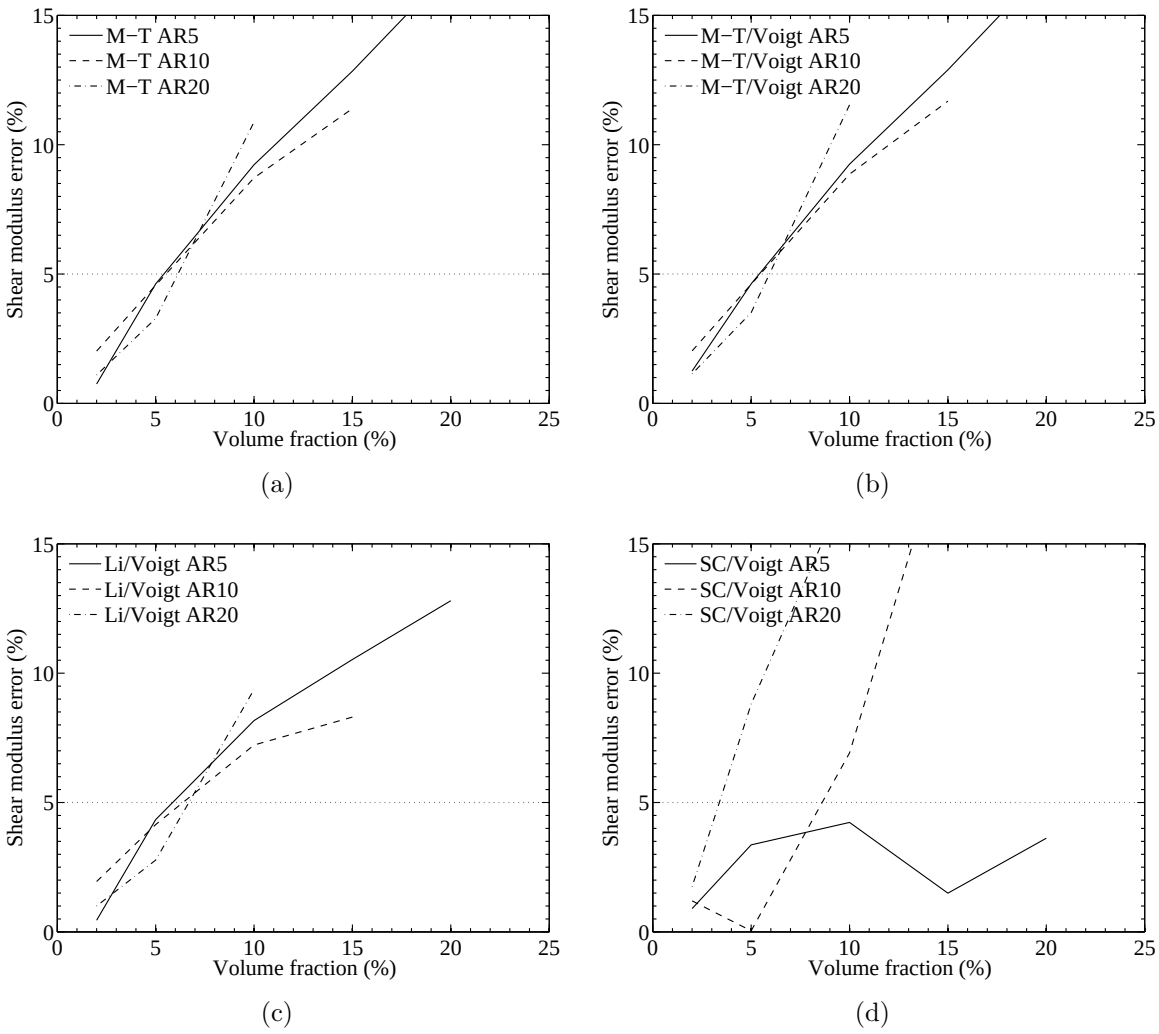

Figure 4.10 Shear modulus errors for the models of a) M-T, b) M-T/Voigt, c) Li/Voigt and d) SC/Voigt with respect to the numerical results for ROFRCs for fibers aspect ratios of 5, 10 and 20 and contrast of properties of 300 as a function of the fibers volume fraction. The dotted line presents a 5% error tolerance.

and Li/Voigt provide the most accurate estimations of the effective shear modulus of ROFRCs for aspect ratios up to 100 (validated for volume fractions up to 5%). No analytical model provides accurate estimations for larger aspect ratios. The accuracy of all three models, i.e. M-T, M-T/Voigt and Li/Voigt, practically is not affected by the properties contrast. None of the models are accurate for high volume fractions (higher than 5%).

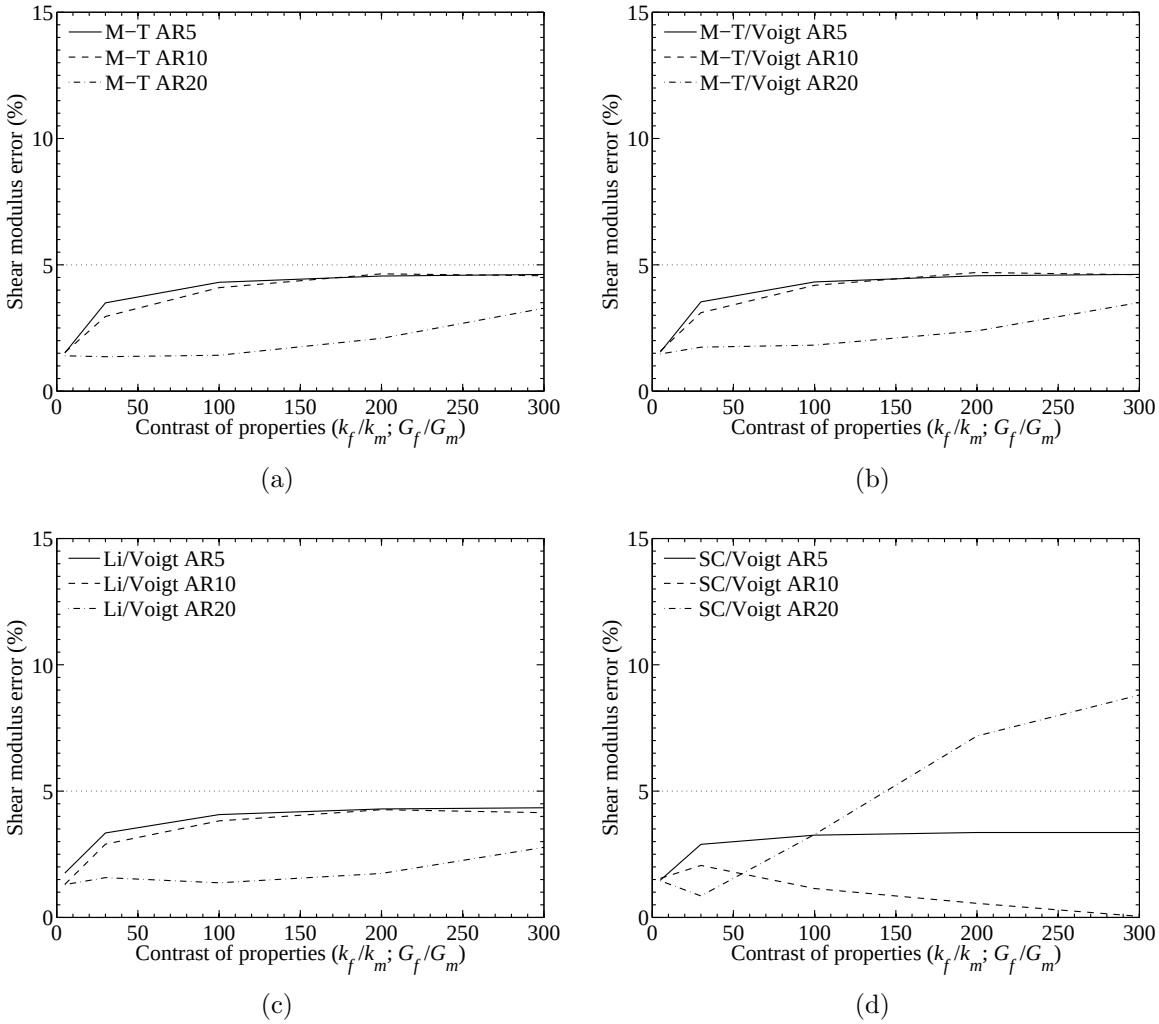

Figure 4.11 Shear modulus errors for the models of a) M-T, b) M-T/Voigt, c) Li/Voigt and d) SC/Voigt with respect to the numerical results for ROFRCs at 5% volume fraction for fibers with aspect ratios of 5, 10 and 20 as a function of the contrast of properties. The dotted line presents a 5% error tolerance.

4.6.3 Very long fibers

It was shown in Figures 4.4(a-d) that the analytical models do not accurately reproduce the aspect ratio saturation limit. Consequently, no model accurately predicts the elastic properties of ROFRCs for aspect ratios larger than 90. In addition, it is impossible to model such composites using the current computational resources. However, the aspect ratio saturation limit provides a practical venue for an accurate reproduction of the effective properties of very high aspect ratio fiber composites via the modeling of the composite with the fibers at the aspect ratio saturation limit. It was hereby determined that the aspect ratio

saturation limit for ROFRCs is approximately 90 for a volume fraction of 2%, but is higher for a volume fraction of 5%. A similar aspect ratio saturation limit (approximately 90) was shown in the study of Tucker III and Liang (1999) for the axial Young modulus of aligned fiber composites at 20% volume fraction. Our results suggest that the aspect ratio saturation limit depends on the fibers volume fraction. However, the available FE results are insufficient to support this claim and this hypothesis should be studied further when the computational resources are available.

4.7 Conclusion

The analytical models predictions of the elastic properties of ROFRCs were compared to accurate effective properties determined using FE numerical homogenization of the appropriate RVE. The comparisons were performed for a wide range of aspect ratios (up to 120), properties contrast (up to 300) and volume fractions only up to 20% due to computational challenges encountered during microstructure generation and meshing).

The main conclusions are:

- The analytical models of M-T, M-T/Voigt and Li/Voigt provide accurate estimations of the bulk and shear moduli of low volume fraction (tested up to 5%) ROFRCs up to an aspect ratio of 90, which was found to be the aspect ratio saturation limit.
- For higher aspect ratios (over 90), the effective properties should be determined using numerical homogenization of the RVE using the aspect ratio saturation limit.
- The model of Li/Voigt provides the best suited model for bulk modulus predictions for volume fractions over 5%.
- No model accurately predicts the shear modulus for volume fractions over 5%.

Therefore, it is concluded that if a single model was to be chosen for predicting the effective elastic properties of ROFRCs, the two-step method of Li/Voigt provides most accurate estimations over the largest range of microstructure parameters. The two major cases of non-validity of the Li/Voigt model were found, first, for the bulk and shear moduli predictions for aspect ratios over 100 and, second, for the shear modulus predictions at volume fractions over 5%. Numerical homogenization of the RVE is still needed in these cases. Indeed, very long fibers and high volume fractions are the most sought microstructures in industrical applications. Unfortunately, those same microstructures impose the most difficult challenges in terms of microstructure generation methods and computational time and memory requirements. Therefore, future studies should focus on improving the numerical homogenization process for ROFRCs to extend the range of computable microstructures. In parallel, efforts should be employed to develop analytical models that are best suited for ROFRCs with very

high aspect ratios and volume fractions of fibers.

4.8 Acknowlegments

The work of Hadi Moussaddy was funded by the National Science and Engineering research Council of Canada (NSERC). Most of the computations were performed on supercomputers financed by the Canadian Foundation for Innovation (CFI) and the NSERC. These computers are hosted by the Fluid Dynamics Laboratory (LADYF) of École Polytechnique de Montréal.

CHAPTER 5

GENERAL DISCUSSION

In the following, certain limitations of the new RVE quantitative definition are discussed and a general formulation is introduced to apply the new criterion to anisotropic materials. In addition, the parameters affecting the aspect ratio saturation limit in ROFRC are briefly discussed.

5.1 Range of applicability of determined RVEs

It should be noted that all determined RVE parameters (n, r) in Chapter 3 are exclusive to the corresponding targeted property (bulk or shear modulus), fibers aspect ratio, properties contrast, boundary conditions and the average effective properties expression (e.g., $\bar{Z}$ or $\hat{Z}$). For example, the determined RVE parameters (n, r) for the case of [k, AR=50, contrast=300, PBCs, $\hat{k}$], where the notation [targeted property, aspect ratio, contrast, boundary conditions, estimator] has been adopted, can not be used to compute accurate effective properties using another estimator, e.g. [k, AR=50, contrast=300, PBCs, $\bar{k}$], or for a larger aspect ratio, e.g. [k, AR=100, contrast=300, PBCs, $\hat{k}$]. It was demonstrated in Chapter 3 that the RVE size increases for larger aspect ratios. In other studies it was demonstrated that the RVE size increases for larger properties contrasts (Ostoja-Starzewski, 2006). Thus, it is possible to conservatively use determined RVE parameters (n, r) of a first microstructure, to other microstructures with lower aspect ratio and/or properties contrast, given that all other parameters are similar. For example, the RVE determined for the case of [k, AR=100, contrast=500, PBCs, $\hat{k}$] can be used for a microstructure with lower aspect ratio [k, AR=50, contrast=500, PBCs, $\hat{k}$] or lower properties contrast [k, AR=100, contrast=300, PBCs, $\hat{k}$].

5.2 Generalizing the new RVE quantitative definition

This study was limited to ROFRCs within linear elasticity and effective isotropy. However, the proposed averaging criterion in Eq.4.23 can be generalized to other microstructures including anisotropic materials where every component of the stiffness tensor $\mathbf{C}$ is a property that has to satisfy the acceptance criteria:

$$\frac{|\hat{\mathrm{C}}_{ijkl} - \overline{\mathrm{C}}_{ijkl}|}{\hat{\mathrm{C}}_{ijkl}} = \frac{|\hat{\mathrm{C}}_{ijkl} - \underline{\mathrm{C}}_{ijkl}|}{\hat{\mathrm{C}}_{ijkl}} \leq \epsilon_{tol}, \tag{5.1}$$

where

$$\hat{\mathbf{C}} = \frac{\overline{\mathbf{C}} + \underline{\mathbf{C}}}{2}. \tag{5.2}$$

However, the influence of the tolerance on the positive definitiveness of the resulting effective tensor should be thoroughly studied in order to guarantee thermodynamically consistent properties. This is let for future works.

5.3 Effect of the computation rule for the effective properties

For illustration purposes, the effect of using different expressions to compute the average Young's moduli is discussed. The apparent Young's modulus was computed using different relations from the arithmetic $\overline{\mathbf{C}}$ and harmonic $\underline{\mathbf{C}}$ mean apparent elasticity tensors as:

$$\overline{\mathrm{E}}_{\mathrm{Y}} = \frac{9\overline{k} + \overline{G}}{3\overline{k} + \overline{G}}, \tag{5.3a}$$

$$\overline{\overline{\mathrm{E}}}_{\mathrm{Y}} = \frac{9\overline{\overline{k}} + \overline{\overline{G}}}{3\overline{\overline{k}} + \overline{\overline{G}}}. \tag{5.3b}$$

The average Young's modulus was also computed with a limited number of components of the compliance tensor:

$$\overline{\mathrm{E}'}_{\mathrm{Y}} = \frac{1}{3}\left(\frac{1}{\overline{\mathrm{C}}^{-1}{}_{1111}} + \frac{1}{\overline{\mathrm{C}}^{-1}{}_{2222}} + \frac{1}{\overline{\mathrm{C}}^{-1}{}_{3333}}\right), \tag{5.4a}$$

$$\overline{\overline{\mathrm{E}'}}_{\mathrm{Y}} = \frac{1}{3}\left(\frac{1}{\underline{\mathrm{C}}^{-1}{}_{1111}} + \frac{1}{\underline{\mathrm{C}}^{-1}{}_{2222}} + \frac{1}{\underline{\mathrm{C}}^{-1}{}_{3333}}\right). \tag{5.4b}$$

Other expressions could also be used to calculate Young's modulus. Figure 5.1 present the average Young's moduli as a function of the number of fibers for ROFRCs at 5% volume fraction, properties contrast of 300 and fibers aspect ratio of 10, 20 and 30. For all aspect ratios, $\overline{\mathrm{E}}_{\mathrm{Y}}$ and $\overline{\overline{\mathrm{E}}}_{\mathrm{Y}}$ apparently converge towards a Young's modulus value that is larger than that of $\overline{\mathrm{E}'}_{\mathrm{Y}}$ and $\overline{\overline{\mathrm{E}'}}_{\mathrm{Y}}$. The gap between estimations is larger at higher aspect ratios. These results show that the relation used to extract the apparent properties from the apparent stiffness tensor has an impact on the accuracy of the former.

For instance, the arithmetic mean apparent stiffness tensor of 11 realizations containing

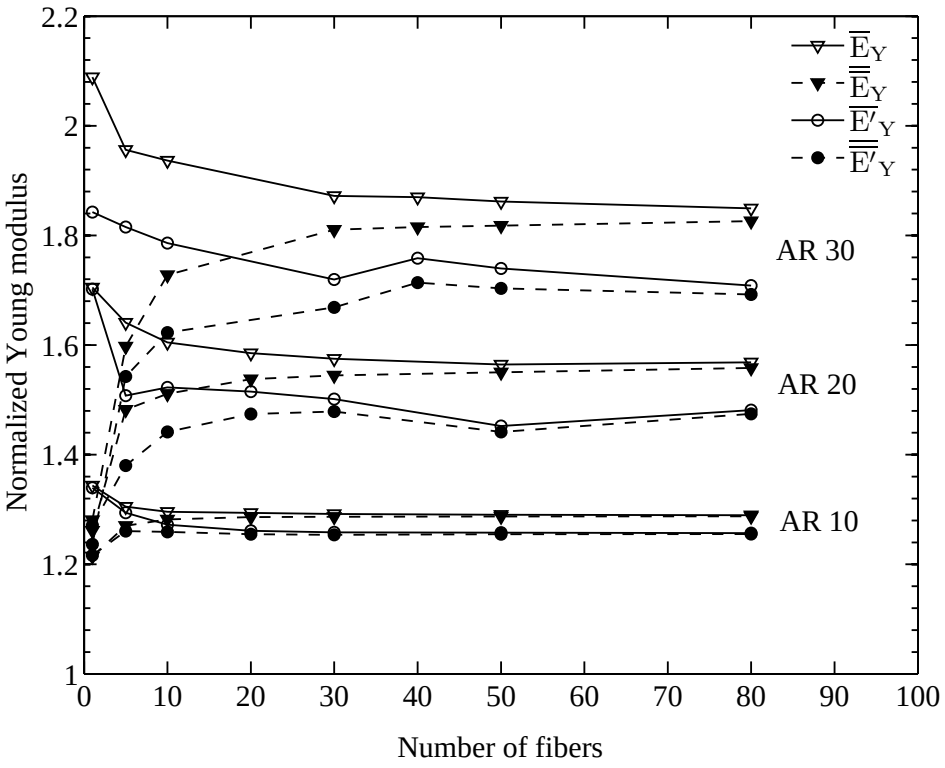

Figure 5.1 Normalized Young's moduli with respect of that of the matrix as a function of the number of fibers for ROFRCs of volume fraction 5%, properties contrast of 300 and fibers aspect ratios of 10, 20 and 30.

80 fibers of aspect ratio 30 is given by:

$$\overline{\mathbf{C}}^{r=11}_{\text{AR=30; } n=80} = \begin{bmatrix} 4.4680 & 1.9081 & 1.9193 & 0.0297 & -0.1071 & -0.0223 \\ 1.9087 & 4.6390 & 1.9230 & -0.0369 & -0.0037 & -0.0858 \\ 1.9189 & 1.9222 & 4.5590 & 0.0297 & -0.1232 & -0.0365 \\ 0.0304 & -0.0370 & 0.0303 & 3.0367 & -0.0428 & -0.0030 \\ -0.1072 & -0.0040 & -0.1232 & -0.0436 & 3.0719 & 0.0421 \\ -0.0220 & -0.0855 & -0.0363 & -0.0033 & 0.0419 & 3.0682 \end{bmatrix}, \qquad (5.5)$$

whereas the corresponding compliance tensor is given by:

$$\overline{\mathbf{C}}^{r=11}_{\text{AR=30; } n=80}{}^{-1} = \begin{bmatrix} 0.2992 & -0.0860 & -0.0895 & -0.0030 & 0.0067 & -0.0014 \\ -0.0861 & 0.2862 & -0.0846 & 0.0051 & -0.0061 & 0.0065 \\ -0.0894 & -0.0846 & 0.2929 & -0.0029 & 0.0085 & 0.0003 \\ -0.0031 & 0.0051 & -0.0029 & 0.3295 & 0.0044 & 0.0004 \\ 0.0067 & -0.0060 & 0.0085 & 0.0045 & 0.3262 & -0.0045 \\ -0.0014 & 0.0064 & 0.0003 & 0.0004 & -0.0045 & 0.3262 \end{bmatrix}. \quad (5.6)$$

The values of $\overline{\mathrm{E}}_{\mathrm{Y}} = 3.70$ GPa and $\overline{\mathrm{E}'}_{\mathrm{Y}} = 3.42$ GPa are obtained (8% difference between the two values). This can be explained by the anisotropy observed in the average apparent elasticity tensors. The isotropy error of $\overline{\mathbf{C}}^{r=11}_{\text{AR=30; } n=80}$ can be calculated following Eq.3.10:

$$\Lambda = \begin{bmatrix} 5.41\% & 4.12\% & 4.73\% & 0 & 0 & 0 \\ 4.15\% & 1.79\% & 4.93\% & 0 & 0 & 0 \\ 4.71\% & 4.89\% & 3.48\% & 0 & 0 & 0 \\ 0 & 0 & 0 & 5.05\% & 0 & 0 \\ 0 & 0 & 0 & 0 & 6.26\% & 0 \\ 0 & 0 & 0 & 0 & 0 & 6.14\% \end{bmatrix}. \quad (5.7)$$

The maximum isotropy error (6.26%) is of the same order than the Young's modulus difference (8%) and can partially explain the discrepancies observed in Figure 5.1. While $\overline{\mathrm{E}'}_{\mathrm{Y}}$ is calculated using only three components of a non-perfectly isotropic tensor, $\overline{\mathrm{E}}_{\mathrm{Y}}$ involves all non-zero components of the elasticity tensor, hence accounts for the variability of the apparent elasticity tensor components. This observation highlights the risks of using relations involving specific (in the sense of a limited number of) components of the elasticity tensor in order to determine effective properties from finite volumes. This is a practice that is commonly used in published homogenization works. However, it was not possible in this thesis work to show that one definition is superior to the other and this should but studied further in future works.

5.4 Microstructure effects on the aspect ratio saturation limit

The aspect ratio saturation limit has been determined to be around 90 for a volume fraction of 2% and a properties contrast of 300. A slightly larger saturation limit was observed for a higher volume fraction of 5% at the same contrast. Therefore, it is suggested that the volume fraction affects the aspect ratio limit. Moreover, a smaller limit around 20 was

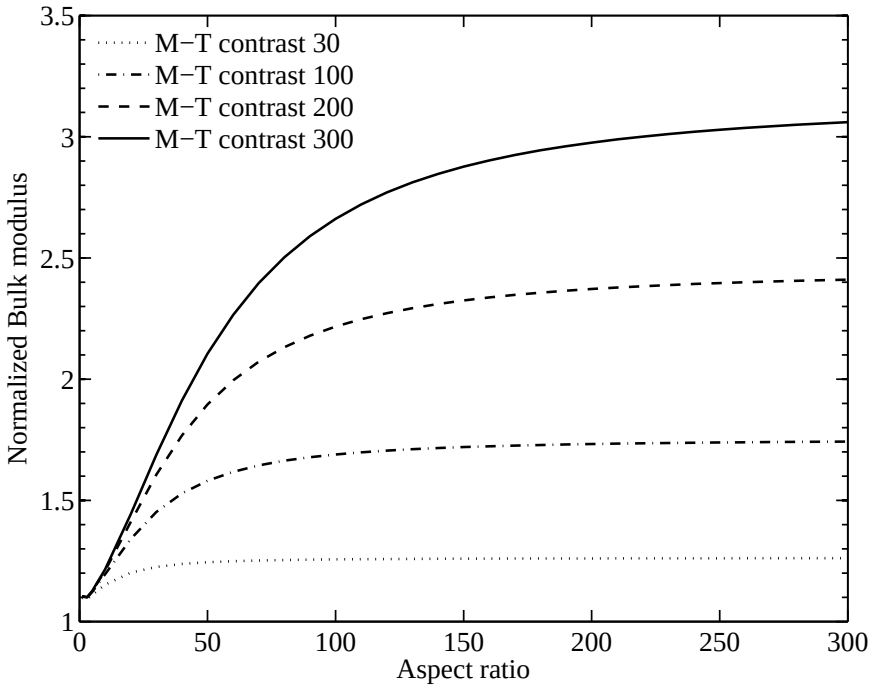

(a)

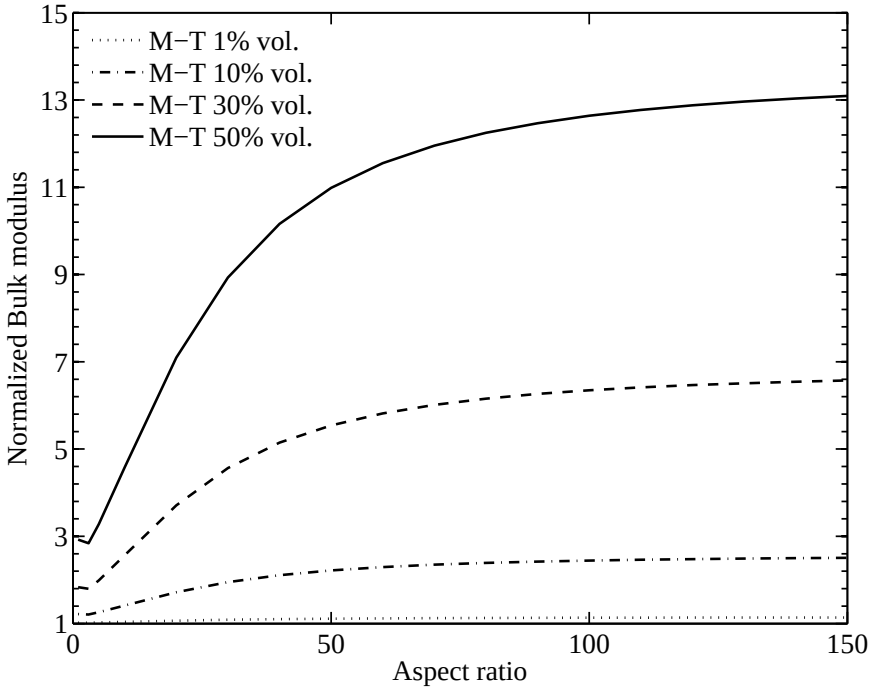

(b)

Figure 5.2 Analysis of the effect of the properties contrast and volume fraction on the aspect ratio saturation limit. a) M-T estimates of the effective bulk modulus as a function of the fibers aspect ratio for contrast of properties, of 30, 100, 200 and 300. b) M-T estimates of the effective bulk modulus as a function of the fibers aspect ratio for volume fractions of 1%, 10%, 30% and 50%.

observed in Mortazavi *et al.* (2013) for a lower properties contrast of 50. Comparisons between both cases suggest that the saturation aspect ratio depends also on the properties contrast. Although analytical methods do not show accurate saturation aspect ratios, they may provide more insight on the effect of those parameters. Figure 5.2(a) presents the M-T estimates of the effective bulk modulus as a function of the fibers aspect ratio for contrast of properties, of 30, 100, 200 and 300. It is observed that higher contrasts have a higher aspect ratios. Figure 5.2(b) presents the M-T effective bulk modulus estimations as a function of the fibers aspect ratio for volume fractions of 1%, 10%, 30% and 50%. Similarly, it is observed that larger volume fractions exhibit larger aspect ratio saturation limits. Further examination of accurate numerical homogenization results is necessary in order to analyze the effect of each parameter on the aspect ratio saturation limit.

CONCLUSION

The first objective of this thesis was to assess RVE quantitative definitions with respect to their estimations of the effective properties. ROFRCs were adopted to conduct the assessment of the different quantitative definitions. It was demonstrated that the property stability criterion, which is the most commonly used criterion for RVE determination, is inappropriate for determining RVEs of ROFRCs with moderate to high aspect ratios of fibers (over 20). Similar conclusions were obtained for the criterion based on the standard deviation of the apparent properties. The validity of published works relying on those criteria is questionable. Single microstructures that yield isotropic elasticity tensors, within a tolerance, computed accurate effective properties. Thus, an isotropic finite volume of a ROFRC can be considered as its RVE. The applicability of this concept onto other microstructures (e.g., spheres, disks, grains,etc.) is uncertain.

The newly proposed averaging criterion computes accurate estimations of ROFRC effective properties, within a given tolerance. Moreover, the averaging criterion does not necessitate the computation of the apparent properties at different volume sizes to study the convergence, as the stability criterion does. This reduces substantially the computational cost related to the RVE determination process. The estimation given by the average of the arithmetic and harmonic means computed accurate properties for volumes smaller than that of all other quantitative definitions, thus further reducing the needed RVE size for a prescribed tolerance. Using the new RVE quantitative definition, the determined RVEs edge lengths were found to be around half the fiber length for aspect ratios larger than 10. Such a correlation allows firsthand quick estimations of RVE sizes for ROFRCs. A generalization of this quantitative definition was given for anisotropic microstructures.

The second objective of this thesis was to assess the analytical models predictions of the effective elastic properties of ROFRCs. The analytical models included one-step and two-step homogenization methods. One-step methods included the models of M-T and SC while two-step methods included that of Dil/Voigt, Dil/Reuss, M-T/Voigt, M-T/Reuss, Li/Voigt, Li/Reuss, SC/Voigt and SC/Reuss. The analytical models predictions were compared to accurate effective properties computed by numerical homogenization following the new RVE quantitative definition. The comparisons were performed for a wide range of aspect ratios (up to 120), properties contrast (up to 300) and volume fractions only up to 20% due to computational challenges. More than 2500 microstructures were generated, meshed and solved under PBCs in the course of this study.

All two-step models involving Reuss model as a second step underestimated the effective elastic bulk and shear moduli of ROFRCs. The one-step SC scheme and the two-step method of SC/Voigt overestimated the effective properties. The analytical models of M-T, M-T/Voigt and Li/Voigt provided accurate estimations of the effective properties of low volume fraction (up to 5%) ROFRCs up to an aspect ratio of 90. For aspect ratios over 90, the effective properties of numerical homogenization stabilized, hence attaining the saturated aspect ratio. The analytical models failed at predicting the aspect ratio saturation limit, hence overestimated the effective properties for aspect ratios over 90. Numerical results suggest that the saturated aspect ratio depends on the properties contrast and volume fraction. For aspect ratios over the saturation limit, numerical homogenization of the RVE is still needed to compute accurate effective properties.

For volume fractions over 5%, the model of Li/Voigt is the best suited for bulk modulus predictions (tested up to 20%), whereas no model accurately predicts the shear modulus. Numerical homogenization is still the only accurate method for determining effective properties of ROFRCs with volume fractions over 20%.

Recommendations

Assessment of RVE quantitative definitions for different microstructures and behaviors:

The current study has assessed RVE quantitative definitions for ROFRCs. Although the RVE quantitative definitions can be applied to any heterogeneous material, the conclusions of the assessment are not necessarily transferable to other types of microstructures such as randomly dispersed spheres or disks. This study proves that RVE quantitative definitions are not necessarily accurate. Similar assessment studies are necessary for other types of microstructures in order to have confidence in RVE quantitative definitions. For simpler microstructures with lower properties contrast, the need of very large volumes to conduct the assessment can be replaced by the exact criterion of convergence of the bounds of uniform displacement and traction boundary conditions.

Reducing the computational burden of numerical homogenization:

Lower cost alternative methods are needed for each step of the numerical homogenization process.

1. **Microstructure generation method:** In this work, numerical homogenization has been limited to relatively low volume fractions and numerous difficulties were faced for

the simulation of fibers of high aspect ratio. The most challenging and time consuming operation that prevented the numerical homogenization of such microstructures is the random generation algorithm. A combination of numerical and theoretical works should be conducted to find the maximum packings of high aspect ratio fibers. Considerable advancements in generation algorithms have been achieved for simple microstructures such as aligned fibers or randomly dispersed spheres. For example, efficient molecular dynamics like simulations in Ghossein and Lévesque (2012) approached the theoretical volume fraction limit of spheres packings of 74% within seconds of simulation. Dynamic simulations should be applied to ROFRC microstructures of high aspect ratios. The randomness of fiber orientations should be monitored under such simulations. Forcing a certain state of spatial arrangement has already been implemented in some microstructure generation methods (Altendorf and Jeulin, 2011b).

2. **Numerical resolution techniques:** FE is the most popular numerical scheme for computing accurate local fields of heterogeneous microstructures. However, the discretization of microstructures with inclusions of high aspect ratios largely increases the computation memory and time. Mesh-free methods (Belytschko *et al.*, 1996; Li and Liu, 2002), as an alternative to FE method, have shown a promising potential and has found applications on various numerical problems including homogenization of composite materials (Li *et al.*, 2011). Basically, such methods consist of including shape functions describing the microstructure in the original analytical formulation. Efforts should be employed in exploring the applicability of mesh-free techniques to random microstructures such as ROFRCs.
3. **Boundary conditions:** It has been demonstrated in many works that PBCs converge at a faster rate towards the effective properties than their uniform counterparts (Terada *et al.*, 2000; Kanit *et al.*, 2003). One can examine other sets of boundary conditions in a search for faster convergence rates. Moreover, implementing interpolated PBCs proposed by Nguyen *et al.* (2012) does not require periodic meshing and periodic geometries. Even though no enhancements are expected regarding the convergence rate, interpolated PBCs simplify the microstructure generation and meshing procedures.
4. **Efficient RVE determination methods:** In this thesis, it was demonstrated that new quantitative definitions can determine accurate effective properties for smaller material volumes. Particularly, the arithmetic and harmonic means of apparent elasticity tensors have collectively presented an efficient estimation of the apparent properties. Other formulations can be sought to find more efficient estimations, thus reducing the volume size needed for a prescribed tolerance.
5. **Microstructure simplifications:** Other simplifications of the numerical homogeniza-

tion process can be examined. Lusti and Gusev (2004) compared the elastic properties of ROFRCs to those of composites reinforced by aligned fibers of the same aspect ratio followed by an orientational averaging procedure. Although their study showed good agreement between the results of both methods, the RVE was not determined for neither microstructure. Simplifying the microstructure of ROFRCs by that of aligned fibers would considerably reduce the computational cost of numerical homogenization.

Studying the aspect ratio saturation limit:

Composites reinforced by very long fibers are the most sought microstructures in industrial applications. However, it was found that no analytical model delivers accurate predictions for such microstructures and numerical homogenization is still necessary. The aspect ratio saturation limit can be used to simulate ROFRCs with very long fibers. The results of this thesis suggest that the aspect ratio saturation limit depends on the properties contrast and the volume fraction. Determining the aspect ratio saturation limit for different microstructure parameters can provide a deeper understanding of ROFRCs. It was also demonstrated in this thesis that the analytical models of M-T, M-T/Voigt and Li/Voigt provided accurate estimations of the effective properties up to the aspect ratio saturation limit. Upon the knowledge of the saturated aspect ratio, one can use those analytical models, within their validity range, to determine the effective properties. Moreover, a correlation between the saturated aspect ratio and the microstructure parameters, combined with the appropriate analytical model, can provide a quick and accurate estimation of the effective properties of ROFRCs with very long fibers.

Assessment of analytical estimates of inclusion stresses:

In the present work, the assessment of analytical models was limited to their estimates of the effective elastic moduli. However, analytical models can also provide estimates of stress and strain phase averages under a given load. Accurate computations of phase average stress in fibers allows to identify the orientations of fibers that experience the maximum averaged stresses under given loads. Based on the M-T one-step method for randomly oriented inclusions, Duschlbauer *et al.* (2003) provided explicit analytical expressions for the average stresses acting in individual reinforcements of arbitrary orientation, shape, and material embedded in a matrix under a macroscopic loading. For a ROFRC with fibers of aspect ratio 5, at 15% volume fraction, and relatively low properties contrast of 5, they found excellent agreement between analytical estimates of the phase average stress with that predicted by numerical results. It is recommended to use currently generated finite volumes in the as-

sessment of the analytical models estimates of the fibers average stresses for a wide range of microstructural parameters.

REFERENCES

ABAQUS Analysis User's Manual (2010). *ABAQUS Analysis User's Manual, version 6.10*. Dassault Systemes.

ALTENDORF, H. and JEULIN, D. (2011a). Random-walk-based stochastic modeling of three-dimensional fiber systems. *Physical Review E*, 83, 041804.

ALTENDORF, H. and JEULIN, D. (2011b). Stochastic modeling of a glass fiber reinforced polymer. P. Soille, M. Pesaresi and G. Ouzounis, éditors, *Mathematical Morphology and Its Applications to Image and Signal Processing*, Springer Berlin Heidelberg, vol. 6671 of *Lecture Notes in Computer Science*. 439–450.

BARELLO, R. B. and LÉVESQUE, M. (2008). Comparison between the relaxation spectra obtained from homogenization models and finite elements simulation for the same composite. *International Journal of Solids and Structures*, 45, 850–867.

BELYTSCHKO, T., KRONGAUZ, Y., ORGAN, D. and FLEMING, M. (1996). Meshless methods: An overview and recent developments. *Computer Methods in Applied Mechanics and Engineering*. 3–47.

BENVENISTE, Y. (1987). New approach to the application of mori-tanka's theory in composite materials. *Mechanics of Materials*, 6, 147–157.

BENVENISTE, Y., DVORAK, G. J. and CHEN, T. (1991). On diagonal and elastic symmetry of the approximate effective stiffness tensor of heterogeneous media. *Journal of the Mechanics and Physics of Solids*, 39, 927–927.

BÖHM, H. J. (2012). A short introduction to basic aspects of continuum micromechanics.

BÖHM, H. J., ECKSCHLAGER, A. and HAN, W. (2002). Multi-inclusion unit cell models for metal matrix composites with randomly oriented discontinuous reinforcements. *Computational Materials Science*, 25, 42–53.

BORNERT, M., BRETHAU, T. and GILORMINI, P. (2001). *Homogénéisation en mécanique des matériaux*. Hermès.

BUCATARU, I. and SLAWINSKI, M. A. (2009). Invariant properties for finding distance in space of elasticity tensors. *Journal of Elasticity*, 94, 97–114.

BUDIANSKY, B. (1965). On the elastic moduli of some heterogeneous materials. *Journal of the Mechanics and Physics of Solids*, 13, 223 – 227.

CAMACHO, C. W., TUCKER, C. L., YALVAÇ, S. and MCGEE, R. L. (1990). Stiffness and thermal expansion predictions for hybrid short fiber composites. *Polymer Composites*, 11, 229–239.

CHAWLA, N., SIDHU, R. and GANESH, V. (2006). Three-dimensional visualization and microstructure-based modeling of deformation in particle-reinforced composites. *Acta Materialia*, 54, 1541 – 1548.

DONEV, A., CISSE, I., SACHS, D., VARIANO, E. A., STILLINGER, F. H., CONNELLY, R., TORQUATO, S. and CHAIKIN, P. M. (2004). Improving the density of jammed disordered packing usingellipsoids. *Science*, 303, 990–993.

DRUGAN, J. and WILLIS, J. R. (1996). A micromechanics-based nonlocal constitutive equation and estimates of the representative volume element size for elastic composites. *Journal of the Mechanics and Physics of Solids*, 44, 497–524.

DUSCHLBAUER, D., PETTERMANN, H. and BÖHM, H. (2003). Mori-tanaka based evaluation of inclusion stresses in composites with nonaligned reinforcements. *Scripta Materialia*, 48, 223 – 228.

ESHELBY, J. D. (1957). The determination of the elastic field of an ellipsoidal inclusion, and related problems. *Proceedings of the Royal Society of London. Series A. Mathematical and Physical Sciences*, 241, 376–396.

FARHAT, C., CRIVELLI, L. and ROUX, F.-X. (1994). Transient feti methodology for large-scale parallel implicit computations in structural mechanics. *International Journal for Numerical Methods in Engineering*, 37, 1945–1975.

FARHAT, C. and ROUX, F.-X. (1991). Method of finite element tearing and interconnecting and its parallel solution algorithm. *International Journal for Numerical Methods in Engineering*, 32, 1205–1227.

FARHAT, C. and ROUX, F. X. (1994). Implicit parallel processing in structural mechanics. *Computational Mechanics Advances*, 2, 1–124.

FEDER, J. (1980). Random sequential adsorption. *Journal of Theoretical Biology*, 87, 237–254.

FERRARI, M. (1991). Asymmetry and the high concentration limit of the mori-tanaka effective medium theory. *Mechanics of Materials*, 11, 251 – 256.

GAVAZZI, A. and LAGOUDAS, D. (1990). On the numerical evaluation of eshelby's tensor and its application to elastoplastic fibrous composites. *Computational Mechanics*, 7, 13–19.

GHOSSEIN, E. and LÉVESQUE, M. (2012). A fully automated numerical tool for a comprehensive validation of homogenization models and its application to spherical particles reinforced composites. *International Journal of Solids and Structures*, 49, 1387–1398.

GITMAN, I. M., ASKES, H. and SLUYS, L. J. (2007). Representative volume: Existence and size determination. *Engineering Fracture Mechanics*, 74, 2518–2534.

GUSEV, A. A. (1997). Representative volume element size for elastic composites: a numerical study. *Journal of the Mechanics and Physics of Solids*, 45, 1449–1459.

HARPER, L. T., QIAN, C., TURNER, T. A., LI, S. and WARRIOR, N. A. (2012). Representative volume elements for discontinuous carbon fibre composites - part 2: Determining the critical size. *Composites Science and Technology*, 72, 204–210.

HASHIN, Z. and SHTRIKMAN, S. (1961). Note on a variational approach to the theory of composite elastic materials. *Journal of the Franklin Institute*, 271, 336–341.

HASHIN, Z. and SHTRIKMAN, S. (1962a). On some variational principles in anisotropic and nonhomogeneous elasticity. *Journal of the Mechanics and Physics of Solids*, 10, 335 – 342.

HASHIN, Z. and SHTRIKMAN, S. (1962b). A variational approach to the theory of the elastic behaviour of polycrystals. *Journal of the Mechanics and Physics of Solids*, 10, 343 – 352.

HASHIN, Z. and SHTRIKMAN, S. (1963). A variational approach to the theory of the elastic behaviour of multiphase materials. *Journal of the Mechanics and Physics of Solids*, 11, 127–140.

HAZANOV, S. and HUET, C. (1994). Order relationships for boundary conditions effect in heterogeneous bodies smaller than the representative volume. *Journal of the Mechanics and Physics of Solids*, 42, 1995 – 2011.

HILL, R. (1963). Elastic properties of reinforced solids – some theoretical principles. *Journal of Mechanics and Physics of Solids*, 11, 357–372.

HILL, R. (1965). A self-consistent mechanics of composite materials. *Journal of the Mechanics and Physics of Solids*, 13, 213–222.

HORI, M. and NEMAT-NASSER, S. (1993). Double-inclusion model and overall moduli of multi-phase composites. *Mechanics of Materials*, 14, 189 – 206.

HU, G. and WENG, G. (2000a). The connections between the double-inclusion model and the ponte castañeda-willis, mori-tanaka, and kuster-toksoz models. *Mechanics of Materials*, 32, 495 – 503.

HU, G. K. and WENG, G. J. (2000b). Some reflections on the mori-tanaka and ponte castañeda-willis methods with randomly oriented ellipsoidal inclusions. *Acta Mechanica*, 140, 31–40.

HUA, Y. and GU, L. (2013). Prediction of the thermomechanical behavior of particle-reinforced metal matrix composites. *Composites Part B: Engineering*, 45, 1464–1470.

HUANG, M. and LI, Y.-M. (2013). X-ray tomography image-based reconstruction of microstructural finite element mesh models for heterogeneous materials. *Computational Materials Science*, 67, 63–72.

HUET, C. (1990). Application of variational concepts to size effects in elastic heterogeneous bodies. *Journal of the Mechanics and Physics of Solids*, 38, 813–813.

KANIT, T., FOREST, S., GALLIET, I., MOUNOURY, V. and JEULIN, D. (2003). Determination of the size of the representative volume element for random composites: Statistical and numerical approach. *International Journal of Solids and Structures*, 40, 3647–3679.

KARI, S., BERGER, H. and GABBERT, U. (2007). Numerical evaluation of effective material properties of randomly distributed short cylindrical fibre composites. *Computational Materials Science*, 39, 198–204.

KUSTER, G. and TOKSÖZ, M. (1974). Velocity and attenuation of seismic waves in two-phase media: Part i. theoretical formulations. *Geophysics*, 39, 587–606.

LENHARDT, I. and ROTTNER, T. (1999). Krylov subspace methods for structural finite element analysis. *Parallel Computing*, 25, 861–875.

LI, L., WEN, P. and ALIABADI, M. (2011). Meshfree modeling and homogenization of 3d orthogonal woven composites. *Composites Science and Technology*, 71, 1777 – 1788.

LI, S. and LIU, W. K. (2002). Meshfree and particle methods and their applications. *Applied Mechanics Review*, 55, 1–34.

LIELENS, G., PIROTTE, P., COUNIOT, A., DUPRET, F. and KEUNINGS, R. (1998). Prediction of thermo-mechanical properties for compression moulded composites. *Composites Part A: Applied Science and Manufacturing*, 29, 63 – 70.

LIU, J. Z., ZHENG, Q. S., WANG, L. F. and JIANG, Q. (2005). Mechanical properties of single-walled carbon nanotube bundles as bulk materials. *Journal of the Mechanics and Physics of Solids*, 53, 123–142.

LUBACHEVSKY, B.D.; STILLINGER, F. P. E. (1990). Disks vs. spheres: contrasting properties of random packings. *Journal of Statistical Physics*, 64, 501–24.

LUSTI, H. R. and GUSEV, A. A. (2004). Finite element predictions for the thermoelastic properties of nanotube reinforced polymers. *Modelling and Simulation in Materials Science and Engineering*, 12, S107–S119.

MAN, W., DONEV, A., STILLINGER, F. H., SULLIVAN, M. T., RUSSEL, W. B., HEEGER, D., INATI, S., TORQUATO, S. and CHAIKIN, P. M. (2005). Experiments on random packings of ellipsoids. *Physical Review Letters*, 94, 198001–1–4.

MILTON, G. (2002). *The Theory of Composites*. Cambridge University Press.

MORI, T. and TANAKA, K. (1973). Average stress in matrix and average elastic energy of materials with misfitting inclusions. *Acta Metallurgica*, 21, 571–4.

MORTAZAVI, B., BANIASSADI, M., BARDON, J. and AHZI, S. (2013). Modeling of two-phase random composite materials by finite element, mori–tanaka and strong contrast methods. *Composites Part B: Engineering*, 45, 1117–1125.

MOULINEC, H. and SUQUET, P. (1994). A fast numerical method for computing the linear and nonlinear mechanical properties of composites. *Comptes Rendus de l'Academie des Sciences, Serie II (Mecanique-Physique-Chimie-Astronomie)*, 318, 1417–23.

MOULINEC, H. and SUQUET, P. (1998). A numerical method for computing the overall response of nonlinear composites with complex microstructure. *Computer Methods in Applied Mechanics and Engineering*, 157, 69–94.

MOUSSADDY, H., LÉVESQUE, M. and THERRIAULT, D. (2011). Comparing finite element and analytical micromechanical modeling of randomly oriented single walled carbon nanotubes reinforced nanocomposites. *The 26th Annual Technical Conference of the American Society for Composites/2nd Joint US-Canada Conference on Composites*. Montreal, Quebec, Canada.

MOUSSADDY, H., THERRIAULT, D. and LÉVESQUE, M. (2013). Assessment of existing and introduction of a new and robust efficient definition of the representative volume element. *Submitted to the International Journal of Solids and Structures*.

MURA, T. (1982). *Micromechanics of defects in solids*. springer edition.

NEMAT-NASSER, S. and HORI, M. (1993). *Micromechanics: Overall Properties of Heterogeneous Materials*. North-Holland.

NGUYEN, V. D., BECHET, E., GEUZAINE, C. and NOELS, L. (2012). Imposing periodic boundary condition on arbitrary meshes by polynomial interpolation. *Computational Materials Science*, 55, 390–406.

ODEGARD, G. M., GATES, T. S., WISE, K. E., PARK, C. and SIOCHI, E. J. (2003). Constitutive modeling of nanotube-reinforced polymer composites. *Composites Science and Technology*, 63, 1671–1687.

OSTOJA-STARZEWSKI, M. (1998). Random field models of heterogeneous materials. *International Journal of Solids and Structures*, 35, 2429–2455.

OSTOJA-STARZEWSKI, M. (1999). Scale effects in materials with random distributions of needles and cracks. *Mechanics of Materials*, 31, 883 – 893.

OSTOJA-STARZEWSKI, M. (2002). Microstructural randomness versus representative volume element in thermomechanics. *Journal of Applied Mechanics*, 69, 25–35.

OSTOJA-STARZEWSKI, M. (2006). Material spatial randomness: From statistical to representative volume element. *Probabilistic Engineering Mechanics*, 21, 112 – 132.

PELISSOU, C., BACCOU, J., MONERIE, Y. and PERALES, F. (2009). Determination of the size of the representative volume element for random quasi-brittle composites. *International Journal of Solids and Structures*, 46, 2842–2855.

PIERARD, O. (2006). *Micromechanics of inclusion-reinforced composites in elasto-plasticity and elasto-viscoplasticity: modeling and computation*, Universié Catholique de Louvain.

PIERARD, O., FRIEBEL, C. and DOGHRI, I. (2004). Mean-field homogenization of multi-phase thermo-elastic composites: a general framework and its validation. *Composites Science and Technology*, 64, 1587–1603.

PONTE CASTAÑEDA, P. and SUQUET, P. (1997). Nonlinear composites. Elsevier, vol. 34 of *Advances in Applied Mechanics*. 171 – 302.

PONTE-CASTAÑEDA, P. and WILLIS, J. (1995). The effect of spatial distribution on the effective behavior of composite materials and cracked media. *Journal of the Mechanics and Physics of Solids*, 43, 1919 – 1951.

RANGANATHAN, S. I. and OSTOJA-STARZEWSKI, M. (2008). Universal elastic anisotropy index. *Physical Review Letters*, 101, 055504.

SAB, K. (1992). On the homogenization and the simulation of random materials. *European Journal of Mechanics, A/Solids*, 11, 585–607.

SALMI, M., AUSLENDER, F., BORNERT, M. and FOGLI, M. (2012). Various estimates of representative volume element sizes based on a statistical analysis of the apparent behavior of random linear composites. *Comptes Rendus Mécanique*, 340, 230–246.

SANDLER, J. K. W., KIRK, J. E., KINLOCH, I. A., SHAFFER, M. S. P. and WINDLE, A. H. (2003). Ultra-low electrical percolation threshold in carbon-nanotube-epoxy composites. *Polymer*, 44, 5893–5899.

SCHJODT-THOMSEN, J. and PYRZ, R. (2001). The mori-tanaka stiffness tensor: Diagonal symmetry, complex fibre orientations and non-dilute volume fractions. *Mechanics of Materials*, 33, 531–544.

STROEVEN, M., ASKES, H. and SLUYS, L. (2004). Numerical determination of representative volumes for granular materials. *Computer Methods in Applied Mechanics and Engineering*, 193, 3221 – 3238.

SUQUET, P. (1997). *Continuum micromechanics*. Springer.

TALBOT, J., SCHAAF, P. and TARJUS, G. (1991). Random sequential addition of hard spheres. *Molecular Physics: An International Journal at the Interface Between Chemistry and Physics*, 72, 1397 – 1406.

TERADA, K., HORI, M., KYOYA, T. and KIKUCHI, N. (2000). Simulation of the multi-scale convergence in computational homogenization approaches. *International Journal of Solids and Structures*, 37, 2285 – 2311.

TORQUATO, S. (2002). *Random Heterogeneous Materials*. Springer.

TRIAS, D., COSTA, J., TURON, A. and HURTADO, J. E. (2006). Determination of the critical size of a statistical representative volume element (srve) for carbon reinforced polymers. *Acta Materialia*, 54, 3471–3484.

TUCKER III, C. L. and LIANG, E. (1999). Stiffness predictions for unidirectional short-fiber composites: Review and evaluation. *Composites Science and Technology*, 59, 655–671.

WILLIS, J. (1981). Variational and related methods for the overall properties of composites. Elsevier, vol. 21 of *Advances in Applied Mechanics*. 1 – 78.

WITHERS, P., STOBBS, W. and PEDERSEN, O. (1989). The application of the eshelby method of internal stress determination to short fibre metal matrix composites. *Acta Metallurgica*, 37, 3061–3084.